DANMARKS OG GRØNLANDS GEOLOGISKE UNDERSØGELSE **RAPPORT 2021/59**

Studies of geological properties and conditions for deep disposal of radioactive waste, Denmark. Phase 1, report no. 8

Conceptual 1D modeling of nuclides transport in low permeable formations

Jolanta Kazmierczak, Sachin Karan & Rasmus Jakobsen

GEOLOGICAL SURVEY OF DENMARK AND GREENLAND
DANISH MINISTRY OF CLIMATE, ENERGY AND UTILITIES

G E U S

DANMARKS OG GRØNLANDS GEOLOGISKE UNDERSØGELSE **RAPPORT 2021/59**

Studies of geological properties and conditions for deep disposal of radioactive waste, Denmark Phase 1, report no. 8

Conceptual 1D modeling of nuclides transport in low permeable formations

Jolanta Kazmierczak, Sachin Karan & Rasmus Jakobsen

GEOLOGICAL SURVEY OF DENMARK AND GREENLAND
DANISH MINISTRY OF CLIMATE, ENERGY AND UTILITIES

G E U S

Preface

The present report is a contribution to a major geological project with the purpose to investigate whether suitable geological sites for a deep repository for the Danish radioactive waste can be identified. The Geological Survey of Denmark and Greenland (GEUS) has been given the task to identify, map, and characterize formations of low permeable rocks occurring with continuous lateral extension at 500 meters depth with thicknesses of 100 meters or more. This report is part of a series of ten reports presenting the results of the first phase of the project, which is carried out mainly as a desk study.

The geological characterisation and evaluation will provide the geological basis for the selection of two sites where, during the second phase of the geological project, detailed geological site investigations will be carried out. These two sites will be selected through a process of information sharing and dialogue between the Ministry of Higher Education and Science (MHES) and the local municipalities. The new geological data generated in the project's second phase will be used as input to a safety case when a disposal solution has been developed by the Danish Decommissioning (DD). The safety case must demonstrate that the geological properties in combination with the engineered barriers of the repository can provide the required safety for disposal on both short and long term.

In a preceding feasibility study, it was concluded that at 500 meters depth potential host rocks occur in claystones in the Jurassic and Lower Cretaceous sections, in Upper Cretaceous chalk and marl, and in Precambrian crystalline basement rocks. In this phase of the geological project, the geological properties and subsurface conditions related to these stratigraphic intervals and rock types are reviewed, and the potential host rocks' capability to retard radionuclides is investigated by conceptual 1D numerical modelling. In addition, natural processes potentially influencing short and long-term stability are identified and described.

Information gathered in the geological reports no. 2-8 forms the basis for a subdivision of Denmark into 11 areas where each area is characterized by the potential host rock type occurring at 500 meters depth, the barrier rocks in overlying sections, and the structural framework. The areas are defined to enable characterization and evaluation of the Danish subsurface at depths to 500 meters. The evaluation is based on requirements and criteria for deep geological disposal, which are defined based on international experience and recommendations. Each area is characterized and evaluated with regards to whether the geological properties and conditions are favourable for deep disposal of the Danish radioactive waste. The results of the project's first phase are presented in the following ten geological reports:

1. Requirements and criteria for initial evaluation of geological properties and conditions
2. Geological setting and structural framework of Danish onshore areas
3. Upper Cretaceous – Paleocene chalk, limestone and marl distribution and properties
4. Jurassic and Lower Cretaceous claystone distribution, sedimentology, and properties
5. Precambrian crystalline basement distribution and properties
6. Subsurface distribution of Jurassic and Cretaceous fine-grained formations based on seismic mapping
7. Evaluation of long-term stability related to glaciations, climate and sea level, groundwater, and earthquakes
8. Conceptual 1D modelling of nuclide transport in low permeable formations
9. Karakterisering og evaluering af geologiske egenskaber og forhold i 500 meters dybde (In Danish)
10. Characterisation and evaluation of geological properties and conditions at 500 meters depth (This report is an English translation of report no. 9, to be published late 2022)

This report is Report no. 8. It describes the purpose of carrying out numerical modeling of nuclide transport during various phases of a geological siting project. The results of conceptual 1D models for sensitivity studies of potential host rocks' effectiveness with regard to retardation of nuclide transport are presented.

Table of contents

0. Dansk Sammendrag (In Danish)

I 2018 vedtog Folketinget, at en langsigtet løsning for håndtering af Danmarks radioaktive affald skal indeholde lokalisering for et muligt dybt geologisk slutdepot, som kan tages i brug senest i 2073 (Folketingets beslutning B90; Danish Parliament, 2018). Det radioaktive affald består af cirka 10.000 m^3 lavradioaktivt affald og mindre mængder af mellemradioaktivt affald, inklusiv 233 kg særligt affald, men intet højradioaktivt varmegenererende affald. De Nationale Geologiske Undersøgelser for Danmark og Grønland (GEUS) har af Folketinget fået tildelt opgaven med at undersøge, om der eksisterer områder i en dybde omkring 500 meter i den danske undergrund, der har de nødvendige geologiske egenskaber for etablering af et sikkert slutdepot for det radioaktive affald.

Det geologiske slutdepotprojekt omhandler de geologiske forhold, der skal tages i betragtning inden en eventuel beslutning om etablering af et dybt geologisk slutdepot for det danske radioaktive affald. De geologiske undersøgelser udføres sideløbende med aktiviteter hos Uddannelses- og Forskningsministeriet (UFM), der er overordnet ejer af slutdepotprojektet, og Dansk Dekommissionering (DD), som har ansvaret for at opbevare affaldet, indtil det skal slutdeponeres (MHES, 2021). Socio-økonomiske forhold, endeligt depotkoncept og -design, sikkerhedsforhold m.v. er ikke en del af det geologiske projekt, men varetages af UFM.

Retningslinjer for identificering af områder egnede til dyb geologisk slutdeponering
Internationale anbefalinger til de geologiske undersøgelser, der skal lede til identificering af en egnet lokalitet for dyb geologisk deponering af radioaktivt affald, er præsenteret af bl.a. det Internationale Atom Energi Agentur (IAEA, 2011) og Norris (2012) – her oversat til dansk:

"At identificere og kortlægge lav-permeable bjergarter, der udgør tilstrækkeligt tykke formationer (mere end 100 meter), og som har en kontinuert lateral udbredelse (flere kilometer i hver retning) indenfor studieområdet. Formationen skal være homogen og må ikke indeholde betydelige diskontinuiteter så som store forkastninger og sprækker. Formationen skal være så mineralogisk homogen og ensartet som muligt. De geologiske forhold skal være stabile på både kort sigt og indenfor en længere tidshorisont afhængigt af affaldets karakter."

Projektet vil følge retningslinjer fra IAEA (IAEA, 2011; IAEA, 2018a; IAEA, 2018b), Det Nukleare Agentur under OECD (NEA, 2005; NEA, 2008; NEA, 2012) og EU-direktiver indenfor området (EU, 2011).

Som bemærket af IAEA (IAEA, 2018a; IAEA, 2018b), er det ikke muligt at udpege ét enkelt område som det bedst egnede baseret på de geologiske egenskaber, idet det er umuligt at undersøge og karakterisere alle naturlige variationer af de geologiske egenskaber ned til 500 meters dybde indenfor et givent område. Opgaven er derimod at identificere et egnet område, der samlet set kan opfylde de definerede krav til sikkerhed og funktionalitet af depotet, samtidig med at etableringen af et geologisk slutdepot i området er teknisk mulig og accepteret af beslutningstagere og interessenter.

Omfanget af de geologiske undersøgelser, der er nødvendige at udføre, er defineret på basis af erfaringer fra lignende projekter i bl.a. Frankrig (ANDRA, 2005), Sverige (SKB, 2007), Schweiz (SFOE, 2008; Nagra, 2017), Holland (COVRA, 2017) og Finland (POSIVA, 2017a,

b). Kontakter er i løbet af projektet etableret til flere af disse organisationer med henblik på udveksling af erfaringer samt rådgivning og kvalitetssikring for det geologiske slutdepotprojekt. Som et resultat af dette internationale samarbejde, blev der i første fase af slutdepotprojektet udført et review af de definerede geologiske kriterier (præsenteret i Rapport nr. 1), hvor kommentarer og anbefalinger er afrapporteret i Blechschmidt et al. (2021).

På baggrund af flere årtiers undersøgelser af de lokale geologiske forhold har nogle lande besluttet at etablere et dybt slutdepot i marine lersten (ANDRA-Frankrig, COVRA-Holland, Nagra-Schweiz). I Sverige (SKB) og Finland (POSIVA) er det besluttet at etablere dybe geologiske slutdepoter i krystallinsk grundfjeld. Mange andre lande arbejder stadig med lokaliseringsprojekter, og udover krystallinsk grundfjeld og lersten er også kalksten, mergel og salt vurderet som mulige bjergarter for deponering afhængigt af de lokale geologiske forhold.

Det geologiske projekt vedrørende et muligt slutdepot i 500 meters dybde
Forud for det igangværende geologiske projekt blev en screening af den danske undergrund foretaget med henblik på at undersøge, om lavpermeable bjergarter findes i 500 meters dybde i den danske undergrund. Denne screening viste, at i 500 meters dybde findes jurassiske og kretassiske lagserier, der indeholder tætte formationer af lersten og kalksten samt prækambrisk grundfjeld bestående af granit og gnejs. Alle disse bjergartstyper kan under de rette omstændigheder have geologiske egenskaber, der gør dem egnede som værtsbjergart for et dybt geologisk slutdepot (Gravesen, 2016). Baseret på dette arbejde blev undersøgelserne i nærværende projekts første fase igangsat.

Det geologiske slutdepotprojekt blev påbegyndt i januar 2019 og forventes at forløbe over en 7-årig periode. Projektet udgør den geofaglige del af det samlede projekt om et muligt dybt geologisk slutdepot, som er defineret i Folketingets beslutning B90 (Danish Parliament, 2018). Det geologiske projekt varetages af GEUS' personale med bidrag fra eksterne forskningsinstitutioner, konsulentfirmaer og internationale eksperter, hvor det er nødvendigt. På grundlag af en karakterisering og evaluering af undergrundens geologiske egenskaber i projektets første fase, skal to lokaliteter udvælges til detaljerede geologiske undersøgelser i projektets anden fase. Uddannelses- og Forskningsstyrelsen (UFS) har ansvaret for at tilrettelægge og gennemføre en dialogproces, der inden udgangen af 2022 kan føre til afklaring af muligheden for at etablere et partnerskab mellem UFM og én eller flere kommuner om gennemførelsen af detaljerede geologiske undersøgelser.

I projektets første fase er de forskellige bjergarter kortlagt og deres egenskaber er beskrevet i det omfang, der findes data. Det skal i den sammenhæng bemærkes, at den tilgængelige information er ujævnt fordelt både geografisk og geologisk. De eksisterende data fra 500 meters dybde er hovedsageligt indsamlet fra tidligere olie- og gasefterforskningsboringer og relaterede seismiske undersøgelser og i mindre grad fra geotermiske, geotekniske og videnskabelige undersøgelser. De fleste dybe boringer i Danmark har haft som hovedformål at påvise tilstedeværelsen af sandsten og karakterisere deres reservoiregenskaber, hvorfor det er meget sparsomt med data fra de lavpermeable bjergarter som lersten og kalksten, der kan anvendes som værtsbjergarter, og som nærværende slutdepotprojekt har fokus på. Den nuværende kortlægning af undergrundens geologi er derfor behæftet med varierende grad af nøjagtighed og pålidelighed for de forskellige parametre, særligt for de lavpermeable bjergarter, som er vigtige for et geologisk sludepot. Gennemgangen af de eksisterende data har

bidraget til at identificere områder med manglende geologiske data og informationer, hvor det er vigtigt at sikre indsamling af nye data i den næste fase af projektet.

I projektets anden fase skal detaljerede geologiske undersøgelser, som nævnt, foretages på to valgte lokaliteter. Undersøgelserne vil omfatte indsamling af seismiske profiler med geofysiske metoder og boring af dybe borehuller. I borehullerne udtages bl.a. borekerner og vandprøver, og der indsamles petrofysiske målinger for efterfølgende analyser med henblik på karakterisering af forseglingsegenskaberne og geotekniske egenskaber. Disse data vil indgå bl.a. i modellering af stoftransport, bestemmelse af geokemisk retardation, seismisk kortlægning og vurdering af geoteknisk stabilitet. De geologiske og geotekniske egenskaber vil også have indflydelse på hvilket depotdesign, der er teknisk muligt og sikkerhedsmæssigt forsvarligt i undergrunden. De indsamlede data og analyser vil efterfølgende indgå i en sikkerhedsvurdering, der skal afklare, om det samlede depotkoncept med de geologiske barrierer i kombination med de konstruerede barrierer kan levere den nødvendige sikkerhed for deponering på både kort og lang sigt.

Opsummering af Rapport nr. 8: Konceptuel 1D modellering af nuklid transport i lavpermeable formationer (Conceptual 1D modelling of nuclide transport in low permeable formations)

Nærværende rapport beskriver resultaterne fra de numeriske modelberegninger, der er udført i den første fase af det geologiske slutdepotprojekt. Modelberegningerne har til formål at bidrage til en indledende vurdering af mulighederne for geologisk slutdeponering i lavpermeable bjergarter i Danmark.

På nuværende tidspunkt er der begrænset viden om bjergartsegenskaber og hydrogeologiske forhold i 500 meters dybde i den danske undergrund. Derfor er man pt. nødt til at basere vurderinger af mulig transport af radioaktive nuklider fra lag i 500 meters dybde til det ferske grundvand, der bruges til drikkevand på en række antagelser og konceptuelle betragtninger. Dette betyder, at modelberegninger, som dem, der præsenteres i nærværende rapport, ikke er særligt nøjagtige i forhold til at beskrive f.eks. transporttider fra 500 meters dybde til det ferske grundvand. Den viden, der er nødvendig for at øge nøjagtigheden af de numeriske stoftransportberegninger, og dermed for at give en mere sikker vurdering af forskellige bjergarters potentiale som værts- og/eller barrierebjergart, omfatter bl.a. data om de fysisk/kemiske bjergartsegenskaber, den mineralogiske bjergartssammensætning, de hydrogeologiske egenskaber, den grundvandskemiske sammensætning samt specifikke geokemiske egenskaber i forhold til de radioaktive stoffer, der findes i det danske affald. Disse egenskaber vil være relateret til lokale, stedspecifikke forhold.

Der er for nuværende overordnet tre typer af lavpermeable bjergarter, der i Danmark potentielt vil kunne anvendes til placering af et geologisk slutdepot: Krystallinsk grundfjeld, kalksten og lersten. Der findes adskillige studier, inklusivt studier fra Skandinavien, hvor det er påvist, at krystallinske bjergarter kan udgøre et geologisk slutdepot. Derfor er krystallinske bjergarter ikke medtaget i nærværende modelstudie, idet det eksisterende datagrundlag ikke kan kvalificere denne vurdering yderligere i en dansk kontekst. Baseret på det nuværende kendskab

og vidensniveau om den danske undergrund, er det derfor vurderet relevant at opstille konceptuelle numeriske modeller for de lavpermeable sedimentære bjergarter kalksten og lersten.

Som nævnt er det i nærværende arbejde valgt at gennemføre en række konceptuelle modelstudier. Det vil sige, at modellerne ikke repræsenterer specifikke lokaliteter i Danmark men derimod en generel betragtning af den geologiske lagfølge, hvori relevante lavpermeable bjergarter under forskellige antagelser indgår. Antagelserne relaterer sig til hydrogeologiske forhold og parameterværdier, der så vidt muligt repræsenterer den aktuelle viden i Danmark. Modelleringen er udført med henblik på: (1) at evaluere barriereeffektiviteten af de lavpermeable sedimentære bjergarter, og (2) at identificere hvilke geologiske, hydrogeologiske og geokemiske parametre, som har den største betydning for transport af nuklider i undergrunden. Dette vil give retningslinjer for dataindsamling og design af det videre modelarbejde i slutdepotprojektets efterfølgende faser.

Modelstudiet er todelt, hvor bjergarternes barriereegenskaber vurderes i del 1 på baggrund af konservative stoftransportsimuleringer. Således antages det i disse modeller som et konservativt scenarium, at lækagen fra et muligt slutdepot sker øjeblikkeligt og effekten af nedbrydning, retardation/sorption, densitetsstrømning og/eller spredning i et 2D/3D domæne er ikke medtaget. Modellernes resultater repræsenterer derfor en situation med en forventet større risiko for påvirkning af det ferske grundvand, end der reelt vil være ved fremtidig slutdeponering i kalksten eller lersten. Adskillige scenarier med forskellige parameterværdier og randbetingelser er i del 1 vurderet ved stokastisk at generere værdier for den hydrauliske ledningsevne inden for et udfaldsrum, som er baseret på de eksisterende data, der findes for kalksten og lersten i Danmark (beskrevet i Rapport nr. 3 og 4, jf. Kapitel 9.1 for reference). Det vil sige, at et antal lige sandsynlige værdier for den hydrauliske ledningsevne er genereret for de forskellige geologiske enheder i modellerne under antagelse af forskellige randbetingelser og stoftransport parameterværdier. Randbetingelser og parameterværdier er ligeledes baseret på den tilgængelige viden.

I del 2 vurderes barriereegenskaberne på baggrund af stoftransportsimuleringer af radioaktive nuklider, hvor effekten af henfald og opløselighed er inkluderet. Årsagen til, at andre transportmekanismer, f.eks. sorption og densitetseffekter, ikke er inkluderet, og at der i denne første fase af slutdepotprojektet udelukkende er arbejdet med 1D repræsentationer af undergrunden, er dels, at det mangelfulde eksisterende datagrundlag og dels, at mange af disse mekanismer vil være stof- og stedsspecifikke, hvilket ikke er muligt at tage højde for på nuværende tidspunkt. De hydrogeologiske parametre, der er anvendt i modellerne i del 2, er baseret på medianværdier for de eksisterende datasæt for henholdsvis kalksten og lersten.

Det er væsentligt at bemærke, at de simulerede gennembrudstider, og deraf afledte vurderinger, der præsenteres i rapporten, repræsenterer én specifik konceptuel geologisk model for hver værtsbjergart og samtidig, som nævnt, en situation med forventet større risiko for påvirkning af det ferske grundvand end der reelt vil være ved slutdeponering i kalksten eller lersten. Det er derfor forventningen, at nye, flerdimensionelle modeller, der baseres på stedspecifikke data, i slutdepotprojektets næste fase vil resultere i væsentligt længere gennem-

brudstider end præsenteret i denne rapport. De simulerede gennembrudstider og -koncentrationer i denne første fase af slutdepotprojektet bør derfor udelukkende anvendes til en første indledende kvalificering af henholdsvis kalksten og lersten som værtsbjergarter – samt til at vurdere hvilke parametre, der har betydning for stoftransport fra 500 meters dybde til grundvandet.

Resultaterne for del 1, hvor der foretages modellering med simpel konservativ stoftransport, viser, at:

- I tilfældet, hvor et slutdepot placeres i kalksten i 500 meters dybde, simuleres der gennembrud af den gennemsnitlige maksimale koncentration i indvindingsdybden for grundvand inden for 33.000 til 530.000 år.
- I tilfældet, hvor et slutdepot placeres i lersten i 500 meters dybde, simuleres der ikke gennembrud af den gennemsnitlige maksimale koncentration i indvindingsdybden for grundvand inden for 1 million år.
- Det er afgørende for nøjagtigheden på den simulerede transporttid og de maksimale koncentrationer, at følgende stedspecifikke parametre bestemmes så nøjagtigt som muligt, da disse naturligt kan variere flere størrelsesordener:
    - Bjergarternes hydrauliske ledningsevner, inklusivt variationer inden for en specifik bjergart.
    - Den hydrauliske gradient.
    - Diffusionskoefficienten, som også vil være stofspecifik.
- Det er mindre afgørende for nøjagtigheden på den simulerede transporttid og de maksimale koncentrationer at have en nøjagtig bestemmelse af f.eks. bjergarternes porøsitet og geologiske laggrænser, da disse ofte varierer mindre end en størrelsesorden.

Resultaterne for del 2, hvor der er medtaget henfald og opløselighed af specifikke radioaktive nuklider i modellerne, viser, at:

- Tiden, der går, indtil det første gennembrud af nuklid i grundvandet ses ved transport fra et slutdepot i 500 meters dybde, er mere end dobbelt så lang, når lersten er værtsbjergart sammenlignet med kalksten som værtsbjergart.
- Koncentrationen af nuklider i grundvandet, som er forårsaget af transport fra et slutdepot i 500 meters dybde, vil i høj grad være afhængig af halveringstider og opløselighed af nukliderne. Med de anvendte hydrauliske egenskaber, og 1D konceptuelle repræsentationer af undergrunden, ses det f.eks., at for scenariet med kalksten som værtsbjergart vil kun nuklider med halveringstider over 100.000 år, og den største opløselighed, nå grundvandet inden for en periode på 1 million år. Tilsvarende resultater opnås med lersten som værtsbjergart, men med gennembrud af kun de mest opløselige og langsomt henfaldende nuklider – og i lavere koncentrationer end med kalksten som værtsbjergart.

Ovenstående resultater viser, at både kalksten og lersten potentielt set kan udgøre en værtsbjergart for et geologisk slutdepot, idet der for begge typer af værtsbjergart ses lange gennembrudstider for de konservative stoftransportsimuleringer. Resultaterne viser endvidere, at lersten som værtsbjergart giver en større tilbageholdelse af nuklider end kalksten som værtsbjergart. Kalksten giver dog allerede i de simple 1D konceptuelle modeller en væsentlig tilbageholdelse af nuklider, og faktorer, der ikke er medtaget i de konceptuelle modeller, så

som nedbrydning, sorption, densitetseffekter og stofspredning i 3D, vil reelt betyde, at nuklider tilbageholdes væsentligt større omfang i begge typer af værtsbjergarter.

Det skal bemærkes, at modelscenarierne med lersten som værtsbjergart for simpelhedens skyld er baseret på en konceptuel model med 170 meter homogen lersten og et slutdepot placeret 70 meter under toppen af denne lersten. Som beskrevet i Rapport nr. 4 (jf. Kapitel 9.1 for reference) er de lersten, der findes i en dybde af 500 meter i Danmark ofte heterogene med hyppig forekomst af sandlag på flere meters tykkelse. Effekten af disse sandlag på stoftransporten fra 500 meters dybde til grundvandet er ikke vurderet i denne første fase af slutdepotprojektet, men det forventes, at en sådan vurdering inkluderes i de mere avancerede 3D numeriske modeller, der opstilles i projektets næste fase.

Derudover, vil depotkoncept og de konstruerede barrierer i et endeligt slutdepot bidrage til yderligere tilbageholdelse af nukliderne i det radioaktive affald.

Modelberegningerne viser stor spredning i de beregnede gennembrudstider. For at mindske denne usikkerhed, er det nødvendigt for den kommende modellering i slutdepotprojektets fase 2 at indsamle stedspecifikke hydrogeologiske og geokemiske data med henblik på bestemmelse af de ovenfor nævnte styrende parametre, herunder også parametre, der ikke er inkluderet i de nuværende modeller. Endelig er en god bestemmelse af det hydrauliske system også vigtig i forhold til vurderingen af 3D strømning.

1. Introduction

In 2018, the Danish Parliament agreed that the long-term solution for Denmark´s radioactive waste should include a deep geological repository operating no later than 2073 (Danish Parliament, 2018). The waste is temporarily stored by the Danish Decommissioning (DD) on the Risø peninsula. It amounts to more than 10,000 m^3 and comprises mostly low-level radioactive waste (LLW), and a minor volume of medium-level waste MLW), including 233 kg special waste – but no high-level radioactive material (HLW).

The Geological Survey of Denmark and Greenland (GEUS) has been given the task by the Danish Parliament to investigate whether areas can be identified where potential host rock with suitable properties for geological disposal is present at 500 meters depth. The task is carried out in parallel with activities by the Danish Ministry of Higher Education and Science (MHES), being the project owner, and DD, being responsible for management of the radioactive waste including storage of the waste and final disposal.

The geological project was initiated in 2019 and is expected to be carried out within a period of approximately seven years. The bulk of the workload will be undertaken by staff members at GEUS, with contributions from external consultancy companies, organisations, and experts as needed. The geological siting project comprises two major phases. The current first project phase is a desk study with the purpose to map and characterize geological properties and conditions of potential host rocks in the Danish subsurface, mainly based on existing data. In the second project phase of the geological project, detailed geological investigations will be carried out at two specific sites to investigate whether the geological properties are suitable for safe disposal of radioactive waste in a deep geological repository at these specific sites. The two sites must be selected in a dialogue-based process between MHES and the local municipalities. Subjects and conditions, such as socio-economic issues, activities relating to civil participation, disposal facility design, safety cases, and other non-geological issues will be addressed and handled separately by MHES and DD with contributions from GEUS where relevant.

1.1 Guidelines for identification of deep geological repository sites

International recommendations on geological studies required to identify suitable sites for deep disposal of radioactive waste have been presented by e.g. the International Atomic Energy Agency (IAEA, 2011) and Norris (2012) as follows:

"*To identify and map layers of low-permeable rock types that are sufficiently thick (more than 100 meters) and which have a continuous lateral extension (several km^2) throughout the entire study area. The rock body should also be sufficiently homogeneous and represent no significant discontinuities like fractures and faults. Furthermore, the rocks should be as mineralogical homogeneous and uniform as possible. The geological conditions should be stable in the short term as well as in the long term.*"

These recommendations as well as experience from siting projects in other countries have been used to identify investigations that need to be performed in the Danish project. Experience from other countries include France (ANDRA, 2005), Holland (COVRA, 2018), Switzerland (SFOE, 2008; Nagra, 2017), Sweden (SKB, 2007) and Finland (POSIVA, 2017a, b).

In some countries, based on several decades of comprehensive subsurface studies, it has been concluded that marine claystones and clay rich carbonates (marl) may constitute suitable host rocks for a final geological disposal. Therefore, extensive research on clay deposits is continuously ongoing and makes available significant amounts of data and experiences that may be valuable for this project (e.g. ANDRA-Belgium, COVRA-Holland, Nagra-Switzerland). In the Czech Republic, a former limestone mine is used for disposal of institutional waste comprising radioactive material similar to the components in the Danish waste. In other countries, including Sweden, Finland, and Norway, it has been decided to establish final repositories in crystalline bedrock. When relevant, the current project in Denmark will draw on experiences of others and cooperate with relevant radioactive waste disposal organisations. Furthermore, the project will follow guidelines from IAEA (IAEA 2011; IAEA 2018 a,b), the Nuclear Energy Agency (NEA (OECD), 2005; NEA 2006; NEA, 2008; NEA, 2012) and the EU directive regarding this field (EU, 2011).

As noted by the IAEA (2018 a, b), the impossibility of finding “the safest site” based on rock properties should be emphasised, because it is not possible to investigate and determine the detailed nature of every possible site. Instead, the key to find a suitable site will be to have it fulfil the required level of safety and performance, and that establishing a repository here is also acceptable to decision makers and stakeholders.

1.2 The deep geological repository project

A geological screening of the Danish subsurface layers present at 500 meters depth was carried out prior to initiation of the current geological siting project, to investigate whether low permeable rocks occur at this depth. The screening showed that the Jurassic and Cretaceous stratigraphic intervals at 500 meters depth comprise chalk, limestone, marl, and claystone, and the Precambrian basement comprises crystalline rocks in terms of gneiss and granite, which may all potentially provide a host rock for a deep geological repository (Gravesen, 2016). Based on this work, it was recommended to further analyse and characterize the geological conditions and barrier effectiveness of the geological formations at depths to 500 meters below the surface, which resulted in a decision to initiate the first phase of the present project.

The first phase of the present geological siting project comprises a geological review of all data available in the GEUS archives, the drilling-sample storage facilities, and from literature. The data have been used to map and describe relevant properties of the rock types identified at depths to around 500 meters, as well as natural processes potentially influencing the short- and long-term geological stability. The results form the basis of a subdivision into geologically different areas which are characterised and evaluated regarding the areas’ potential suitability for deep disposal as described in the project’s Report No. 9 (cf. Chapter 7.1 for reference).

The geological desk studies were carried out as separate work packages and presented in a number of reports (Reports No. 2-7; cf. Chapter 7.1 for references) addressing the following issues: overview of the onshore geological setting in Denmark; subsurface mapping based on seismic data and well data; a geological description of the three rock types chalk, claystone and crystalline basement, respectively, and issues potentially influencing long-term geological stability, such as climate conditions, possible glaciations, earthquake risks and groundwater conditions. Based on the results of the geological desk studies, conceptual 1D numerical modelling was performed to identify properties and conditions with high importance for the rocks' barrier-effectiveness for retardation of the radionuclides (Report No. 8; cf. Chapter 7.1 for reference).

Information on the subsurface geological formations onshore Denmark is quite scattered and of highly varying quality. The archives and databases comprise 2D seismic data of different vintages and quality as they are acquired for different purposes. Well data exist mainly from deep wells drilled for hydrocarbon exploration, some geothermal wells, and other technical/scientific drillings. Thus, as the data from various regions of Denmark varies in vintage, quality and level of detail, the current picture is by no means comprehensive. However, the geological desk studies combined with some new sedimentological and stratigraphic studies, and initial sensitivity studies from the conceptual 1D modelling have proven highly valuable; both in detailed mapping and identifying rock types, as well as in identifying major data gaps and critical parameters, for which it is important to obtain information during the next phase of the project.

The characterisation and evaluation carried out in this first phase of the project provide the geological basis for selection of two sites for detailed geological investigations in the second phase of the project. A dialogue-based process for the site selection is managed by MHES.

As part of the detailed investigations in the second phase of the project, new data and information will be collected at the two sites to further evaluate whether the geological properties and conditions are favourable for deep disposal. Thus, the second phase sets off with planning and preparation for the investigations, which include acquisition of seismic data and the drilling of deep boreholes (deeper than 500 meters) at each site. The extensive data sampling program will, among others, include drill-cores, well logs, and groundwater samples - thus, providing samples and measurements for laboratory analyses and various other studies. Based on the new data, a characterisation and evaluation of the geological suitability of the two sites will be made. This characterisation will also be used by DD for identification of a suitable repository design and for evaluation of the combined retention capacity of the engineered and the geological barriers as input to a safety case.

2. General introduction to numerical modeling for geological repositories

Prior to the selection of a disposal site and the construction of a repository, the protection of human health and the environment from radiation and possibly released nuclides must be ensured. The combined effectiveness of a host rock formation, the engineered barrier system, and the overlying effective containment zone (ECZ) in protection of human health and environment from influence of the radioactive waste is assessed by reactive transport modeling (Selroos and Follin, 2014; De Windt and Spycher, 2019). The data and simulation outcomes must: (1) demonstrate if a given site meets basic safety- and construction requirements, (2) permit the comparison between different sites, and (3) assess the impact of the repository on environment and society (Ström et al., 2008; Selroos and Follin, 2014).

The identification of suitable geological disposal sites for radioactive waste includes reactive transport models at various stages of the geological siting project as part of a narrowing down process (IAEA, 2011). Models are made for different purposes during different stages varying from initial conceptual models to complex site-specific models based of the data acquired during the detailed geological site investigations. It is noted that the international studies cited in the present Chapter 2 are generally dealing with high-level radioactive waste (HLW), which have been the focus of geological repository studies. The Danish waste comprises mainly LLW, but the experience from HLW studies will be applied where pertinent.

2.1 Modeling – purpose

In the present initial project phase, chalk, claystone and crystalline basement rocks occurring at depths of approximately 500 meters below ground level are considered as potential host rock formations for a radioactive waste repository. As part of the assessment of the rocks' retardation capability, conceptual modeling of nuclides transport in different rock types is carried out in this initial phase without knowing the specific repository location. This is similar to other countries' methodology (ANDRA, 2005 b, c; Luo et al., 2013). The purpose is to investigate how various geological parameters influence the retardation capacity and whether some parameters have a larger impact on retardation capacity than others. Conceptual reactive transport models are commonly developed based on the existing data, i.e. underground research laboratories and borehole data (ANDRA, 2005b, c; Luo et al., 2013; Luo et al., 2014a, b; Selroos and Follin, 2014). Reactive transport models at this phase are usually limited to a few selected nuclides, including those that with the highest possibility can have an impact on the biosphere because of their high concentrations in the radioactive waste or long decay time (ANDRA, 2005b). Such models are used in preliminary estimates of barrier properties in various geological settings.

Conclusions from the initial phase are used as input to the process for the selection of specific suitable sites for the second phase of detailed investigations as well as for identification of data gaps that should be filled in during the detailed site investigations.

In the second phase, base case site-specific models are often set up for selected locations (Follin et al., 2008; Sawada et al., 2015). The models are based on site specific data and analyses acquired from the detailed site studies. Modeling of geological disposal of radioactive waste in this and following phases is carried out in accordance with IAEA safety standards and ensures transparency and traceability of the data and modeling assumptions (IAEA, 2011). Objectives of the modeling at this phase are: (1) to obtain a high level of understanding of flow and transport processes at the specific site (Follin et al., 2008; Schwartz, 2012; Sawada et al., 2015), and (2) to assess performance of a potential radioactive waste repository under the normal, recent environmental conditions based on the temporal range of the data available for the considered location (Lim, 2006; Brommundt et al., 2014; Enssle et al., 2014; Verma et al., 2015). The base case models for the radioactive waste repositories are based on the comprehensive understanding of the modeled system based on diverse observations and provide the best match between the conceptual interpretation, measured values and simulation results (ANDRA, 2005b). Sensitivity analysis at this phase is typically run by setting up alternative base case models to identify parameters with the highest impact on seal capacity and to address the uncertainties of key parameters (e.g. ANDRA, 2005b). The alternative models are used to test the worst-case scenarios of the repository impact for instance by ignoring chemical retention of geological units (ANDRA, 2005b), assuming immediate release of nuclides from the system of the engineered barriers (ANDRA, 2005b), or increasing of the host rock formation permeability based on the assumption that there are undetected fracture networks (ANDRA, 2005c; Schwartz, 2018). The aim of the alternative models is often, even though they may overestimate the repository impact, to check if the geological and engineered barriers are able to contain the nuclides migration in cases of errors in the data collection, conceptual understanding of the system, or construction of the engineered barriers (ANDRA, 2005c; Schwartz, 2018).

In the final phase of a typical modelling exercise, long-term safety is assessed by reactive transport models, which are based on the base case site-specific models. These models are used to estimate behaviour of repository under the changing conditions such as glaciations, sea level changes, earthquakes, failure of the engineered barriers, and anthropogenic catastrophes (ANDRA, 2005b, c; Selroos and Painter, 2012; Vidstrand et al., 2014; Enssle et al., 2014; Schwartz, 2018). The models are run for normal evolution scenarios and altered evolution scenarios. The normal evolution scenarios account for expected engineered (e.g. gradual failure of containers and seals, generation of gas), geological (e.g. changes in geological medium as a result of expected glaciations and earthquakes, self-healing of the geological medium), and hydrogeological (e.g. changes in sea level and hydraulic gradients) evolution of the repository site (ANDRA, 2005c; Schwartz, 2018). The purpose of the altered evolution scenarios is to quantify if the long-term safety requirement is fulfilled in the accidental situations, e.g. simultaneous failure of multiple engineered barriers at the beginning of repository operation period or incorrect characterization of geology comprising fractures network (ANDRA, 2005c).

Simple numerical models limit influence of model complexity on the interpretation of reality and are appropriate at the initial modeling phases (ANDRA, 2005c) while in the later phases, the complexity of the models, and included parameters, increase (IAEA, 2011). For instance, the modeling of the hydrogeological conditions in the regions selected for geological disposal of radioactive waste in Swiss claystone was based on relatively simple regional models consisting of 13 layers (Luo et al., 2013) to more complex local models considering alternative

geologies and variations in parameters distribution (Luo et al., 2014a, b). The far field models (covering a part of the regional area) for transport of nuclides from repositories in the crystalline basement rocks in Sweden were developed from simplified models considering host rock formation into complex models comprising retention models for backfill tunnels and overlying sedimentary rocks as well as various combinations of hydraulic parameters (Follin et al., 2008; Selroos and Painter, 2012).

Research of the site for geological disposal of radioactive waste in Denmark is in its initial phase, and therefore the present work has focused on setting up simple and conceptual numerical models for assessment of the potential host rock formations and identification of feasible formations for further detailed investigations. Specific modeling objectives of the initial phase are described in Sections 4 and 5.

2.2 Modeling approach

Reactive transport models for geological repositories of the radioactive waste should be developed in an iterative process consisting of investigation and data collection stages alternating with modeling stages until a desired level of confidence in understanding the flow and transport processes of the modeled systems is achieved (Ström et al., 2008) and Figure 1. The confidence level acquired in the modeling studies must ensure that repository safety requirements and performance criteria are fulfilled (Ström et al., 2008; IAEA, 2011).

Uncertainties concerning safety should be assessed quantitatively and qualitatively (IAEA, 2011). The sources of the uncertainty in the reactive transport modeling are those related to the ability of representation of the real system (input data, parameter values and modeling assumptions) and unpredictability of the evolution of the repository and its environment over long time spans (IAEA, 2011). It is important to address uncertainties throughout the entire modeling process, starting at the initial modeling phases (ANDRA, 2005b), and to estimate the influence of the specific parameters on the safety performance of the repository site (Ström et al., 2008). If variations in a parameter have a minor influence on the safety assessment of the geological disposal of the radioactive waste, the acquisition of detailed data and complete understanding of that parameter at the site are not required (Ström et al., 2008). Preliminary models, based on the existing data serve only as a guide to the future studies (Ström et al., 2008). Thus, the basic uncertainty analysis identifying the critical parameters is needed in the initial modeling phase. In the later modeling phases, uncertainty of the data related to critical parameters used in modeling should be reduced (IAEA, 2011) by further data acquisition, alternative conceptualization of the system and consistency checks between the data and different models (Ström et al., 2008). For instance, extensive modeling studies were conducted for flow and transport in fractured granite in Finland, from a regional scale to the near field scale, to understand and reduce uncertainty connected to the interpretation of the tests conducted in open boreholes and conceptualization of these boreholes in flow and transport models. In the initial phase, the focus was on understanding the major and minor features of the groundwater system based on the hydraulic head measurements, while further tasks aimed at reducing model uncertainty by acquisition and implementation of additional data sets, e.g. measured flows in the crystalline basement rocks, in the models (Vidstrand et al., 2015; Sawada et al., 2015).

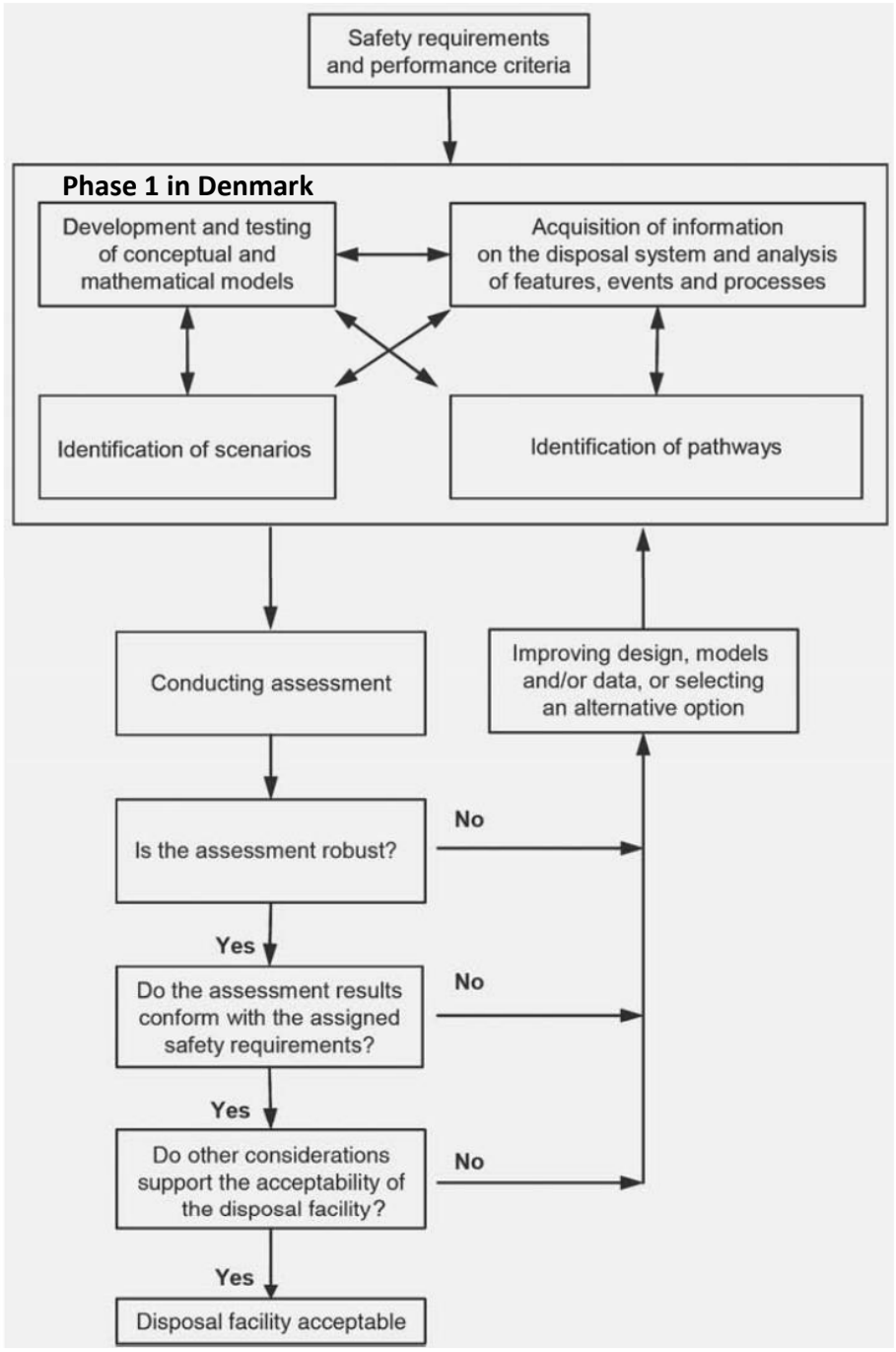

Figure 1. *Example of the iterative approach to the safety assessment (IAEA, 2011).*

Figur 1. *Eksempel på den iterative metodik for sikkerhedsvurdering (IAEA, 2011).*

It is common practice that uncertainty and confidence in the model input data are assessed continuously combining manual evaluation, expert assistance and reviews and mathematical modeling (Follin et al., 2008; Sawada et al., 2015). Multi-disciplinary input data for the models (geology, rock mechanics, thermal properties, hydrogeology, hydrogeochemistry, transport

properties) are checked for consistency (Figure 2) and adapted and simplified to the modeling purposes (Ström et al., 2008). All sources of the uncertainty are noted during the iterative process: accuracy of the measurements, data understanding, deficiencies, exclusion and biases and uncertainties related to the modeling approach. The uncertainties, if important for the safety analysis of the repository performance, are addressed by additional data collection or alternative modeling scenarios, including alternative geometries or parametrization of the model domains (Ström et al., 2008).

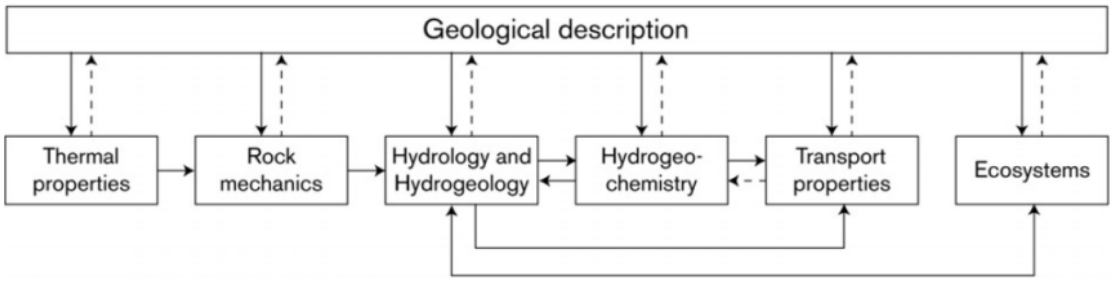

Figure 2. *Feedback loops between different discipline descriptions (Ström et al., 2008).*

Figur 2. *Indbyrdes afhængigheder for forskellige faglige beskrivelser (Ström et al., 2008).*

Sensitivity and uncertainty analyses are performed to achieve understanding of the behaviour of the system and governing parameters under the recent conditions and various site evolution scenarios and events (IAEA, 2011). To ensure the high level of confidence, developed models should be supported by laboratory and in-situ experiments (De Windt and Spycher, 2019) as well as paleo-hydrogeological studies (IAEA, 2011).

Sawada et al. (2005) presented influence of the uncertainties on the results of groundwater flow simulations at the regional scale of geological repositories of radioactive waste. They set up five independent conceptual groundwater flow and transport models for a fractured granitic rock in Japan using the same data set obtained during the investigation phase and different modeling codes. Uncertainties in the parameters and processes resulted in differences in the travel time up to several orders of magnitude, and travel lengths differences in the modeled area within a factor of 3, and thus huge variations in predicted discharge areas for a given particle (Sawada et al., 2005), Figure 3. The major sources of discrepancies were the effective porosity, definition of the boundary conditions and conceptualization of the major fault zones (Sawada et al., 2005).

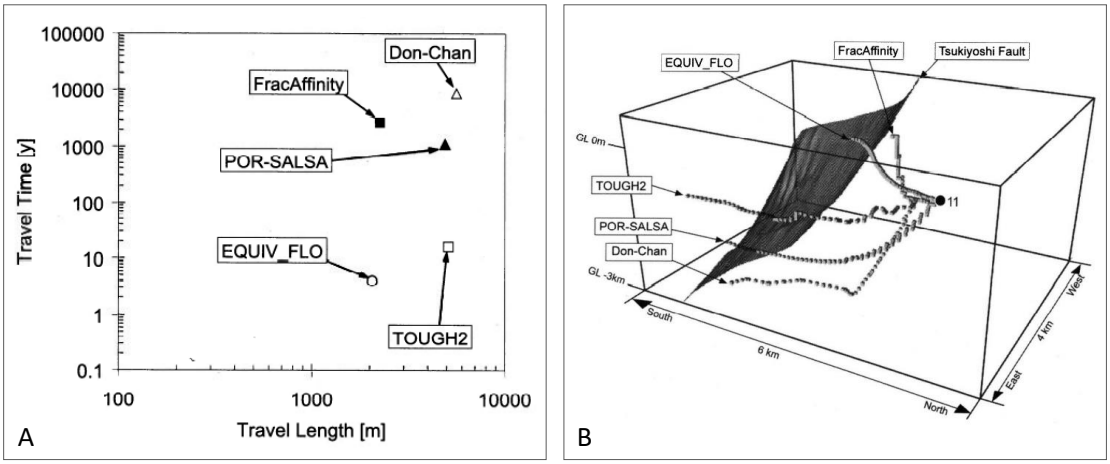

Figure 3. *Influence of the uncertainty in parameters and processes on the modeling results. A. Particle travel time from the same starting point (shown in panel B as point 11) obtained using different modeling codes. The names in the boxes depict the applied modeling code. B. Simulated groundwater travel paths from the starting point 11 using different modeling codes (Sawada et al., 2005).*

Figur 3. *Påvirkning af parameter- og procesusikkerheder på modelleringsresultater.*
A. Simulerede partikelopholdstider fra samme startlokalitet (vist i figur B som punkt 11) ved brug af forskellige modelleringskoder.
B. Simulerede partikelbaner i grundvandet fra startlokalitet punkt 11 ved brug af forskellige modelleringskoder (Sawada et al., 2005).

2.3 Modeling levels and time scales

The models used to simulate geological disposal of radioactive waste include a complex set of thermal, hydrogeological, mechanical and geochemical processes on a time scale of hundreds of thousands of years (De Windt and Spycher, 2019). They consist of regional, far field and near field sub-models where regional models describe large scale recharge and discharge areas and flow patterns, far field models are located in specific areas of the regional models and simulate nuclides transport from the repository to the biosphere, and near field models comprise detailed engineered construction of the repository and assess the safety performance of the basic canister and tunnel design (Luo et al., 2013, 2014a; De Windt and Spycher, 2019), Figure 4.

Regional models comprise major geological formations and regional fractures and mainly simulate flow and advective transport. Their horizontal and vertical extent allows predicting the regional flow patterns and obtaining knowledge about regional discharge and recharge areas. Output from the regional models provides groundwater flow data and locations of the recharge and discharge areas for the far field models (Luo et al., 2013, 2014a, b).

The far field models estimate the potential of the host rock formation to delay transport and release of nuclides and radiation into the biosphere in case of leakage from a system of engineered barriers (Selroos and Painter, 2012; Schwartz, 2018; De Windt and Spycher,

2019). They also estimate an influence of the repository construction on the groundwater resources and exploitation of thermal and mineral waters (Luo et al., 2013). The far field models characterize groundwater flow and nuclides transport processes in complex systems with often multiple hydraulic domains, pressure, salinity and temperature gradients, two-phase flow (gas and fluid or fluid and ice), and time varying boundary conditions, i.e. changes in aquifer recharge, sea level, salinity and atmospheric/ice pressure at the top surface (Vidstrand et al., 2014). The major hydraulic domain considered in the far field models is fractured or unfractured host rock formation, although the engineered and soil domains may also be considered. Introduction of for instance backfilled tunnels into the far field models of crystalline basement rocks results in reduction of the dose of non-sorbing nuclides (Selroos and Painter, 2012). The far field models cover time spans of up to 2 Myr (Schwartz, 2012, 2018), representing the lifetime of actinides. Geological information in the far field models is more detailed than in the regional models and includes local aquifers (Luo et al., 2013, 2014a) and networks of regional and local fractures as well as deformation zones generated during the construction of a repository (Follin et al., 2008). Flow and transport simulations are based on the complex sets of parameters allowing for simulation of advection, dispersion, diffusion and reactive transport of nuclides from a deep subsurface to the biosphere (Selroos and Painter, 2012; Trinchero and Iraola, 2020). Groundwater flow predicted in the far field models is used as input data for the near field models (Selroos and Painter, 2012).

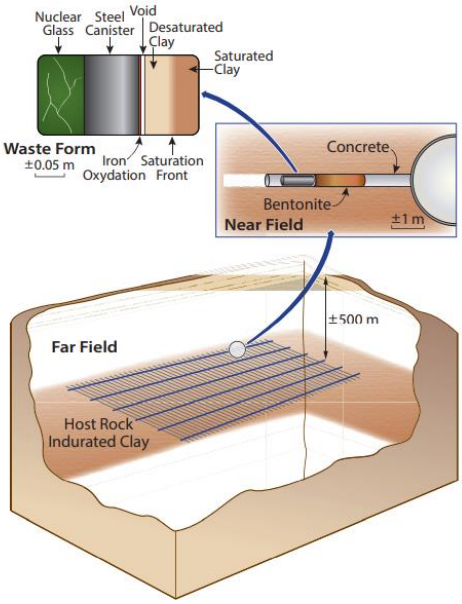

Figure 4. *Illustration of the scale related to far field and near field models (De Windt and Spycher, 2019).*

Figur 4. *Illustration af skala relateret til fjernområde- og nærområde modeller (De Windt and Spycher, 2019).*

Near field models estimate the effectiveness of engineered multiple barrier systems in preventing release of nuclides from the repository (Lim, 2006; Brommundt et al., 2014). These models are often called THMC models, as they simulate different thermal (T), hydrogeological (H), mechanical (M), and chemical (C) processes on a scale of a radioactive waste repository. These processes include container corrosion, canister failure caused by earthquakes (Selroos and Painter, 2012) or production defects (Schwartz, 2018), production and release of gases in the engineered barriers and from the waste (Enssle et al., 2014), and changes in the engineered and geological barriers as a result of, e.g. release of heat from the waste or changes in saturation of the host rock after closing of the repository (De Windt and Spycher, 2019). The near field models are run for a predicted lifetime of a repository and simulate processes occurring on the time scale of thousands of years (De Windt and Spycher, 2019). The near field models, including engineered solutions, are typically provided by the waste and repository owner, and their output is used in the far field transport models (Selroos and Painter, 2012).

2.4 Flow and nuclides transport – governing equations

Nuclides are transported in liquid and/or gaseous phases either with advection or diffusion as the major transport process through the porous rock matrix and complex fracture systems. Advection is a bulk motion of the substance with the flowing fluid. Diffusion is the random movement of chemical components and gaseous phases leading to transport from the areas of high concentration to areas of low concentration.

Flow of fluid through a porous medium is described by Darcy's law (e.g. Zheng and Bennett, 2002):

$$\mathrm{q} = \frac{Q}{A} = -\mathrm{K}\frac{\mathrm{dH}}{\mathrm{dL}} \qquad \text{(Equation 1)}$$

where q is a Darcy velocity, Q is volumetric flow rate through an area (A), K is hydraulic conductivity and dH is the change in hydraulic head along the distance (dL), i.e. dH/dL is the hydraulic gradient.

Hydraulic conductivity (K) and permeability (k) describe the ability of the host rock formations and overlying sediments to transmit water. Permeability is a property of a solid material itself, while hydraulic conductivity is additionally dependent on fluid viscosity and density. Hydraulic conductivity and permeability are related according to the equation (e.g. Zheng and Bennett, 2002):

$$\mathrm{k} = \frac{\mathrm{K}\mu}{\delta \mathrm{g}} \qquad \text{(Equation 2)}$$

where μ and δ are fluid viscosity and fluid density (both being temperature dependent), and g is the gravitational constant.

Darcy's equation can be developed further to describe multiphase flow (e.g. Muskat and Meres, 1936):

$$q_\beta = -\mu_\beta^{-1} k_{r\beta} k(\nabla P_\beta - \delta_\beta \times g) \quad \text{(Equation 3)}$$

where q_β is Darcy velocity of a phase β, either liquid or gas, with given dynamic viscosity (μ_β) and mass density (δ_β), k is the absolute permeability, $k_{r\beta}$ is the relative permeability to a phase β, ∇P_β is the pressure gradient, and g is the gravitational constant.

While hydraulic conductivity (K) represents the rate of flow of water with given viscosity and density in a unit of cross-sectional area, transmissivity (T) is the rate at which water flows over the whole saturated thickness of the aquifer (b) under a unit hydraulic gradient, (Fetter, 2001):

$$T = Kb \quad \text{(Equation 4)}$$

The transport of nuclides is governed by the advection-dispersion equation (e.g. Zheng and Bennett, 2002):

$$\frac{dc}{dt} = -v\frac{dc}{dx} + D_L\frac{d^2c}{dx^2} - \frac{dq}{dt} \quad \text{(Equation 5)}$$

$$D_L = D_e + \alpha_L v \quad \text{(Equation 5a)}$$

where: c is the solute concentration in water, t is time, v is the pore water flow velocity, x is distance, q is the solute concentration in the solid phase, D_L is the hydrodynamic dispersion coefficient, D_e is the effective diffusion coefficient, and α_L the dispersivity.

The diffusive transport rate depends on the concentration difference and effective diffusivity, and is described by the equation (e.g. Zheng and Bennett, 2002):

$$F = -D_e\frac{dc}{dx} \quad \text{(Equation 6)}$$

where: F is the diffusive mass flux, D_e is the effective diffusion coefficient, c is the solute concentration in water and x is distance.

The dominant transport process in nuclides transport models is specified by a numerical parameter called the Peclet number. The Peclet number (P_e) is the ratio of advective transport (T_c) to diffusive transport (T_d) (e.g. Zheng and Bennett, 2002):

$$P_e = \frac{T_c}{T_d} \quad \text{(Equation 7)}$$

Advective transport is dominant in the models with $P_e \rightarrow \infty$ (e.g. Zheng and Bennett, 2002). E.g. diffusive transport was dominating for the P_e values <0.3 and an advection dominant regime had P_e values >300 in the near field models described by Lim (2006).

2.5 Model conceptualization – flow modelling

Flow velocity of liquid and gaseous phases and related contaminants transport are governed by boundary and initial conditions in the model domain (Section 2.5.1) and by hydraulic properties of the host rock formations (Section 2.5.2). The governing variables at the boundary conditions are hydraulic head (Equation 1), pressure (Equation 3), salinity (density) and temperature gradients (Equations 2 and 3). Hydraulic head and pressure differences initiate gradient driven advective flow while salinity (density), and temperature changes influence viscosity and density driven flow. The major hydraulic properties governing the flow velocity are a group of groundwater conductance parameters comprising hydraulic conductivity, permeability, transmissivity (Equations 1–4), and porosity.

2.5.1 Boundary and initial conditions

Hydraulic head, pressure, salinity (density) and temperature gradients govern advective contaminant transport in the reactive transport modeling for radioactive waste repositories (Equations 1–3). The section summarizes practices in assignment of the initial and boundary conditions in models for radioactive waste repositories and shows the implications of variations in the boundary conditions on the output of transport models.

The boundary conditions are often set as Dirichlet boundary conditions, i.e. specified hydraulic head, pressure, salinity and temperature (Sawada et al., 2005; Luo et al., 2014a, b; Schwartz, 2018). These boundary conditions are applied at the horizontal surfaces comprising top and bottom of the model domain and at the vertical surfaces representing the lateral model boundaries (e.g. Brommundt et al., 2014; Vidstrand et al., 2014; Schwartz, 2018). Values of the boundary conditions assigned at the bottom of the model domain depend on the domain depth, the depth of the constructed repository and type of host rock formation. Model boundaries at each modeling level, regional, far field and near field, are set in a distance from the model volume representing the repository in order to reduce the boundary effects on the flow patterns in the repository and its proximity (Brommundt et al., 2014; Vidstrand et al., 2014). E.g. fixed conditions assigned to the boundaries of the far field model should have limited control on hydraulic heads and flow paths at the repository location.

Modeling studies for radioactive waste repositories use a nested modeling approach, in which the near field models are cut out from the far field models and the far field models are subtracted from the regional models. In the nested modeling approach, geological and hydrogeological conditions set at each of the modeling levels are transferred without changes to the more detailed models, e.g. thickness of the geological layers and the geological structure at the given location does not change between the regional, far field and near field models (Luo et al., 2013). The consistency in the hydrogeological conditions enables the possibility of transfer of e.g. hydraulic heads simulated in the regional model into boundary conditions of the far field model. The conditions (e.g. specified head, salinity) predicted by the regional model at the borders of the far field model are assigned to the boundary conditions of the far field model. Likewise, the boundary conditions for the near field model are extracted from the results of the far field simulation (Luo et al., 2014a, b).

2.5.1.1 Regional and far field models

Flow of fluids is governed by hydraulic gradients (Equation 1). Hydraulic heads at the upper boundary of regional and far field models are set either as a fixed head at the measured or predicted groundwater levels (Schwartz, 2012, 2018; Luo et al., 2014b) or correlated to the terrain surface (ANDRA, 2005c; Sawada et al., 2005). In the latter case, the upper boundary is modeled as an outflow boundary with drainage to the surface when calculated hydraulic heads exceed terrain surface and recharge of the host rock formations when the difference between hydraulic heads and terrain surface is negative (ANDRA, 2005c). The hydraulic heads are maintained by the recharge assigned to the upper model boundary (Sawada et al., 2005; Luo et al., 2014a, b; Vidstrand et al., 2014). The recharge values are set either at steady-state throughout the simulation period (Sawada et al., 2005) or have transient values, e.g. for the glacial and periglacial periods (Vidstrand et al., 2014) and sea level changes (Schwartz, 2018). Regional surface water bodies (rivers, lakes, sea) are modeled as fixed hydraulic heads (Sawada et al., 2005). Hydraulic conditions in the basic models simulating long time periods (up to 1 Myr) are often described as steady-state (ANDRA, 2005c; Luo et al., 2014b; Schwartz, 2018).

Sensitivity of the safety performance of the repository to changes in hydraulic heads caused by, e.g. changing the sea level and increasing erosion rates is checked by simulation of various hydraulic gradients in the base case geological setting (Schwartz, 2012, 2018). These sensitivity analyses are carried out by increasing/decreasing of hydraulic gradients in the modeled domains (Schwartz, 2012, 2018) which influence the location of the groundwater discharge zones. Vidstrand et al. (2014) showed that the discharge locations of nuclides leaking from a repository in crystalline basement rocks were farther away from the repository area at lower sea levels than during the recent sea stage. Furthermore, during periglacial periods the discharge sites closed completely because of a decreasing impact of the hydraulic gradient and significantly lowered flux rates at the location of the repository. Small groundwater fluxes were also modeled for a completely submerged site (Vidstrand et al., 2014). On the other hand, transient water-level conditions in a basalt only had small effects on the peak radioactive doses which increased only by a factor of 3 at discharge sites (Schwartz, 2018).

Bottom model boundaries of the regional and far field models are often assumed to be at the depths of a couple of thousands of meters and thus set as no flow boundaries, e.g. for the repositories in French (ANDRA, 2005c), Swedish (Vidstrand et al., 2014), and Japanese (Sawada et al., 2005) granite massifs or in Swiss claystone (Luo et al., 2014a, b). Horizontal hydraulic gradients in the deep subsurface are low (Schwartz, 2018) and here vertical flow may be the dominant flow direction (ANDRA, 2005b). However, vertical boundary conditions are usually set as no flow boundaries at drainage divides of the shallower aquifers and at the crest lines and fault zones acting as aquitards (ANDRA, 2005c; Sawada et al., 2005; Follin et al., 2008; Schwartz, 2012, 2018).

Occurrence of no-flow conditions at the outer model boundaries can be disturbed by regional fracture structures enabling flow beyond the defined boundary condition. For instance, in the crystalline basement rocks in Sweden, the particle discharge locations in the recent conditions were controlled by outcropping of the regional fractures (Vidstrand et al., 2014). Fractured deformation zones were also a major location for recharge of the glacial meltwater into

the aquifer (Vidstrand et al., 2014). Different hydraulic properties used for the regional fracture zone in the granite massif in Japan resulted in a variation of the particle travel times by several orders of magnitude (Sawada et al., 2005), Figure 3. Thus, a good understanding of the regional tectonic structures is needed when deciding on the reactive transport model boundaries (Luo et al., 2014a; Schwartz, 2018).

Pressure at the upper boundary, under normal conditions, i.e. no glaciations, is at a steady-state and equals that of the atmosphere (0.1 MPa) or has values following the recent day topography and bathymetry (Schwartz, 2012, 2018; Vidstrand et al., 2014). In the simulations of glacial conditions, a transient pressure beneath the ice sheet is set at the top model boundary (Vidstrand et al., 2014). In these cases, the gaseous phase is neglected, and the modeled phases are liquid and frozen fluid (Vidstrand et al., 2014).

The influence of changing recharge and pressure conditions at the upper model boundary on groundwater fluxes at the repository depth is presented in Figure 5. Groundwater discharge during the ice sheet transgression (upward Darcy fluxes) is controlled by the specified head at the ice sheet front location and the outcropping deformation zones (Figure 5c, e). The Darcy flux in a case when the ice sheet margin is located above the repository is two orders of magnitude higher than in a case when the ice sheet margin advances further than the repository location (Figure 5c, d, e, f). The ice sheet advance over the unfrozen ground has the greatest influence on the groundwater discharge (Figure 5e) while the permafrost conditions are reducing the groundwater fluxes (Figure 5b, c). Groundwater flux at the periglacial conditions (Figure 5b) is significantly reduced compared to the temperate conditions (Figure 5a) and the downward flux direction is dominant.

Pressure at the bottom boundary of the regional and far field models is either allowed to be flexibly adjusted, especially if the conditions at the repository depth are not well known (Schwartz, 2018) or is set at a measured value (Brommundt et al., 2014). Pressure in the initial models comprising single-phase flow is often set at a steady-state (Schwartz, 2018). At the subsequent, more advanced modeling stages two-phase flow (gas and liquid) is introduced, and transient changes in the pressure field distribution are enabled (Schwartz, 2018), except of the cases where the quantity of the released gaseous phase can be neglected (i.e. ANDRA, 2005c). Two-phase transport models are usually run for a shorter time period, on a scale of thousands of years (Schwartz, 2012).

The upper model boundary often has zero salinity and a temperature corresponding to the average yearly air temperature at the studied site (Schwartz, 2018). Temperature distribution in the remaining part of 3D model domains is site specific and either homogeneous even up to 1000 meters depth (Sawada et al., 2015) or heterogeneous and increasing with depth (Schwartz, 2018). E.g. temperature in the model of the granite site in Sweden increases by 0.01 °C/m over a depth of 1200 meters (Joyce et al., 2014).

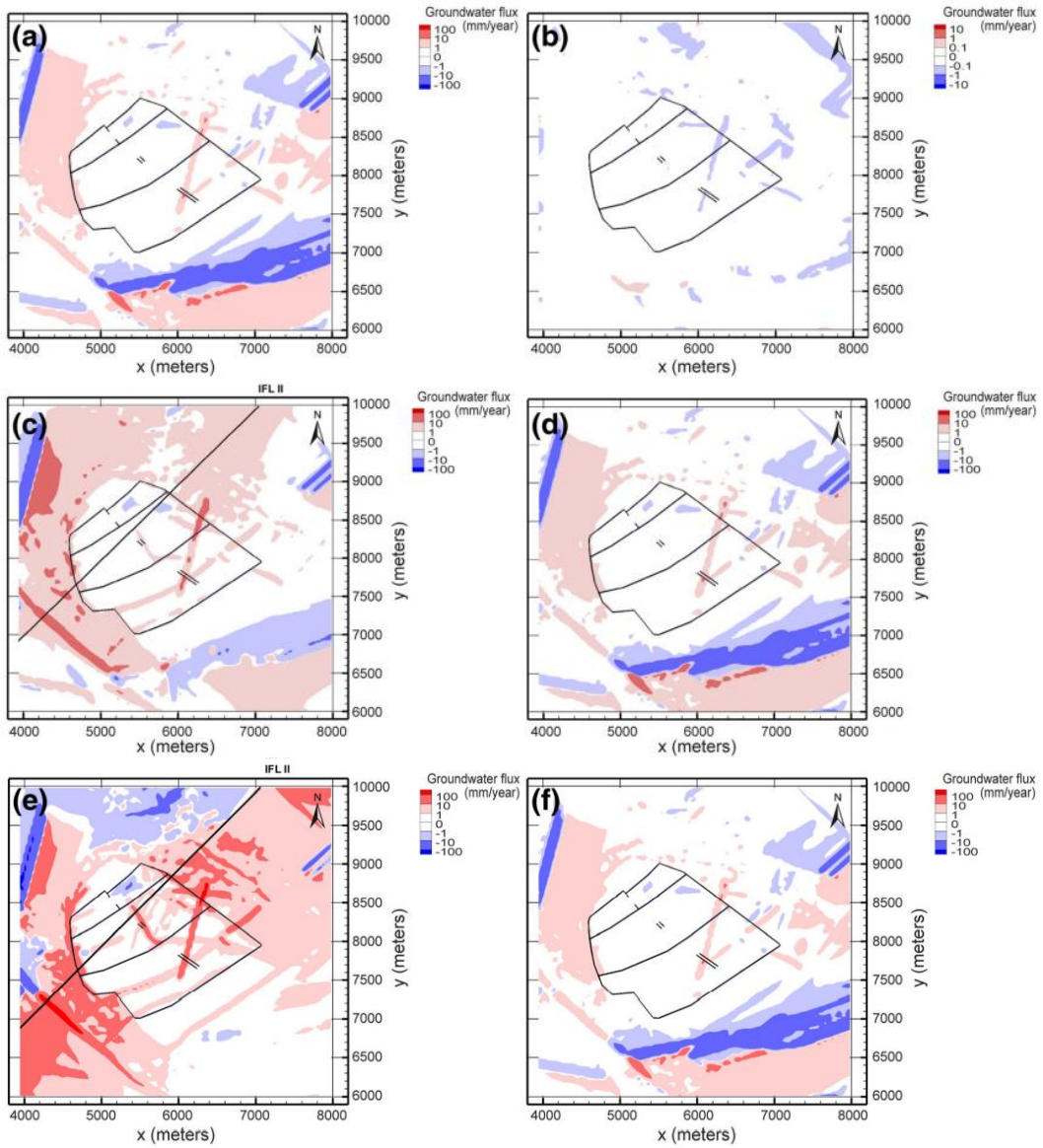

Figure 5. *Vertical Darcy flux at the repository depth in a crystalline basement rock, Sweden, in various climate conditions: (a) temperate, (b) periglacial, (c, d) ice sheet advance over permafrost with the ice sheet front location (IFL II) at the repository site (c) and south-east from the repository site (d), (e, f) ice sheet advance over unfrozen ground with the ice sheet front location (IFL II) at the repository site (e) and south-east from the repository site (f). Repository area is marked with the black lines (Vidstrand et al., 2014).*

Figur 5. *Vertikal Darcy flux ved et slutdepots dybde i krystallinske bjergarter i Sverige simuleret ved forskellige klimatiske forhold: (a) tempereret, (b) periglacialt, (c, d) isfremstød over permafrost med isfremstødets front (IFL II) ved depotets lokalitet (c) og syd-øst for depotets lokalitet (d), (e, f) isfremstød over ikke-frossen jord med isfremstødets front (IFL II) ved depotets lokalitet (e) og syd-øst for depotets lokalitet (f), (Vidstrand et al., 2014).*

At the initial phase, 3D models are commonly run assuming a freshwater environment in the entire model domain (ANDRA, 2005b, c; Luo et al., 2014a, b). Occurrence of salinity gradients is not considered in e.g. model scenarios of French granite, where salinity is regarded to be much lower than in the coastal settings in Sweden and Finland (ANDRA, 2005c). In the following phases, as additional data are collected, density flow is introduced by adding brine fractions to the liquid phase or assigning the observed water salinity (Schwartz, 2012; 2018; Vidstrand et al., 2014) and introducing brine diffusivity (Schwartz, 2012, 2018). Salinity at the bottom boundary is often held constant throughout the simulation time (Schwartz, 2012, 2018; Vidstrand et al., 2014). The fixed salinity value at the model bottom influences simulated evolution of the salinity and groundwater flux at the repository depth (Vidstrand et al., 2014). Thus, the models with density driven flow can be initialized in two stages. First a model with zero salinity in the entire domain is run. In the second step salinity gradients are introduced and diffusivity of salt is calibrated to match the observed conditions (Schwartz, 2012).

It is important to ensure that discretization of the models at steady-state conditions allows to maintain the present, measured pressure, temperature and salinity gradients throughout the entire simulation time of even up to 1 Myr (Schwartz, 2012, 2018). In cases when some of the conditions are transient over time, the size of the cells at the bottom model boundary should be adjusted to i.e. maintain the constant salinity throughout the simulation time, and to allow to account for changes in the pressure occurring due to the release of a gaseous phase during the repository operation (Schwartz, 2012).

2.5.1.2 Near field models

Boundary and initial conditions in the near field models are site specific at the local scale and depend on the repository design. As the Danish repository design is not known at the moment, a detailed review of the boundary and initial conditions in the near field models is not relevant for the recent research stage. A short example of the influence of the repository design on the nuclides transport in the near field models is shown in Figure 6. The transport of nuclides in the near field model of the repository in the unfractured granite massif in Japan was strongly influenced by the direction of the hydraulic gradient and changed by application of different boundary conditions. Variations in the flow directions through the engineered barriers resulted in changes of the residence time on one order of magnitude (Figure 6, Lim, 2006).

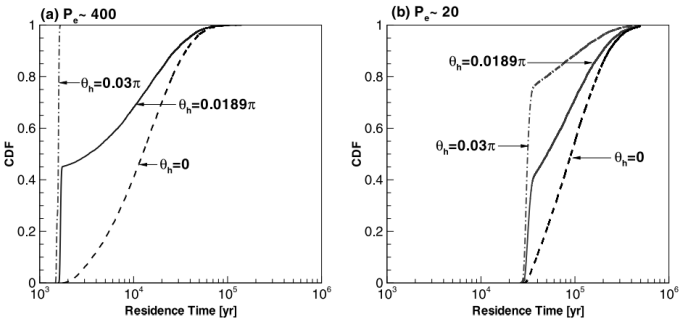

Figure 6. *Influence of the changes in the flow direction in radians (θh) through the engineered barriers of the radioactive waste repository on the residence time of Cs-135 in the system dominated by advective (a) and advective-diffusive (b) transport. Pe is a Peclet number (see Equation 7), and CDF is a Cumulative Distribution Function (Lim, 2006).*

Figur 6. *Påvirkning af ændringer i strømningsretningen i radianer (θh) gennem de konstruerede barrierer for det radioaktive depot i forhold til opholdstiden for Cs-135 i et system domineret af advektiv (a) og advektiv-diffusiv (b) transport. Pe er Peclet tallet (se Ligning 7), og CDF er den kumulative fordelingsfunktion (Lim, 2006).*

2.5.2 Geology and hydrogeological properties

For disposal sites located in crystalline basement rocks, Follin et al. (2008) suggested groundwater flow from the deep subsurface to the discharge areas to occur through three hydrogeological domains: hydraulic rock mass domains, hydraulic conductor domains and hydraulic soil domains. Hydraulic rock mass domains are low (or non-) permeable, unfractured or slightly fractured rock matrixes where flow by advection is limited. Hydraulic conductor domains consist of preferential flow paths, i.e. fracture networks or fractured deformation zones created during construction of the radioactive waste repository, where advective flow of liquid and gas phases is significant. Hydraulic soil domains are porous, unconsolidated sediments above host rock formation and other consolidated formations (Follin et al., 2008). The classification may also be applied to other formations such as chalk and claystone. Geometry and hydraulic properties of the rock mass domains and conductor domains govern advective transport of nuclides through the host rock formation. Soil domains are usually less important in the models of the deep subsurface flow, although they may influence the results of reactive transport modeling of nuclides (Selroos and Painter, 2012).

On the regional and far field scale, flow patterns are highly influenced by layer distribution, thickness and occurrence of regional folds and fractures. In a pre-feasibility modeling study of granite for the geological disposal of radioactive waste, ANDRA (2005c) tested the influence of three morpho-structural configurations of the French granite massifs on the travel time from the repository located at 500 meters depth to the discharge sites at the surface. The modeled settings were: (1) granite massif with an upper boundary layer in the form of an inclined plane covered by overlying deposits with varying surface topography, (2) granite massif with an upper layer boundary in the form of a dome covered by overlying deposits with varying surface topography and (3) granite massif with an upper layer boundary in the form of a depression and overlying deposits with a flat topographical surface. The differences

in geology between the models led to changes in the modeled hydraulic gradients. Simulation results showed that groundwater travels the longest distance before discharging at the surface outlets in the dome structure while in the depression setting the travelled distances are the shortest (ANDRA, 2005c). For non-fractured, low permeable host rock formations an important geometrical feature is layer thickness. A sensitivity study in the 130 meters thick Callovo-Oxfordian claystone layer in France showed that increasing of the claystone thickness by 10 meters on both sides of the repository of radioactive waste would reduce flow velocities by approximately 33% compared to the base case scenario. The longer travel time leaves more time for the decay of nuclides, thus the mass of I-129 exiting the host layer was reduced by 25% and outflow of Cl-36 by 100% (ANDRA, 2005b).

In the modeling study of Opallinus clay as host rock formation in four regions of Switzerland, Luo et al. (2013, 2014a, b) stress the importance of implementation of relevant regional faults in the groundwater flow models since they can have a large effect on the overall flow directions in the local aquifers depending on the hydraulic parameters of the tectonic structures (connecting or isolating fractures). Sensitivity analysis on the regional faults in Switzerland showed that variations in the fractures transmissivity (no flow, low and high transmissivity) resulted in the shift of groundwater discharge areas from the local rivers to locations outside of the model domain (Luo et al., 2014a, b). Fractures are highly conductive, forming preferential flow and transport paths and thus, crucial to address in modeling studies from regional to the near field scale. Fractures in the host rock formation can be divided into fractures generated by tectonic activity and fractures created during the repository construction, so called deformation zones, or excavation damaged zones. The scale of the deformation zones depends on rock mechanics and excavation methods.

Groundwater velocity and flow patterns are controlled by hydraulic parameters: porosity, hydraulic conductivity/transmissivity (or permeability), Equations 1–4. A relationship between the horizontal and vertical values of the hydraulic parameters is represented by an anisotropy ratio that is e.g. a ratio of horizontal hydraulic conductivity (K_h) to vertical hydraulic conductivity (K_v).

Porosity is the fraction of the host rock formation where the pore space between grains is filled with liquid and/or gas phase. The part of the porosity where the transport of liquid and gas phases takes place is called effective porosity. Effective porosity in the models with unfractured rock matrix separated from the fracture networks is assigned independently to various hydraulic domains. The unfractured rock matrix has often an effective porosity one or two orders of magnitude lower than the hydraulic conductor domains, i.e. fractures, interbeds of high permeable deposits (Schwartz, 2018; Trinchero and Iraola, 2020). Effective porosity in the models comprising continuous porous media is calculated by combining effective porosities of fracture networks and unfractured rock matrix (Hadgu et al., 2017; Appendix A). Sedimentary rocks, e.g. claystone, have much higher porosity than unfractured crystalline basement rocks because of the presence of pore space between the clay minerals in the rock. Limited knowledge about the effective porosity may be a source of large uncertainty in the simulation results, for instance porosity used in five conceptual models set up independently for a granite massif in Japan varied by three orders of magnitude resulting in the variation of travel times of the same particle from several years to several thousand years (Sawada et al., 2005). However, such large differences in porosity only occur between highly fractured rock and very low porosity rocks such as crystalline basement rocks. For the Danish

subsurface, matrix porosities can be fairly well determined within the same order of magnitude.

The matrix of claystone and unfractured crystalline basement rocks are characterized by low permeability/hydraulic conductivity compared to the fractured zones and e.g. sandy interbeds, and consequently slower advective transport of nuclides (ANDRA, 2005b; Schwartz, 2018; Trinchero and Iraola, 2020). In the fractured deposits, e.g. crystalline basement rocks, the transport of solutes takes place in a two-dimensional system which can be divided into two one-dimensional problems, transport along the fracture and into/out of the matrix (Trinchero and Iraola, 2020). Low transmissivity of the fractures in the host rock formation can significantly delay the transport of nuclides to the surface. The estimated travel time of I-129 in the granite massifs of France varied from hundred thousand years to several hundred thousand years, depending on the fracture transmissivity (ANDRA, 2005c).

Porosity, permeability, hydraulic conductivity and transmissivity increase in deformation zones created during the repository construction (Lim, 2006; Enssle et al., 2014). Mineral precipitation/dissolution and clay swelling can also affect hydraulic parameters. Highly alkaline waters seeping through biomicrite clay at Maqarin, Jordan caused precipitation of cement-like phases sealing fractures (Steefel and Lichtner, 1998). Fractures in granite massifs of France and Japan are sealed with minerals of hydrothermal origin (ANDRA, 2005c; Yoshida et al., 2013). At Yucca Mountain, Nevada, USA reactive transport modeling supported by laboratory experiments showed that porosity and permeability in volcanic tuffs were decreased by precipitation of calcite from the infiltrating water (Spycher et al., 2003). Host rock formation properties may also be changed by temperature changes. Thus, thermal parameters of the host rock formation comprising thermal conductivity, specific heat capacity and temperature are additional governing factor in, e.g. modeling of repositories of HLW emitting heat (Verma et al., 2015; Johnson et al., 2019), or where evolution of a repository in glacial and periglacial periods is modeled (Vidstrand et al., 2014). However, the thermal parameters are not of importance at the recent phase for the Danish settings, since the Danish radioactive waste is non-heat emitting intermediate level radioactive waste and the recent modeling studies are in the initial modeling phase.

The hydraulic parameters are commonly assigned to the model domain at the cell basis with a homogeneous parameter value within a cell (Sawada et al., 2005; Luo et al., 2014a; Schwartz et al., 2018). In the unfractured rocks, the assigned parameter value represents the hydraulic properties of the rock matrix. Parameter values assigned to the cells representing the fractured rocks are estimated by combining hydrogeological properties of the rock matrix and fractures. Regional fractures, if considered to be sufficiently thick, can also be inserted on a cell basis as areas with higher hydraulic conductivities (ANDRA, 2005c; Figure 7). The fractured host rock formations can also be modeled as channel networks, parametrizing only the networks of fractures or a combination of a channel fracture parametrization with parameters applied at the cell basis for the unconsolidated sedimentary rocks can be used (Sawada et al., 2005; Hadgu et al., 2017). Thus, fracture models are categorised into hydrogeological models as Discrete Fracture Networks (DFN), Equivalent Continuous Porous Media (ECPM), or/and Continuous Porous Media (CPM), e.g. ANDRA (2005c), Selroos and Painter (2012), and Hadgu et al. (2017), Appendix A. A common approach is to nest smaller DFN far field and near field models within larger CPM regional and far field models (Figure

8; ANDRA 2005c; Selroos and Painter, 2012). Testing of different ranges and distribution of the hydraulic parameters is commonly a part of sensitivity studies in flow and transport modeling (ANDRA, 2005c; Schwartz, 2012, 2018; Luo et al., 2014a; Trinchero and Iraola, 2020).

An important property of host rock formations to be considered during the model set up is heterogeneities in geometry and hydraulic properties of fracture networks and rock matrix. For instance, the Callovo-Oxfordian clay in France is a feasible host rock formation for a radioactive waste repository due to its homogeneous properties, i.e. lack of heterogeneities, and constant thickness of 130 meters over a regional scale (ANDRA, 2005b). In studies focusing on understanding the influence of boundary conditions on nuclides transport through the system of engineered and geological barriers, the host rock formation is often set as an unfractured homogeneous porous medium with the hydraulic conductivity equivalent to the combined hydraulic conductivity of the fractures and rock matrix in the considered rock volume (Lim, 2006). In the far field models, sensitivity analysis is often performed on the heterogeneous distribution of parameters (Luo et al., 2014a; Hadgu et al., 2017). Sensitivity analysis on hydraulic parameters in Swiss claystone and limestones settings showed that an increase of hydraulic conductivity in local aquifers may result in decrease of hydraulic heads in some of the aquifers even by 100 meters while heads in the neighbouring aquifers remain nearly unchanged (Luo et al., 2014a).

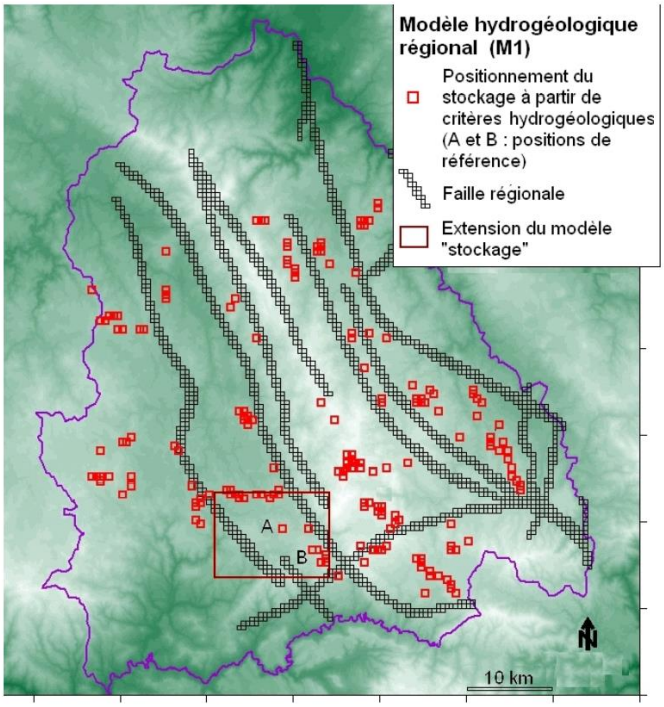

Figure 7. *Regional fractures in the hydrogeological model of French granite massif (ANDRA, 2005c).*

Figur 7. *Regionale sprækker i den hydrogeologiske model for fransk granit (ANDRA, 2005c).*

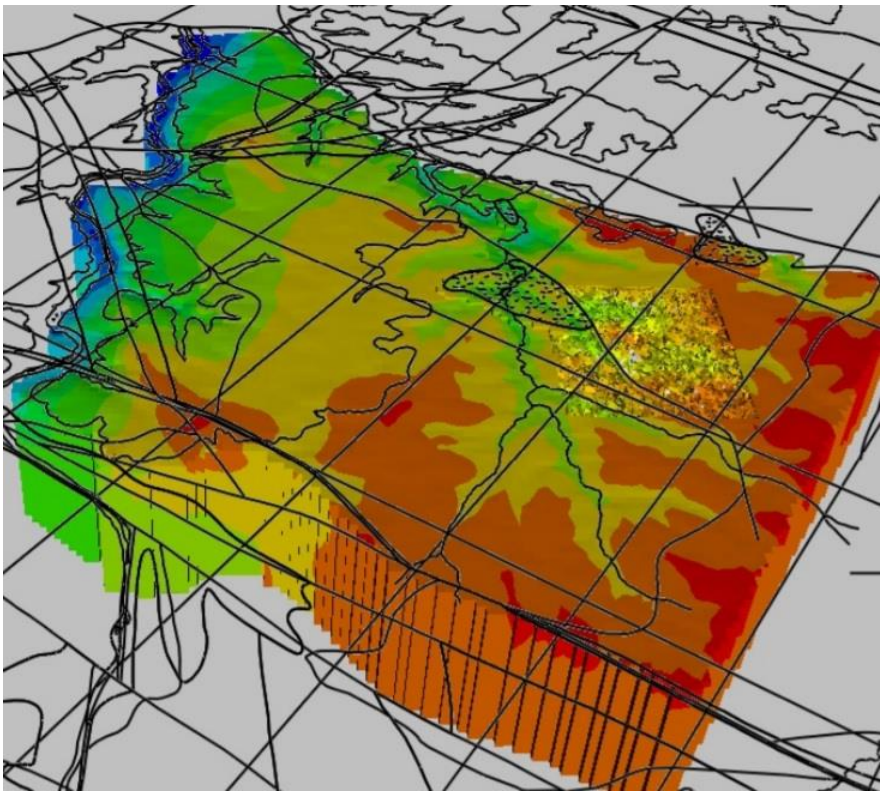

Figure 8. *Far field DFN model nested in the regional up-scaled CPM model of French granite massif (ANDRA, 2005c).*

Figur 8. *Fjernområde DFN model inden for en regionalt opskaleret CPM model af fransk granit (ANDRA, 2005c).*

Heterogeneity in the distribution of hydraulic properties is especially important in fractured media. Higher fracture intensity in the crystalline basement rocks is often found close to the surface (ANDRA, 2005c; Selroos and Follin, 2014). Transmissivity of the fractures in host rock formations is usually highly heterogeneous at each depth of the modeled areas and can vary up to orders of magnitude (Ström et al., 2008). Nevertheless, transmissivity in general decreases with depth (ANDRA, 2005c; Vidstrand et al., 2014). However, it is often observed that hydraulic properties decrease only to a certain depth, for instance, ANDRA (2005c) assumed decrease of hydraulic conductivity in French granite massifs to a depth of 350 meters. Similarly, the hydraulic conductivity of the granite massifs in Japan was two orders of magnitude higher in the uppermost 120 meters of the highly fractured domain compared to the remaining part of the massif (Sawada et al., 2005). The opposite effect is observed at the deformation zones created during the repository construction, where transmissivity and fracture aperture increases at greater depths. These changes result in a decrease of the transport resistance in the deformation zones (Selroos and Painter, 2012).

In addition to hydraulic properties, groundwater flow in the fracture network is also influenced by fracture connectivity, dipping, length, size of the unfractured matrix and surface wetness. Steeply dipping fractures are usually less conductive, for instance granite at the Forsmark site in Sweden was found to have low permeability at depths greater than the occurrence of a gently dipping fracture zone (Ström et al., 2008). Differences in geometric distribution and

connectivity of fractures in the French granite massifs resulted in an offset by a factor of 10 in maximum concentrations of nuclides discharging at the surface (ANDRA, 2005c).

At the early modeling phases, where details about fracture networks are unknown, an often used approach is to model only major fractures on a scale of hectometers to kilometers, and furthermore connectivity between the fractures is assumed. Sensitivity to characterization of average fracturing is tested by scenarios including different fracture distributions and expected ranges of values for the fracture parameters (ANDRA, 2005c).

Fracture distribution can be modeled in deterministic or stochastic approaches (ANDRA, 2005c; Sawada et al., 2005; Selroos and Follin, 2014; Hadgu et al., 2017). Models of regional fractures are often established in a deterministic fashion (ANDRA, 2005c; Sawada et al., 2005). In the feasibility study of French granite, ANDRA (2005c) set up deterministic models of regional fracturing (>300 meters length) based on geophysical data. The models consisted of thousands of fractures modeled in the form of ellipses. Fractures smaller than 50 to 300 meters in length, located in the near field of the repository were modeled in a stochastic form, based on the available data for the minor fracture distributions. The disadvantage of the stochastic model was that it was not possible to reproduce heterogeneities in the fracture density observed in certain sectors of the granite massifs (ANDRA, 2005c).

The second group of fractures, occurring next to the fracture network of natural origin is a fractured deformation zone created during the excavation of the repository. In crystalline basement rocks, this zone is assumed to have a thickness of less than 1 meter (ANDRA, 2005c). The deformation zones usually are modeled with hydraulic parameters orders of magnitudes higher than in the undisturbed rock (ANDRA, 2005c; Enssle et al., 2014).

Sedimentary rocks overlying the host rock formations are sometimes excluded from the flow and nuclides transport models for the geological disposal of the radioactive waste (Sawada et al., 2005). Nevertheless, in some settings the siliciclastic sediments overlying the host rock formation have a thickness of a couple of hundred meters (Schwartz, 2012). Advective transport of nuclides is often faster in the sedimentary rocks overlying the host rock formations as the often occurring siliciclastic sediments usually have higher porosity and permeability than the host rock formations (Schwartz, 2012). In two-phase modeling in siliciclastic sediments overlying the host rock formation, high permeability favoured the flow of liquid phase in comparison to the gas phase while a low permeability had an opposite effect (Schwartz, 2012). On the other hand, the dose modeled at the surface from adsorbing nuclides may be reduced due to sorption processes in the near-surface soils (Selroos and Painter, 2012). Thus, disregarding of the sedimentary, near surface rocks may lead to the pessimistic assessment of the performance of the repository site, although the final doses are not strongly attenuated (Selroos and Painter, 2012).

2.6 Model conceptualization – nuclides transport

The modeled residence time of nuclides in the geological layers depends on advective transport variables, diffusive transport variables, and reactive transport parameters. Advective transport is governed by e.g. hydraulic heads distribution, geology of the system and hydrogeological properties of the layers (Equations 1–5, Sections 2.4 and 2.5). Diffusive

transport is influenced by for instance effective diffusion coefficient, size of the matrix available to the diffusion, porosity, and the concentration gradient (Equation 6, Sections 2.4 and 2.6.1). Reactive transport parameters comprise e.g. a retardation factor being a function of the surface sorption (Section 2.6.2; ANDRA, 2005c; Selroos and Painter, 2012).

2.6.1 Conservative transport

In highly permeable rocks, e.g. near surface sedimentary rocks, fractures, and deformation zones with high hydraulic conductivities, the dominant transport mechanism is advection and dispersion (Equation 5; Zheng and Bennett, 2002; Trinchero and Iraola, 2020). In low permeable claystone, unfractured crystalline basement rocks, and the matrix of the chalk, the dominant transport process is often diffusion (Equation 6; Brommundt et al., 2014; Enssle et al., 2014). For instance, it was estimated that nuclides in the Callovo-Oxfordian clay during 1 Myr would be transported, via conservative transport, 77 meters by diffusion and 0.3 meter by advection (ANDRA, 2005b). Diffusion of nuclides into the rock matrix is assumed to be a reversible process depending on the concentration differences (Selroos and Painter, 2012).

Diffusion parameters used in the models depend on the properties of the host rock formation, properties of solution and type of nuclides. The effective diffusion coefficient is strongly related to the type of nuclides (ANDRA, 2005c; Schwartz, 2012) and depends on the ion mobility (Appelo and Postma, 2005). Ions with larger radius are less mobile and therefore have lower effective diffusion coefficients. The effective diffusion coefficient decreases also with an increase of the viscosity of water (Appelo and Postma, 2005). The effective diffusion coefficient in fractured rocks decreases from the edge of the fractures, where often multiple microfractures are present into the centre of the completely unfractured rock matrix (ANDRA, 2005c). This is due to decrease of the surface available for the diffusion. Effective diffusion coefficients are introduced into models as deterministic or probabilistic values. The deterministic values are often used in cases where the influence of groundwater flow-related parameters on the transport of nuclides are estimated, while the probabilistic values are most often used in the main safety calculation cases (Selroos and Painter, 2012).

The rock matrix size available for diffusion is a parameter used to describe the fractured media in the numerical set up. In the far field models of fractured host rock formations, for simplification and reduction of a required computational power, diffusion from fractures to matrix is modeled as a one-dimensional process occurring perpendicular to the advective flow in the fracture planes (Selroos and Painter, 2012; Trinchero and Iraola, 2020). The matrix size available for diffusion (maximum thickness of diffusion) can be set as limited or unlimited. The limited matrix size allows nuclides and gases to migrate only to a specified distance from the fracture to the inner part of the rock matrix. The unlimited matrix size does not give any limitations on the distance travelled via diffusion through the unfractured rock matrix. The matrix size available for diffusion regulates delay in the arrival times of nuclides to the surface. Travel times of nuclides through the host rock formation increase with increasing distance available for the particle diffusion from the fracture planes into an unfractured rock matrix, where the advective transport can be neglected compared to the fracture networks. The maximum thickness of diffusion is usually smaller in the near field models and the matrix

size available for the diffusion increases with the increasing size of the model and decreasing precision in representation of the fracture networks (ANDRA, 2005c).

Diffusion into unfractured rock matrix significantly delays arrival times of nuclides to the surface. Nuclides diffused into unfractured rock matrix migrate back to the fractures network once the nuclides concentrations in the fractures are lower than in the rock matrix (Trinchero and Iraola, 2020). The sensitivity analysis of diffusion parameters in fractured media often includes decrease in effective diffusion and porosity available to diffusion from the fracture planes leading to underestimation of nuclide arrival. In these cases, a major part of the released nuclides is transported by advection in the fracture networks (ANDRA, 2005c). More complex scenarios with diffusion parameters set as higher values in the excavation damaged zone, due to the occurrence of dense microfractures networks increasing the surface available for the diffusion into unfractured rock matrix, than in the surrounding rocks without micro fracture networks are also tested (ANDRA, 2005c). However, less complicated models without fractures, but with diffusion controlled transport in the host rock are also seen.

2.6.2 Reactive transport

Concentrations of nuclides arriving to the biosphere depend on nuclides half-life and solubility, geochemical parameters of the geological layers and groundwater, and microbial activity. Release of nuclides at the repository location in the far field models can be modeled as a transient Neumann boundary conditions that allows for nuclides injection at a predicted release rate (Schwartz, 2012, 2018; Enssle et al., 2014). The far field simulations may use the near field nuclides mobilization data as input (Schwartz, 2012).

In general, the most soluble nuclides in radioactive waste are Cl-36, Cs-135, I-129, and gaseous C-14 (Schwartz, 2012, 2018). Actinides are insoluble under anoxic conditions and their transport in the deep subsurface is significantly delayed, unless they are transformed into soluble forms in the presence of dissolved oxygen or oxidants produced by the irradiation of water (De Windt and Spycher, 2019). Oxidants produced by the irradiation of water are favourably used by reducing ions in groundwater(e.g. Fe(II)) and thus the oxidants' availability for oxidation of actinides (e.g. insoluble U(IV)) is limited by the groundwater chemistry prior to the repository placement (Odorowski et al., 2017).

The concentration of nuclides in groundwater is diminished by sorption to clay minerals and organic matter in the engineered barriers (clay buffers, backfill), and in the host rock. Sorption is often modeled as a linear, reversible process (Enssle et al., 2014). Sorption capacity of the host rock's micro surfaces is determined by the content of organic matter and clay minerals in the host rock, and the porewater chemistry. The linear, reversible process is in moost cases represented by a linear sorption partition coefficient (or the distribution coefficient), $K_{d,}$ describing the relative concentration of sorbed ions to the concentration in the aqueous phase (Selroos and Painter, 2012). Inclusion of the sorption parameters in complex far field models comprising host rock, backfill tunnels, near surface sedimentary rocks and deformation zones usually increases the safety performance of the repository site (Selroos and Painter, 2012).

Due to the sorption properties of the clay minerals, reactive transport models for nuclides often introduce distribution coefficients of nuclides between sediments with different content of clay minerals (Schwartz, 2012). The content of nuclides prone to sorption is usually higher in the clay-bearing deposits than in other rock types. For multivalent cations, the sorption capacity of the host rock decreases with increasing groundwater salinity due to an increased concentration of major cations competing with nuclides for the sorption sites (Schwartz, 2012).

The near field models often include steep chemical and hydrogeological gradients between the multiple barrier system (engineered materials and host rock formation) and complex geochemical and mechanical reactions. The chemical processes influencing the sorption capacity of a near field are decalcification of cement-based barriers, dissolution of clay-based barriers, precipitation of calcite and zeolites at the barriers interface, swelling/shrinkage of clay backfills and biogeochemical reactions (De Windt et al., 2004).

Nuclide concentrations and radiation doses predicted in the process of reactive transport modeling can be sampled in different parts of the system in order to check if the regulatory limits are met. The currently proposed dose limit in Denmark equals 0.1 mSv/yr (Sundhedsstyrelsen, 2015).

The most common practice is to calculate radiation doses by multiplying nuclides concentrations at the surface discharge points by the landscape dose factor (Selroos and Painter, 2012) or biodose conversion factor (Schwartz et al., 2012, 2018). The landscape dose factor is a result of a detailed biosphere modeling (Selroos and Painter, 2012). The biodose conversion factor considers pathways of exposure to the radiation due to water intake, contact with the contaminated soil, inhalation of radioactive gases and consumption of contaminated food (Schwartz, 2018). Nuclide concentrations can also be checked at the potential depths of recent and future drinking water intakes in aquifers (ANDRA, 2005b) or at the depth of the boundary between fresh and saline water, which has been suggested to correspond to 1 g/L of dissolved solids (Schwartz, 2012).

2.6.3 Nuclide inventory and repository design for transport models

Prior to the modeling studies, the waste producers normally prepare the waste inventories – also called catalogues - dividing radioactive waste into homogenous sets of waste indicating the waste composition and activity, production of gas by radiolysis, heat transfer and irradiation level, and amount and volume of the waste packages. Detailed descriptions of the container materials are also provided and include descriptions of used metallic materials and information on presence of organic matter in the radioactive waste (ANDRA, 2005b, c).

The nuclides in the waste catalogues may to the benefit of the modelling exercise be sorted according to the nuclides half-life and/or type of the emitted radiation. E.g. ANDRA (2005c) divided nuclides into three groups: (1) short-lived nuclides with a half-life up to 6 years, (2) medium-lived nuclides with a half-life of 6 to 30 years, (3) long-lived nuclides with a half-life above 30 years. Danish Decommissioning divided nuclides in the Danish radioactive waste into short-lived (half-life <30 years) β/ϒ nuclides, long lived (half-life >30 years) β/ϒ nuclides,

and α nuclides with a half-life from 3.8 days to 14 × 10^9 years (COWI, 2011a). Nuclides are selected for the modeling studies based on the relevance to the long-term safety of the repository and theoretical transfer times through the geological barrier. Nuclides with very low radioactivity are eliminated. The remaining nuclides are grouped based on solubility, sorption capacity and toxicity into mobile elements, averagely mobile and barely mobile. Typically, the long-lived and most mobile nuclides are picked for feasibility modeling studies, i.e. I-129, Cl-36, Cs-135, C-14, Tc-99, Sn-126, Se-79 and Mo-93, as they pose the highest threat to the human health and environment (ANDRA, 2005c; Lim, 2006; Enssle et al., 2014; Schwartz, 2018).

In the feasibility modeling phases, the input data from the waste inventory usually has the highest certainty compared to hydrogeological data, which are limited in the initial modeling phases (ANDRA, 2005b). In the case where the waste types are continuously decommissioned during the modeling studies, the sensitivity analysis includes variations in the amount of radioactive waste (ANDRA, 2005c).

The decommissioning institution normally delivers preliminary concepts and designs for the repository to be used at the initial modeling stages. The architecture of the repositories is through an iterative process adapted to the expected geological setting and to the outcomes of the modeling studies (ANDRA, 2005c; Ström et al., 2008; Figure 9). However, during the

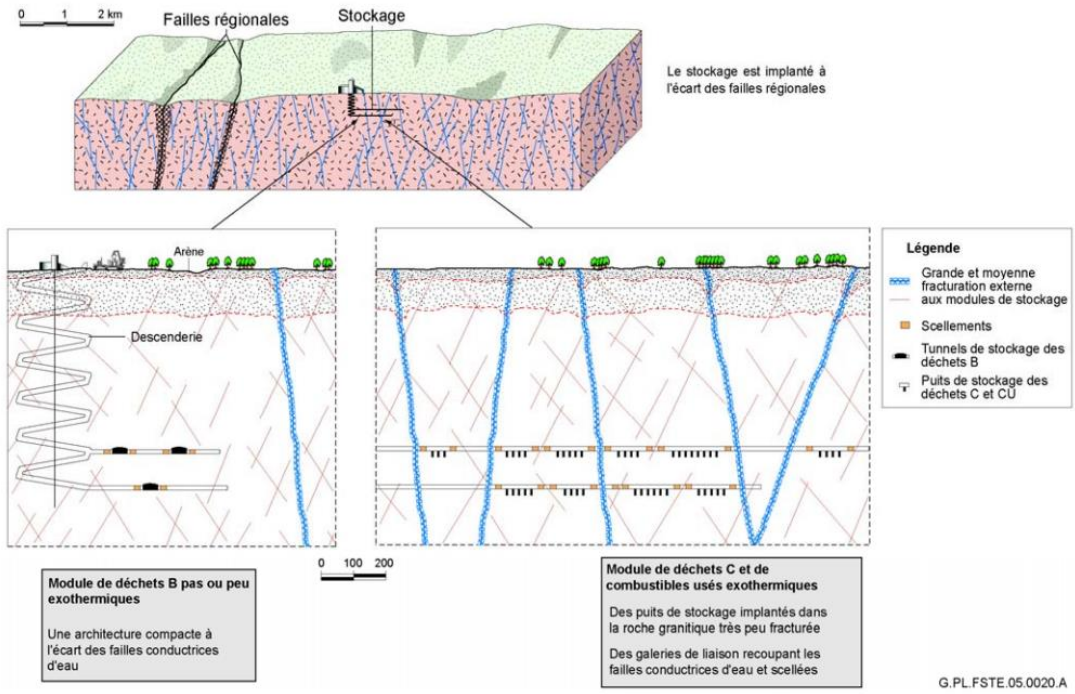

Figure 9. *Adaptation of the repository architecture to the granite fractures (ANDRA, 2005c).*

Figur 9. *Tilpasning af depotets arkitektur i forhold til sprækkerne i granit (ANDRA, 2005c).*

pre-feasibility studies, the focus of the analysis is on the host rock formation rather than on the detailed, complex engineered components (ANDRA, 2005c). In the later phases the detailed models are constructed to check the influence of different canister configurations on the nuclide migration (Lim, 2006). For instance, the changes in the near field release of Cs-135 were significant (factor of 3) between different canister configuration where e.g. canisters were placed parallel and perpendicular, respectively, to the flow direction (Lim, 2006).

2.7 Numerical methods, discretization, codes

Reactive transport models for radioactive waste repositories are commonly three dimensional (3D) and set up using finite elements methods (Sawada et al., 2005; Schwartz, 2012; Selroos and Painter, 2012; Vidstrand et al., 2014), although finite differences method (ANDRA, 2005c; Sawada et al., 2005) and two dimensional (2D) models are also used (Lim, 2006). The size of the model domains in XY dimensions vary from tens of meters for the near field simulations to tens of kilometers for the regional and far field models (ANDRA, 2005c; Sawada et al., 2005; Schwartz, 2012, 2018). Horizontal discretization is usually regular, avoiding numerical dispersion and in tens to hundreds of meters in the far field models (Sawada et al., 2005; Luo et al., 2014a; Schwartz, 2018). In the sensitive areas of the near field models, fine discretization is replaced with analytical solutions to save computation time (Selroos and Painter, 2012). Vertical extent of the regional and far field models varies from a couple of hundred meters to a couple of kilometers (ANDRA, 2005c; Sawada et al., 2005; Schwartz, 2012; Vidstrand et al., 2014). Vertical discretization depends on the model settings and aims to maintain the measured pressure and salinity values throughout the simulation time (Schwartz, 2012, 2018). The models consist of hundreds of thousands of elements (Schwartz, 2012).

One of the software precursors for modeling of geological disposal of radioactive waste was FARF31 (Norman and Kjellbert, 1990). However, the code is not suitable for modeling of the heterogeneous systems with multiple retention models, for instance sorption in the repository tunnels together with matrix diffusion in fractured rock (Selroos and Painter, 2012). During the past two decades numerous mathematical solutions and software were developed for improvement of the performance of the large flow and transport models for the geological disposal of radioactive waste, e.g. Lanteri and Raffourt (2004) reduced computing time of nuclides transport in the finite volume PORFLOW code, Trujillo (2004) applied a mixed finite volume method to simplify the far field simulations, Lim (2006) developed a code for a 2D multiple canister flow and transport modeling, and Bagtzoglou et al. (2009) developed the approach using fuzzy logic to solve the groundwater flow equation in the field of uncertain parameters based on soft/qualitative data.

In Sweden, a combination of four codes – MIKE SHE, ConnectFlow (Serco, 2008), COMP23 (Cliffe and Kelly, 2006) and MARFA (Painter and Mancillas, 2009) was used for modeling of nuclides transport in a near and far field model. A MIKE SHE model was set up for understanding of the shallow, Quaternary aquifers. The output data were used in a simplified finite element ConnectFlow flow model, which allows for flow modeling in fractured media. ConnectFlow allows for nesting CPM and DFN models within a single model domain and for modeling of density-driven flow, including diffusion into the rock matrix. The equivalent flows

at the canister locations were implemented in a near field COMP23 model to estimate release paths at the repository. COMP23 simulates the near field conditions including release and transport of nuclides in the system of the engineered barriers. A far field nuclide transport model was set up in MARFA, suitable for both, fractured and unfractured media, using groundwater travel times and hydraulic resistance estimated in ConnectFlow (Follin et al., 2008; Serloos and Painter, 2012) and nuclide release rates calculated in COMP23 (Selroos and Painer, 2012). MARFA supports heterogeneity of flow pathway properties, all decay chains and temporal variability in nuclide release rates (Selroos and Painter, 2012). ANDRA (2005c) for granite massifs in France also used a combination of ConnectFlow, COMP-23 and FARF-31 (later developed into MARFA). Additionally, FracMan and PathPipe were used for generation of DFN and transport tubes, and Goldsim for volume modeling of engineered barriers (ANDRA, 2005c).

Hadgu et al. (2017) and Trinchero and Iraola (2020) used PFLOTRAN (Mills et al., 2007) for assessment of transport of naturally-occuring nuclides in fractured media. The software is suitable for parallel two-phase simulations without salinity variations. Its non-parallel version is FLOTRAN (Lichtner, 2007). Simulation of the transport of nuclides in fractured and unfractured media can also be conducted in the finite volume DarcyTools code (Svensson et al., 2010), including volumetric up-scaling from discrete fractures networks to an equivalent continuous porous medium (Vidstrand et al., 2014), POR-SALSA handling multi-phase flow with thermal balance, EQUIV_FLO and FracAffinity simulating both saturated and unsaturated flow. The channelized flow in the fracture network excluding the continuous model domain can be simulated in Don-Chan. FEHM (Zyvoloski et al., 2012) is a finite element code used for studies of porous flow in salt formations (Johnson et al., 2019). The code applies equations for conservation of water mass, air mass, and energy. It also includes salt-specific reactions. The code did not cause major convergence problems in the crystalline basement rock settings, but the simulation time is long for large models including periods up to 1 Myr (Schwartz, 2018).

TOUGHREACT is a finite difference code developed for modeling of non-isothermal multiphase flow and reactive transport in porous and fractured media. It is often used in different host rock formation settings for modeling of nuclides transport in the near field and far field of waste repositories (Sawada et al., 2005; Schwartz, 2012, 2018; Brommundt et al., 2014; Enssle et al., 2014). Schwartz (2012) simulated transport of nuclides from a repository in a salt dome through a siliciclastic aquifer using TOUGHREACT for a two-phase flow and TOUGH2-MP for a one-phase scenario, where the aqueous phase was treated as a mixture of water and brine. TOUGH2-MP was also used by Sawada et al. (2005) for flow modeling in the fractured granite massifs in Japan and for multi-phase transport in French clays (Brommundt et al., 2014; Enssle et al., 2014).

One-phase transport of nuclides in variable salinity environments can also be calculated in NAMMU (Serco, 2003) or SUTRA-MS (Hughes and Sanford, 2004). The later only allows for simulation of single chain nuclides.

The initial models focus usually on the advective and diffusive transport of selected nuclides and do not include e.g. multiphase flow or detailed decay chains. Thus, regional and far field models can also be set up using for instance a finite element FEFLOW code. The code allows

for a detailed discretization along important geological features like faults, rivers and boundaries of the geological formations. Contrary to the 2D fracture models common in the other codes, fractures in FEFLOW are introduced as 3D features (Luo et al., 2013, 2014a).

Sensitivity checks regarding numerical methods are usually run for (ANDRA, 2005b):

- Component sensitivity, where the influence of application of different computer codes on the modeling results is checked.
- Sensitivity to different mesh sizes.
- Sensitivity to the various discretization methods.
- Sensitivity to the resolution algorithms.

3. Current knowledge of the Danish waste inventory

3.1 Nuclides inventory and geochemical description

The following section contains a description of nuclides in the Danish waste based on the report prepared by COWI (2011a). The report includes the most recent description of radioactive waste stored at Danish Decommissioning facilities in Risø. However, the description is based on a couple of assumptions, since in the available documentation: (1) there is not data on all individual containers, (2) the lists of nuclides are not always complete, and (3) the activities are not stated for all waste items.

To follow the procedures commonly used in other countries (Section 2.6.3) and ensure the most precise evaluation of the long-term safety of the radioactive waste repository, the nuclides transport models should be based on a clear, complete and detailed description of the radioactive waste in Denmark. Input data to the models comprise: (1) amount and volume of each type of the waste containers, (2) detailed description of the containers engineered barriers, (3) origin of the waste, (4) detailed geochemical description stating fraction of each nuclide, its decay products and its properties (solubility, activity, decay time), and (5) possibility of heat and gas emission, including expected amounts of gaseous nuclides being a product of the decay chains.

The waste stored at the facilities in Risø originates from radiation sources, nuclear fuel, building materials and structures, Risø activities and external origin – industry, hospitals, universities. The list of nuclides considered in the risk assessment performed by COWI (2011a), together with the nuclides half-life, decay radiation and decay chain is given in Table 1.

In addition to the list in Table 1, COWI (2011a) also indicated occurrence of Ac-227, Cd-113 m, Cl-36, Ni-59, Nb-94, Np-237, Mo-93, and Pa-231 in the Danish waste. However, these nuclides are present only in small amounts, and COWI (2011a) decided not to include them in the pre-feasibility study. According to COWI (2011a), the most relevant elements for the long-term risk assessment are uranium and transuranic elements (e.g. isotopes of Am, Np, and Pu) with half-life times up to 14×10^9 yr, present in the nuclear fuel (COWI, 2011a).

The amount of waste considered for the disposal, as for 2008, equaled 4817 m^3. Of this, 178 m^3 was referred to as special waste including: (1) 1.2 kg of irradiated, dissolved uranium, (2) 234 kg of irradiated fuel, (3) 2 t of non-irradiated uranium, (4) core solution and heave water, and (5) waste from other sources (COWI, 2011a). The remaining waste is low- and medium-level waste.

Table 1. *Nuclides considered in the risk assessment by COWI (2011a).*

Tabel 1. *Nuklider inkluderet i sikkerhedsvurderingen udført af COWI (2011a).*

Element	Nuclide	Half-life (yr)	Decay radiation	Daughter
Americium	Am-241	432	8xα 4xβ	Np-237 -> Pb-209, neptunium series
Barium	Ba-133	10.7	EC, ϒ	Cs-133 stable
Calcium	Ca-41	140 000	EC, ϒ	K-41 stable
Carbon	C-14	5 730	β	N-14 stable
Cesium	Cs-137	30	β, ϒ	Ba-137 stable
Cobalt	Co-60	5.27	β, ϒ	Ni-60 stable
Curium	Cm-244	18.1	9xα 6xβ	Pu-240 -> Pb-208, thorium series
Europium	Eu-152	13.3	β, ϒ β, ϒ + 3xα	0.72 Sm-152 stable 0.28 Gd-152 -> Sm-148 -> Nd-144 -> Ce-140 stable
	Eu-154	8.8	β, ϒ	Gd-154 stable
Iridium	Ir-192	0.20	β, ϒ	Pl-192 stable Os-192 stable
Iron	Fe-55	2.7	EC, ϒ	Mn-55 stable
Nickel	Ni-63	96	β	Cu-63 stable
Plutonium	Pu-241	14.4	β	Am-241, neptunium series
	Pu-240	6 500	8xα 4xβ	U-236 -> Pb-208, thorium series
	Pu-239	24 110	8xα 4xβ	U-235 -> Pb-207, actinium series
	Pu-238	87.7	8xα 4xβ	U-234 -> Pb-206, radium series
Radium	Ra-226	1 600	5xα 4xβ	Rn-222 -> Pb-206, radium series
Radon	Rn-222	0.01	5xα 4xβ	Po-218 -> Pb-206, radium series
Samarium	Sm-151	90	β	Eu-151 stable
Selenium	Se-75	0.33	EC, ϒ	As-75 stable
Silver	Ag-108 m	418	EC, ϒ	Pd-108 stable
Strontium	Sr-90	29.1	2xβ	Y-90 -> Zr-90 stable
Technetium	Tc-99	211 000	β	Ru-99 stable
Thorium	Th-230	75 380	6xα 4xβ	Ra-226 -> Pb-206, radium series
	Th-232	14×10^9	6xα 4xβ	Ra-228 -> Pb-208, thorium series
Tritium	H-3	12.3	β	He-3 stable
Uranium	U-234	246 000	7xα 4xβ	Th-230 -> Pb-206, radium series
	U-235	704×10^6	7xα 4xβ	Th-231 -> Pb-207, actinium series
	U-238	$4\,470 \times 10^6$	8xα 6xβ	Th-234 -> Pb-206, radium series

The total activity of nuclides will change as follows within a period of 100 kyr, starting at 2008 (COWI, 2011a):

- In 30 yr, the total activity will be in order of 10^6 GBq with Am-241, Co-60, Cs-137, Eu-154, H-3, Ni-63, Pu-238, and Sr-90 dominating the radiation.
- In 100 yr, the activity will decrease to 10^5 GBq. The dominating sources of radiation will be Am-241, Cs-137 and Ni-63.
- In 1 kyr, the activity will decrease another order of magnitude to 10^4 GBq. The most important nuclides for the radiation will be Am-241, C-14, Ni-63, Pu-239, and Pu-240. In 30 000 years, the nuclides dominating the radiation will be Tc-99, Pu-239, Pu-240, U-238 and U-234 with a total activity decreasing slightly above 10^3 GBq.
- At 100 kyr, the activity will have decreased slightly below 10^3 GBq. The most important nuclides will be uranium and transuranic elements (e.g. isotopes of Am, Np, and Pu) with an increasing amount of radiation coming from daughter products of uranium isotopes.
- Because of the long half-life of uranium and transuranic elements, this level of radiation will decrease very slowly and a level of radiation above 10^2 GBq will remain for billions of years.

Although the above lists the most important nuclides in terms of the level of radiation as a function of time, the potential environmental impact of the nuclides will also depend on their release from the engineered containment, their concentrations, and their behaviour during transport through the geology. The differences in release and transport behaviour may imply that nuclides that are less important, in terms of radiation, may be more important in terms of actual environmental impact because they may reach the groundwater used for drinking water as well as surface waters. The transport behaviour for a given nuclide may also vary depending on the repository rock and overlying rock types.

3.2 Potential host rock formations in Denmark

Based on the geological mapping in the present repository project (c.f. Chapter 9.1 for relevant references), three types of rocks are identified to occur at depths around 500 meters, i.e. crystalline basement rocks, chalk, and claystone. More details with focus on the properties of the potential host rock formations in Denmark are available in the GEUS reports (Gravesen et al., 2021; Jakobsen et al., 2021; Pedersen et al., 2021). Each of these rock types have different properties related to hydraulic flow and transport of nuclides. Consequently, different processes can govern nuclide transport within each of the rock types. Crystalline basement rocks and claystone are considered for hosting radioactive waste repositories in Sweden (Follin et al., 2008), Finland (Sawada et al., 2015), Switzerland (Luo et al., 2013, 2014a, b), and France (ANDRA, 2005b). Chalk and marlstone have also been considered in Switzerland (NAGRA, 2005, 2008).

4. Conceptual modeling of nuclide transport in Danish low permeable formations

Three low permeable rock types occur in the Danish subsurface at depths of 500 meters; crystalline basement rocks, claystone, and chalk (Gravesen et al., 2021; Jakobsen et al., 2021; Pedersen et al., 2021). Crystalline basement rock properties have been studied intensely for radioactive waste repositories in several countries, including Sweden, Finland, France, and Switzerland (ANDRA, 2005c; Follin et al., 2008; Sawada et al., 2015). Likewise, highly compacted claystone abundant in clay minerals including illite, smectite, kaolinite, montmorillonite, and chlorite are considered suitable as host rock formation (ANDRA, 2005b; Baeyens et al., 2014). Chalk occurs widespread in the Danish subsurface and some knowledge exists on its hydrological properties around 500 meters depth (Jakobsen et al., 2021), thus enabling a preliminary assessment of its host rock formation potential. As the information on host rock formation properties of crystalline basement rocks exists from several other studies and no data is available for Danish crystalline basement rocks at 500 meters depth, crystalline basement rock is not included in the current analysis but the current knowledge from other countries is briefly reviewed (Sections 2.5 and 2.6, Appendix A).

The claystone mineralogy and rock properties at depths around 500 meters in the Danish subsurface seem to be quite different from properties of other claystones that were found suitable as host rock formations in France and Switzerland (e.g. ANDRA 2005b, Grambow et al., 2014; Luo et al., 2014a, b; Tsang et al., 2015). Swiss claystone was buried to 3–4 kilometers depth, while the burial depth of Danish claystone occurring at 500 meters depth today was increased during glaciations by approximately 700 meters to 1.2 kilometers. The burial depth differences have resulted in higher diagenesis of Swiss claystone and decreased hydraulic conductivity compared to the Danish claystone. Other important factor are mineralogical differences. The dominating clay mineral in Danish claystone is kaolinite, while Swiss claystone comprises smectite in large amounts, and higher clay content in general. The higher content of kaolinite in the Danish claystone presumably results in a higher relatively higher hydraulic conductivity compared to the Swiss claystone (Mbia et al., 2014). Finally, sand interbeds abundant in Danish claystone (Pedersen et al., 2021) may create preferential flow paths.

The modeling study aims to make a conceptual assessment of the potential for geological disposal of radioactive waste in low permeable sedimentary rocks that are present at 500 meters depth in the Danish subsurface. At present, the information relevant to assessing the effectiveness of the geological barriers at depths to 500 meters is limited. The information needed to assess the host rock potential is related to the physical rock properties, the hydrogeological regime at the specific site of a potential host rock, groundwater chemistry, rock mineralogy as well as the geochemical properties of the nuclides in the inventory (Sections 2.5, 2.6 and 3.1).

The present study is regarded as a preliminary evaluation of the host rock potential based on numerical modeling using conceptualizations under various assumptions. Applied param-

eter values are based on the literature relevant to Danish conditions, i.e. mainly from borehole and geophysical data from Denmark but in some cases Danish data are very limited or lacking, and therefore parameter values were in some cases also estimated from underground research laboratories and specific sites for geological disposal of radioactive waste outside of Denmark.The modeling is made (1) to evaluate the barrier effectiveness of low permeable sedimentary rocks and (2) to identify what parameters related to geological, hydrogeological and hydrogeochemical properties are governing the the subsurface transport of nuclides.

Conceptual modeling analyses were based on common modeling practices (Section 2) to assess the potential of the formations occurring in the Danish subsurface (Figure 10). The results will be used in the subsequent Phase 2 of the repository project to design the most optimal study program and to reduce uncertainty in the upcoming models. This will also encompass flow and transport of nuclides in 2D and 3D hydrogeological domains.

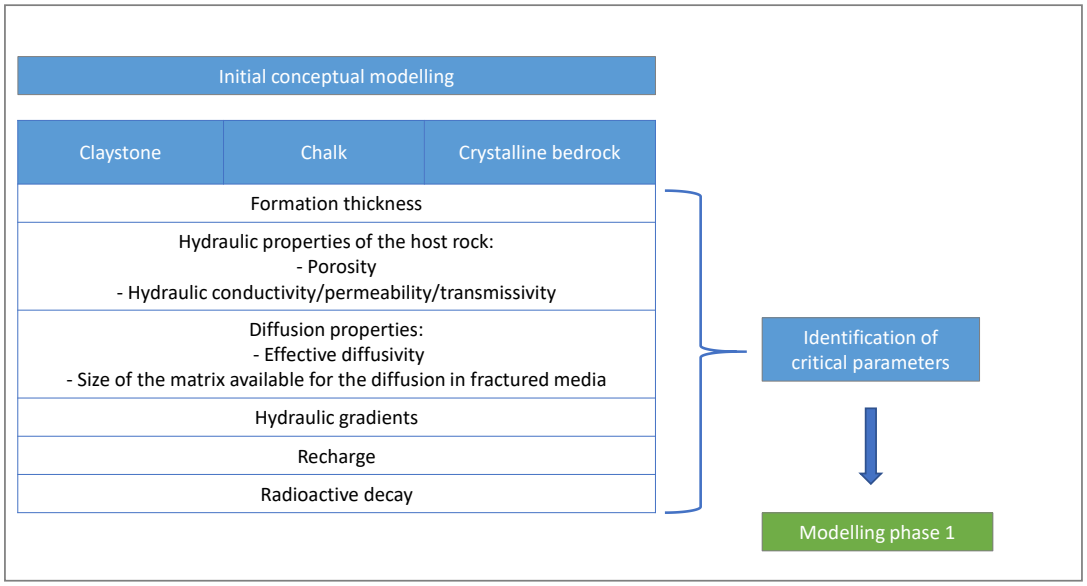

***Figure 10**. Initial modeling phase for the potential Danish host rock formations at 500 meters depth.*

***Figur 10**. Indledende modelleringsfase for de potentielle danske værtsbjergartsformationer i 500 meters dybde.*

It is important to stress that the current numerical evaluation is only a preliminary assessment to gain general knowledge and insights into the host rock formation potential for the chalk and claystone in the Danish subsurface. Further, the conceptual models do not represent a specific site in Denmark, but the geological formations are considered as likely average settings at 500 meters depth. Detailed numerical models providing a better representation of the host rock formation potential at specific sites will be set up as part of Phase 2 of the geological project, where new data are collected at specific potential repository sites.

Previous numerical studies in Denmark were made for different repository concepts than the current focus at 500 meters depth: 1) repository close to the ground level (depth < 30 meters) with unsaturated conditions, 2) repository at a medium depth of up to 100 meters, and (3) a borehole disposal facility at depths of 100–300 meters (COWI, 2011b, c, d). The models comprised a near field model of nuclides release at the repository (COWI, 2011c) and a far field model of groundwater flow and nuclides transport, degradation, and retardation (COWI, 2011b, d). Nuclides included in the modeling studies performed by COWI are listed in Section 3.1.

The near field model was an analytical solution and included the properties of the engineered barriers and the host rock formation and nuclides solubility and sorption. Nuclides release was calculated at 10, 30, 100, 300, 1000, 3000 and 10000 yr (COWI, 2011c).

In the far field model, four conceptual geological settings were investigated and comprised geological layers common at a depth of up to 100 meters in Denmark: fat clay, clay till, Danian and Maastrichtian limestone, and crystalline basement rocks. Fifteen deterministic models were set up using MODFLOW and MT3DMS. All rocks were modeled as a Continuous Porous Medium (CPM) with isotropic properties in the horizontal plane. Limestone at the investigated depth is often fractured and highly permeable. Thus, a setting with highly permeable limestone layer was also tested. The models were run at a steady-state with fixed head and river as the boundary conditions. Constant flux boundaries were applied at the abstraction wells. The models included diffusion, nuclides decay, and sorption. Nuclides release was set as a fixed flux with a fixed concentration. Dilution factors were calculated at the recipients (wells, streams, and coastal waters). Sensitivity analyses were performed for hydraulic conductivity and sorption partition coefficient (K_d). Nuclides were divided, based on the sorption properties and literature data, into seven groups with K_d value from 0 to 200 m^3/kg. The biosphere model was implemented to calculate the received dose (COWI, 2011b, d).

According to COWI (2011d), breakthrough curves (BTCs) for the crystalline basement rocks setting have the lowest concentrations and the latest arrival times compared to the sedimentary rocks. The earliest arrival time and the highest concentrations are in BTCs for the clay till setting. BTCs for the repository in the fat clay are a bit delayed and have lower concentrations compared to the repository located in the limestone. For a repository at a medium depth of up to 100 meters, the location of the repository close to the highly permeable limestone layer has a higher impact on the BTCs arrival time and nuclide concentration than the repository depth and geology of the host rock formation (fat clay or limestone). BTC arrival times are delayed and nuclide concentrations decreased with an increasing borehole depth (COWI, 2011d).

5. Methodology

5.1 Evaluation criteria

To evaluate the host rock potential, far field conceptual 1D models representing type locations for the available low permeable rock types are analyzed using numerical models representing various scenarios described in Section 5.2.2. At the current stage, no specific repository site is identified. As such transport of nuclides from a given geological repository is governed by site-specific hydrological conditions and the hydraulic gradients governing transport of nuclides would also be site dependent. Therefore, to evaluate the feasibility of a given low permeable rock type at the current stage, numerous model conceptualizations could be applied. However, as the output for evaluation is dependent on the conceptualization, it is deemed appropriate to evaluate the feasibility from the simplest starting point possible. The notion is to avoid adding more complexity into the conceptualization than can be justified at the current stage. Thus, 1D conceptual models are applied. The models at the recent stage do not represent nuclides transport at a specified site, and the focus of the numerical analysis is on the host rock formation feasibility and identification of crucial hydraulic properties. Furthermore, the half-life of most of the nuclides in Danish waste is contained within 1 Myr (Table 1). Thus, to limit the computational effort, the simulated time was limited to 1 Myr. Modeling of the nuclides transport in other studies also is commonly limited to 1 Myr (e.g., Schwartz, 2012; Enssle et al., 2014; Hadgu et al., 2017).

The analyses are performed in a two-step approach, where step 1 seeks to compare the host rock potential from a conservative (worst-case) nuclides transport approach. I.e., here it is assumed that nuclide leakage from the deposit depth is instantaneous, effects of retardation and decay are not included, and neither is the effect of spreading in 3D. By using a conservative transport assumption, it allows for comparison of the different host rock formation's potential from an advective and dispersion properties perspective. Nuclide transport is dependent on various geochemical variables, among others solubility, half-life, and sorption. Common for these variables is that they are all compound-specific and vary with changes in groundwater chemistry and the mineralogical composition of the host rock formation (Section 2.6). Therefore, the conservative nuclides transport analysis enables comparison between the different geological barrier conceptualizations without having to consider a specific nuclide.

In step 1, the host rock potential is evaluated in terms of breakthrough curves (BTC) for a simulated leakage of nuclides from the barrier formation in a depth of 495–505 meters. Specifically, the breakthrough time of the maximum relative concentrations is used to infer the effect of the different assumptions, parameter values, and boundary conditions of the scenarios and compare these for the different host rock formation conceptualizations. In Denmark, the main drinking water resource is groundwater and the critical level of nuclides in groundwater for an acceptable yearly dose intake with drinking water should be evaluated at the groundwater abstraction depth. As such, the maximum simulated BTCs are evaluated at a depth corresponding to an assessed average level for groundwater abstraction in the two

conceptual models. The averaged groundwater abstraction levels are further explained in the sections below describing each of the conceptual models (Section 5.2).

In step 2, the reactive transport models were set up and nuclide concentrations were simulated at the average abstraction level defined in the middle of the fractured chalk (Section 5.3). The reactive transport of nuclides is, to a large extent, governed by site and compound-specific factors. These data are not available at the current project stage and thus, the reactive transport model is set using the median hydrogeological properties, with diffusion, solubility, and decay data from the literature. The reactive transport modeling aims to compare the potential of Danish chalk and claystone in preventing nuclides transport to the average groundwater abstraction depth. The inventory for the Danish radioactive waste is currently incomplete (Section 3.1) and therefore the reactive transport model includes the potentially most harmful nuclides identified as described in Section 5.3.2. The 1D calculations do not include the effects of spreading and mixing in 3D in the aquifer and the well, as the focus of the phase 1 is on the evaluation of the potential of Danish chalk and claystone in preventing nuclides transport instead of 3D modeling of nuclides transport at a specific site. The sorption was also excluded from modeling studies at phase 1. The sorption partition coefficient depends on the rock mineralogy and water chemistry (Section 2.6.2). These data are not available for 500 meters depth in Denmark at the recent investigation stage, and therefore high uncertainty would be connected to the sorption partition coefficient values. Thus, the sorption partition coefficient was not included in 1D conceptualizations. The results of the reactive transport models are used to compare the relative effect of the hydraulic properties of the different host rock formations and the solubility and decay of the nuclides on nuclides concentrations at the average abstraction level. A detailed description of the reactive transport model set up, and the selection of nuclides included in the model are given in Section 5.3. In the next phases of the project reactive transport modeling will also be considered in 2D and 3D hydrogeological domains.

5.2 Conceptual models

The data availability of onshore geological formation properties at around 500 meters in the subsurface are scarce and likewise, for the hydrological regime, the knowledge is limited. Further, geochemical properties related to nuclide transport, such as solubility, diffusion, and sorption are compound- and site-specific. Hence, data at the present stage do not justify a detailed conceptualization of the hydrogeological and geochemical setting for the different potential host rock formations. For the potential host rock formations, the conceptual models represent a generic geological setting based on assessments of regional geology. This means that the models do not represent the geology and layer thicknesses of a specific location but a general assessment of an average representative geological setting where the potential host rock formations are present. Therefore, we apply a relatively simplistic approach utilizing literature parameter values and boundary conditions (BC), to evaluate the host rock potential as well as the importance of parameters to be determined in future data collection.

Flow and nuclide transport simulations in 1D were performed with MODFLOW (Harbaugh et al., 2000) and MT3MDS (Zheng and Wang, 1999) as these model codes are sufficient to

simulate the flow and transport processes considered relevant at the present stage. Two model conceptualizations representing chalk and claystone as host rock formations were used. Several studies show that in the deeper subsurface, advective flow is limited and solute transport is diffusion-dominated (e.g. ANDRA 2005b; Enssle et al., 2015; Tsang et al., 2015). If advective flow is present, the flow direction is often horizontal (Luo et al., 2014a, b). However, since the hydrological flow regime is site-specific and unknown at the current stage, the assumption of a possible upwards flow component is maintained. The flow in the model was specified with fixed head boundaries at the top and bottom of the model domain. The upper and lower boundary condition define the hydraulic gradients that were varied to assess the effects of having minimum and maximum gradients. Depending on the hydraulic gradient and porosity, the variation in porewater velocities may also imply diffusive dominated nuclide transport. That is, diffusive dominated transport is often neglected when porewater velocities are greater than 0.1 m/d (Rausch et al., 2005) and as porewater velocities are dependent on Darcy flux and porosity, a situation where the hydraulic gradient is changed the transport regime could change. For instance, in a system with advective transport (porewater velocities > 0.1 m/d), a decrease in gradient would proportionally lower the porewater velocities and potentially below 0.1 m/d. Such a change could shift the transport regime from being advection-dominated to being diffusive-dominated. See Sections 2.4 and 2.5 for further details. Both conceptualizations were discretized in 5-meter cells extending 600 meters to encompass the repository depth in 500 meters The transport simulations in MT3DMS were performed with generalized conjugate gradient solver using the third-order total variation diminishing (TVD) scheme (Zheng and Wang, 1999) where the convergence criteria were set to 1E-5 mg/l and the maximum number of iterations to 200. As the flow solution was steady-state, the number of time steps was set to 1 and the number of transport time steps was 0 meaning that MT3DMS automatically determines the transport step size.

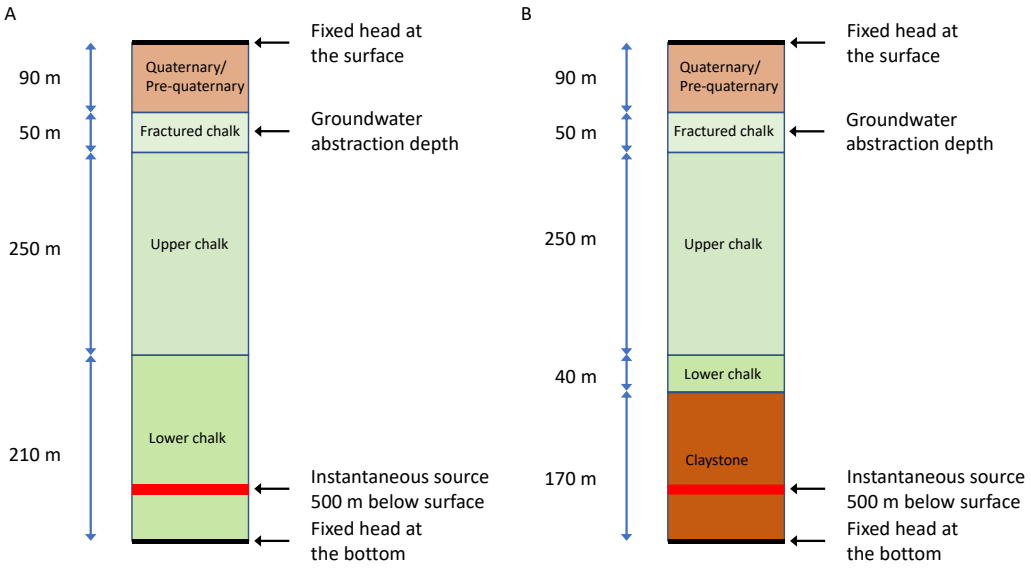

***Figure 11**. Conceptual model for A) chalk as host rock formation, and B) claystone as host rokc formation.*

***Figur 11**. Konceptuel model for A) kalk som værtsbjergartsformation, og B) lersten som værtsbjergartsformation.*

In Denmark, the chalk is ubiquitous except in the most eastern part, Bornholm, where crystalline basement rocks are present essentially to the surface. In the conceptualizations, the average depth to the top of the chalk is assessed in GIS using the map of Mathiesen et al. (2021) and estimated to be at 90 meters. Hence, the sediments from Quaternary and Prequaternary (Cenozoic) sand and clay units are represented from the surface to 90 meters. Studies of chalk at selected sites in Denmark show that the chalk comprises an upper more permeable unit and lower compacted, clay-bearing less permeable unit (Nielsen et al., 2011). The uppermost part of the chalk unit is generally fractured and approximately 1/3 of the total drinking water consumption at the national scale is abstracted from this part (Nilsson and Gravesen, 2018). It is assumed that the fractured zone represents the upper 50 meters of the upper chalk unit. The depth at which the BTC was evaluated, was specified in the middle of the fractured chalk at 115 meters to represent an assumed abstraction depth (Figure 11).

Based on permeability measurements in the chalk (Appendix B), the upper chalk represents the upper 300 meters including the fractured zone, while depths below 300 meters are considered as the lower chalk unit. In the model conceptualization for chalk as the repository barrier formation, the lower chalk unit extends to the bottom of the model domain in 600 meters (Figure 11).

In the model conceptualization for claystone as the barrier formation, the lower chalk unit extends to 430 meters and its lower part was replaced with claystone. The average depth to the top claystone in these areas was estimated in GIS using the map of Lower Cretaceous formations (Mathiesen et al., 2021) and was found to be 430 meters. The geological units overlying claystone had the same extent and lithology as in a conceptual chalk model to eliminate the influence of variations in geology along the flow path on the solute transport and facilitate the comparison of chalk and claystone as host rock formation. The applied hydraulic conductivities for the different units included in the conceptual models are described in Section 5.2.2.

5.2.1 Stochastic modeling

A key parameter in a simulation of flow and solute transport is the hydraulic conductivity, K. Unlike the geochemical properties that are essentially unknown at the present stage, K values representing the Danish subsurface are to some extent available from previous studies but limited to a few locations at 500 meters depth. Therefore, to evaluate the host rock formation potential for chalk and claystone, the current modeling approach relies on a stochastic approach with varying K within the hydrogeological units represented in the model conceptualizations. This approach allows an evaluation of the possible variation in the simulated flow and transport regime related to probable changes in K. With a stochastic variation in K, different assumptions of unknown boundary conditions and parameter values representing worst-case and best-case scenarios were tested to evaluate the output. The different scenarios are explained in detail in Section 5.2.2. Numerous studies have been performed to investigate the geological heterogeneity in terms of variation in K of various geological formations and geostatistical properties describing the variation have been deduced (Gelhar et al., 1992; Sonnenborg and Henriksen, 2005). It is therefore possible to generate an ensemble

of equally probable realizations representing the variation in K within the geological formations. K of a hydrogeological unit representing different geological units within the conceptual models were randomly varied according to its geostatistical properties to provide a number of equally probable model outputs. Randomization based on Latin hypercube sampling was used because of its efficiency in terms of computational power while achieving the same statistical accuracy as other random sampling methods (Zhang and Pinder, 2003).

The K values for the upper unit representing Quaternary and Pre-quaternary sand and clay, and the unit representing the fractured chalk zone were based on calibrated parameter values from the Danish national groundwater model, the DK-model, covering all parts of Denmark (Stisen et al., 2019). The DK-model represents the Danish geology down to the base of the fractured chalk and is calibrated against observed stream discharge and hydraulic head measurements. Thus, the calibrated parameter values are assumed to be representative of the different units implemented in the conceptualization herein. The DK-model is divided into seven regional models each representing different areas in Denmark and hence different Quaternary and Pre-quaternary sand and clay units with varying extent. To implement a generic conceptualization of the Quaternary and Pre-quaternary sand and clay units were considered as one unit in the conceptualizations (Figure 11). This approach required that the Quaternary and pre-Quaternary units including both sands and clay were attributed geostatistical properties of sandy aquifers. The effects of considering the sand and clay as one unit are deemed minor for the results as the impact of changing K in the different scenarios is assessed in the fractured chalk situated below the Quaternary/pre-Quaternary deposits. The sedimentary deposition overlying the crystalline basement rocks at Bornholm is substantially reduced compared to the rest of Denmark. Likewise, for the fractured chalk zone, K was based on the median of the calibrated values within each of the regional models of the DK-model excluding the model representing Bornholm as chalk is not present at Bornholm (Jakobsen et al., 2021; Gravesen et al., 2021).

To generate the ensemble of realizations, the average and the standard deviation together with minimum and maximum expected K values need to be defined. The calibrated K-values representing the different Quaternary-, Pre-quaternary- and fractured chalk layers from the DK-model differ amongst the various regional models, and thus, the median of the calibrated values was assumed to represent the average value while the calibrated maximum and minimum values were used as upper and lower bounds to minimize the effect of extreme values. The standard deviations were derived from literature values (Sonnenborg and Henriksen, 2005). From the permeability measurements of the upper and lower chalk, statistical distributions were made to deduce average values and standard deviations (Appendix B). The averages and the median within each unit of the chalk were similar, and thus, for consistency with the other layers, the medians for upper and lower chalk were used in generating the ensembles.

For claystone, very few measurements of liquid permeability are available from the Fjerritslev Formation (Springer et al., 2020), a low permeable, deep buried cap rock deposit that is not representative for Danish claystone formations at 500 meters depth. Commonly available gas permeabilities measured in Danish claystone are much higher than liquid permeabilities and grossly overestimated due to the drying out of the core related to the storage conditions and permeability measurements methods (Springer et al., 2020). Furthermore, hydraulic conductivity data presented in the literature for French or Swiss claystone (ANDRA, 2005b; Luo

et al., 2014a, b) are not representative of Danish claystone deposited under a different conditions (Pedersen et al., 2021). Thus, average, minimum and maximum values and standard deviations of liquid permeability in Danish claystone were estimated using the measured effective porosities and its relation to liquid permeability described in Mbia et al. (2014). The applied procedure and results are described in Appendix C. The estimated median and harmonic mean values of the permeability varied by two orders of magnitude, where the largest permeability was obtained using the median. For consistency with the other layers, the median for claystone, representing mixed claystone-sandstone layers was used in generating the ensembles, although a stochastic run using the harmonic mean was also performed to evaluate the effect of perfectly layered claystone-sandstone deposits on the conservative transport of solutes. The values applied to generate the ensembles for the variation in K of the different hydrological units are given in Table 2.

Table 2*. Hydraulic conductivity, effective porosity, dispersivity, and gradient used in modeling scenarios.*

Tabel 2*. Hydraulisk ledningsevne, effektiv porøsitet, dispersivitet, og gradienter anvendt i modelscenarierne.*

		K (m/d)	**Effective porosity (%)**	**Dispersivity (m)**	**Diffusion coefficient (m^2/d)**	**Hydraulic gradient (-)**
Quaternary/Pre-quaternary DK-model	Median	4.5	30	-	2.2E-05	-
	Minimum	1.3E-03	23	0.6	2.6E-09	0.001
	Maximum	61.7	38	6	8.0E-05	0.01
	Standard deviation (log)*	0.59	-	-	-	-
Fractured chalk DK-model	Median	3.0E-03	30	-	2.2E-05	-
	Minimum	6.3E-04	15	0.6	2.6E-09	0.001
	Maximum	1468.9	45	6	8.0E-05	0.01
	Standard deviation (log)*	0.43	-	-	-	-
Upper chalk	Median	1.8E-03	43	-	2.2E-05	-
	Minimum	5.2E-04	38	0.6	2.6E-09	0.001
	Maximum	5.7E-03	53	6	8.0E-05	0.01
	Standard deviation (log)	0.16	-	-	-	-
Lower chalk	Median	3.8E-04	30	-	2.2E-05	-
	Minimum	6.9E-05	21	0.6	2.6E-09	0.001
	Maximum	1.7E-03	38	6	8.0E-05	0.01
	Standard deviation (log)	0.21	-	-	-	-
Claystone	Median	1.2E-06	29	-	2.2E-05	-
	Minimum	4.0E-10	11	0.6	2.6E-09	0.001
	Maximum	2.3E-03	44	6	8.0E-05	0.01
	Standard deviation (log)	1.11	-	-	-	-

* Based on Sonnenborg and Henriksen (2005).

5.2.2 Modeling scenarios

The stochastic approach was used in step 1 to compare host rock formation potential from a conservative nuclide transport approach (Section 5.2.1). As such, the stochastic approach represented different ensembles to investigate the effect of changing boundary conditions and parameters values on the nuclide travel times and magnitudes. By changing the hydraulic gradients and hydrodynamic dispersion coefficients (mechanical dispersion and diffusion coefficient values, Equations 1, 5, and 5a) worst- and best-case ensembles were evaluated. Both the hydraulic gradients and the dispersivities were changed by a factor of 10 to arbitrary representing a minimum and maximum. The variation in dispersivity is scale-dependent (Gelhar et al., 1992), and as such, minimum and maximum dispersivity was set to 0.1 and 1% of the model domain length of 600 meters. The variation in the diffusion coefficient is compound- and site-specific, but as information on this is not currently available, minimum and maximum values were based on the available literature values for parent and/or daughter isotopes in the Danish waste and the different sedimentary rocks. The literature values for the diffusion coefficient are listed in Table 3. For the hydraulic conductivities of the Quaternary/Pre-quaternary and fractured chalk, the minimum and maximum were based on the calibrated minimum and maximum values in the DK-model. For the upper and lower chalk, the minimum and maximum hydraulic conductivity and porosity values were based on the

***Table 3**. Diffusion coefficients (m^2/s) compiled from the studies on nuclides transport in sedimentary rocks.*

***Tabel 3**. Diffusionskoefficienter (m^2/s) baseret på undersøgelser af nuklidtransport i sedimentære bjergarter.*

source:	1	2	3	4	5	6	7	MEDIAN
general	5.0E-12 to 2.5E-10		1.5E-11				1.6E-10	8.8E-11
Ac-227	2.5E-10							2.5E-10
Am-241	2.5E-10							2.5E-10
Am-243	2.5E-10							2.5E-10
C-14	5.0E-12 to 1.0E-11			4.9E-11				1.0E-11
Ca-41	2.5E-10 to 5.0E-10					2.0E-10		2.5E-10
Cm-244	2.5E-10							2.5E-10
Cm-245	2.5E-10							2.5E-10
Cm-246	2.5E-10							2.5E-10
Cs-135	2.5E-10 to 5.0E-10	5.0E-11			3.8E-10 to 9.2E-10	2.3E-10		3.2E-10
H-3					2.4E-12 to 3.5E-11			1.9E-11

source:	1	2	3	4	5	6	7	MEDIAN
I-129	5.0E-12 to 1.0E-11	3.0E-14 to 1.6E-11		4.9E-11	2.0E-12	6.9E-12		8.5E-12
Ni-59	2.5E-10 to 5.0E-10							3.8E-10
Np-237	2.5E-10							2.5E-10
Pa-231	2.5E-10							2.5E-10
Pb-210	2.5E-10							2.5E-10
Pu-239	2.5E-10							2.5E-10
Pu-240	2.5E-10							2.5E-10
Pu-241	2.5E-10							2.5E-10
Pu-242	2.5E-10	1.4E-11 to 5.0E-11						3.3E-11
Ra-226	2.5E-10							2.5E-10
Se-79	5.0E-12 to 1.0E-11							7.5E-12
Sn-126	2.5E-10 to 5.0E-10							3.8E-10
Tc-99	2.5E-10 to 5.0E-10							3.8E-10
Th-229	2.5E-10							2.5E-10
Th-230	2.5E-10							2.5E-10
Th-232	2.5E-10							2.5E-10
U-233	2.5E-10							2.5E-10
U-234	2.5E-10	5.0E-11						1.5E-10
U-235	2.5E-10							2.5E-10
U-236	2.5E-10							2.5E-10
U-238	2.5E-10							2.5E-10

1 – ANDRA, 2005b; 2 – Bourgeat et al., 2004; 3 – De Windt et al., 2004; 4 – Enssle et al., 2014; 5 – Grambow et al., 2014; 6 – Tournassat and Steefel, 2015; 7 – LaVenue et al., 1990.

borehole data (Appendix B). Claystone porosity values were collected from borehole data, and hydraulic conductivities were estimated from claystone porosity-permeability relationship in the Danish basin (Appendix C).

An overview of the different parameter values is given in Table 2, where the minimum and maximum parameter values are listed for the hydraulic gradient, dispersivity, and diffusion coefficient which were assumed to be independent of the different hydrological units and each other. The applied minimum and maximum values for effective porosity were varied according to the different hydrogeological units. The variation in hydraulic gradient is indeed site-specific and here the variation ranged a factor of ten to assess the sensitivity of simulated BTC to increasing the hydraulic gradient. It is noted that the median K value for the fractured chalk is relatively low considering that it is representative of fractured media. At the same

time, the maximum K value for the fractured chalk is relatively high. The reason is that fractured chalk is treated as equivalent porous medium in the DK-model, where the variation in K within the chalk is governed by the fracture density. Hence, higher K values represent the fractured part of the chalk while the lower K values represent the non-fractured part of the chalk. The distribution of the K values within the chalk is not normally distributed and neither is the logarithm of the K values (not shown). Therefore, the median K value is implemented despite the relatively low value. The applied median value for the fractured chalk is still larger than the lower chalk formations. As the location, at which the concentration is evaluated in the models, is within the middle of fractured chalk with an extent of 50 meters, the effect of its K value will be minor. Further, the K range within the minimum and maximum values for the fractured chalk are sampled in the generation of the realizations.

Since step 1 entails assessing the breakthrough time for the maximum concentration with varying parameter values, best- and worst-case ensembles are not readily determined. For instance, a realization with a high dispersivity value could lead to a faster breakthrough of maximum concentration relative to a realization with lower dispersivity where the actual magnitude in concentration with increasing dispersivity may be lower. Therefore, as the minimum and maximum values for four parameters were altered, a total of 16 ensembles (2^4) were evaluated according to Table 4. I.e., to generate each of the ensembles, K was randomized while using either the minimum or maximum parameter value for porosity, diffusion coefficient, dispersivity, and hydraulic gradient.

***Table 4**. Ensemble overview using minimum and maximum parameter values in the stochastic model runs. For each ensemble, the K-values for the formations present in the model were varied generating an ensemble for each scenario.*

***Tabel 4**. Ensemble overblik med anvendelse af minimum og maksimum parameter værdier i stokastiske modelkørsler. For hvert ensemble, blev K-værdien for formationerne i modellen varieret for at generere et ensemble for hvert scenarie.*

Ensemble	Effective porosity		Diffusion coefficient		Dispersivity		Gradient	
	Minimum	Maximum	Minimum	Maximum	Minimum	Maximum	Minimum	Maximum
1	X			x	x		x	
2		X		x	x		x	
3	X		x		x		x	
4		X	x		x		x	
5	X			x		x	x	
6		X		x		x	x	
7	X		x			x	x	
8		X	x			x	x	
9	X			x	x			x
10		X		x	x			x
11	X		x		x			x
12		X	x		x			x
13	X			x		x		x
14		X		x		x		x
15	X		x			x		x
16		X	x			x		x

To test the sensitivity of the host rock formation thickness, additional ensembles to Table 4 were simulated. With different thicknesses of the host rock formation, median porosity and diffusion coefficient values, and minimum dispersivity and gradient, K was randomized within the different geological units (Table 5). Thus, in ensembles 17 the host rock thickness was maintained at the initial thickness according to Figure 11. In ensemble 18, the host rock formation thickness was increased by 50% of its thickness above the repository depth, and in ensemble 19 the host rock formation thickness was decreased by 50%. In ensemble 20, which was simulated only for the claystone, an ensemble of stochastic solutions was generated by replacing median hydraulic conductivity in the Latin Hypercube set up with a harmonic mean. The harmonic mean represents a perfectly layered claystone-sandstone system and in Danish claystone it is two orders of magnitude lower than a median hydraulic conductivity. Assumption of a perfectly layered claystone-sandstone system does not represent an average claystone setting at 500 meters in Denmark. Therefore, the best-case scenario for a perfectly layered claystone system was tested in ensemble 20. The median hydraulic conductivity, better representing the bulk properties of Danish claystone at 500 meters, was used in the remaining ensembles. The randomization of the claystone is based on the deduction of the harmonic mean of K and the associated geostatistical parameters (Appendix C), while the K randomization of the remaining units is based on Table 2.

***Table 5**. Ensemble overview using average, minimum and maximum barrier thickness and varying K-values in claystone between median and harmonic mean.*

***Tabel 5**. Ensemble oversigt for anvendelse af gennemsnit, minimum og maksimum barrieretykkelse og varierende K-værdier i lersten i forhold til medianen og det harmoniske gennemsnit.*

	Barrier thickness	Effective porosity	Diffusion coefficient	Dispersivity	Gradient
Ensemble 17	Initial	Median	Median	Minimum	Minimum
Ensemble 18	+50% of initial	Median	Median	Minimum	Minimum
Ensemble 19	-50% of initial	Median	Median	Minimum	Minimum
Ensemble 20*	Initial	Median	Median	Minimum	Minimum

*Only simulated for the claystone, where the K values are represented by the harmonic means.

5.3 Reactive transport modeling

Nuclides transport is site-specific and governed by various factors: (1) repository and engineered barriers design, (2) physical and chemical properties of the engineered barriers, (3) hydrogeological properties and mineralogy of the formation, (4) groundwater chemistry, (5) temporal changes in the properties of the engineered barriers, host rock formation, and groundwater chemistry, and (6) specific nuclide properties, e.g., half-life, solubility, and adsorption (Sections 2.4, 2.5, 2.6 and 3.1). A reactive transport model for one set of parameters representing the clay and chalk as host rock formations is set up instead of using a stochastic ensemble. The reason being that (1) the site-specific information and the repository design are unknown at the current stage, (2) nuclides release and its duration depend on the solubility, groundwater chemistry, and flow rate, (3) the simulation time of the solute transport

models is long and they should be kept relatively simple compared to the flow models to avoid numerical errors (Konikow, 2011), and (4) the host rock formation potential of Danish formations for the worst- and best-case scenarios were estimated and the host rock formation properties were identified in step 1.

5.3.1 Conservative transport model

As the sensitivity of the model to the variation in hydraulic parameters was analyzed in step 1, the conservative transport model was later developed into a reactive transport model constructed using median hydraulic conductivity, effective porosity, diffusion coefficients, minimum hydraulic gradient, and dispersivity (Table 2). The conceptual model setup is similar to that in the stochastic runs (Figure 11). The first arrival time of a conservative tracer (i.e., tracer concentration greater than zero) at the groundwater abstraction depth is used in the process of selecting the nuclides to include in the reactive transport model. Nuclides that decayed to levels with negligible activity prior to the first arrival time were excluded from the reactive transport modeling.

5.3.2 Nuclides selection

Danish radioactive waste comprises 21 waste types and 42 nuclides (COWI, 2011a). 16 of the nuclides reported by COWI (2011a) decay into daughter products through the uranium, thorium, actinium, and neptunium series (Friedlander et al., 1981; Be et al., 2016; Figure 12). Additionally, three short decay series of Pm-147, Sn-113, and Sr-90 occur (Be et al., 2016; Figure 12). The remaining nuclides decay to stable isotopes. The resulting total number of nuclides, parents, and daughters, in the waste, is 100.

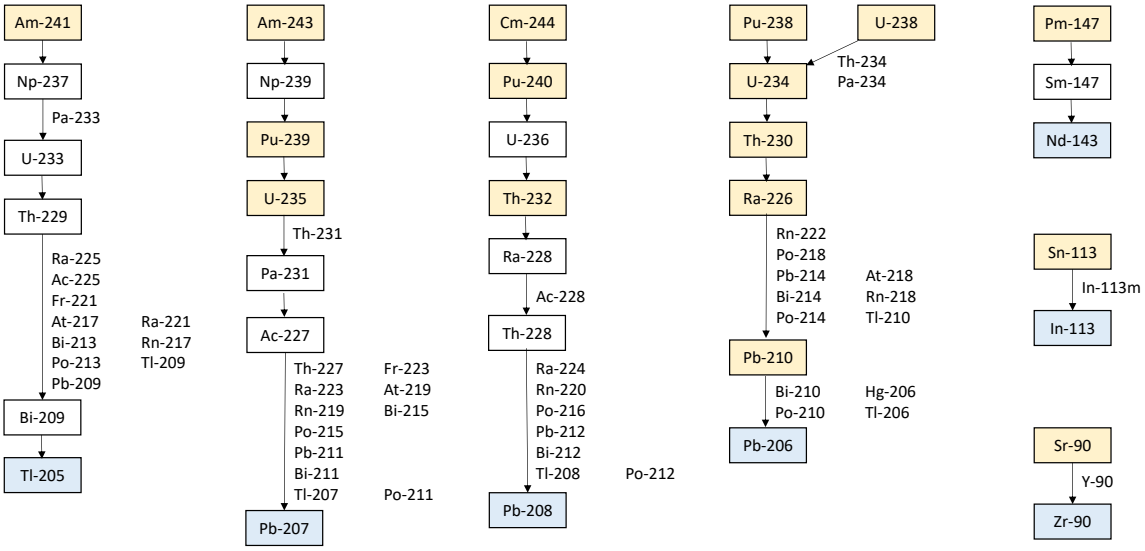

***Figure 12**. Decay chains in Danish radioactive waste. Isotopes marked in yellow are nuclides reported by COWI (2011a). Isotopes marked in blue are the stable decay products. Nuclides with half-life below 1 yr. are indicated along the arrows.*

Figur 12 (forrige side). *Nedbrydningsveje for det danske radioaktive affald. Isotoper markeret med gult er nuklider afrapporteret af COWI (2011a). Isotoper markeret med blå er stabile nedbrydningsprodukter. Nuklider med halveringstider under 1 år er vist langs pilene.*

Prior to the selection of nuclides for reactive transport modeling, decay of the parent nuclides and production and decay of daughter isotopes in each waste type throughout 1 Myr were estimated. The amount of the parent nuclides at the source (*N*) throughout the time (*t*) was estimated using the decay law (Friedlander et al., 1981):

$$N = N_0 \times e^{-\lambda t} \quad \text{(Equation 8)}$$

where N is the amount of the nuclide at the time *t*, N_0 is the amount of the nuclide at the time t_0 and λ is the decay constant related to the half-life ($t_{½}$) by the equation (Friedlander et al., 1981):

$$t_{½} = \frac{ln2}{\lambda} \quad \text{(Equation 9)}$$

The amount of the first daughter isotope (N_2) after the time (*t*) was derived from the equation (Friedlander et al., 1981):

$$N_2 = \frac{\lambda_1}{(\lambda_2 - \lambda_1)} \times N_1^0 \times \left(e^{-t\lambda_1} - e^{-t\lambda_2}\right) + N_2^0 \times e^{-t\lambda_2} \quad \text{(Equation 10)}$$

where λ_1 and λ_2 are the decay constants of the parent and daughter isotopes, respectively, and N_1^0 and N_2^0 are the amount of the parent and daughter isotopes at the time t_0.

The production and decay of the successive daughters were calculated using Bateman's equation (Friedlander et al., 1981):

$$N_n = C_1 \times e^{-t\lambda_1} + C_2 \times e^{-t\lambda_2} + \cdots C_n \times e^{-t\lambda_n} \quad \text{(Equation 11)}$$

$$C_1 = \frac{\lambda_1 \times \lambda_2 \times \ldots \lambda_{n-1}}{(\lambda_2 - \lambda_1) \times (\lambda_3 - \lambda_1) \times \ldots (\lambda_n - \lambda_1)} \times N_1^0 \quad \text{(Equation 11a)}$$

$$C_2 = \frac{\lambda_1 \times \lambda_2 \times \ldots \lambda_{n-1}}{(\lambda_1 - \lambda_2) \times (\lambda_3 - \lambda_2) \times \ldots (\lambda_n - \lambda_2)} \times N_1^0 \quad \text{(Equation 11b)}$$

$$C_n = \frac{\lambda_1 \times \lambda_2 \times \ldots \lambda_{n-1}}{(\lambda_1 - \lambda_n) \times (\lambda_2 - \lambda_n) \times \ldots (\lambda_{n-1} - \lambda_n)} \times N_1^0 \quad \text{(Equation 11c)}$$

where N_n is the amount of the n^{th} daughter after a time (*t*), N_1^0 is the amount of the parent isotope at the time t_0, and λ_1, λ_2… λ_n are the decay constants of the parent and daughter isotopes. (Noting that the term (λ_n - λ_n) is always absent helps in seeing the structure of the equations).

In the next step, the changes in the amount of nuclides in the waste throughout 1 Myr were transformed into activities (A) according to the equation (Friedlander et al., 1981):

$$A = n \times N_a \times \frac{ln2}{t_{½}} \quad \text{(Equation 12)}$$

where n is the amount of moles of isotope and N_a is the Avogadro constant. The activities were transformed into yearly doses (D) by the equation (WHO, 2008):

$$D = A \times h_{ing} \quad \text{(Equation 13)}$$

where h_{ing} is the dose coefficient for ingestion by adults (mSv/Bq) calculated from (WHO, 2008):

$$h_{ing} = \frac{IDC}{GL \times q} \quad \text{(Equation 14)}$$

where *IDC* is individual dose criterion equal to 0.1 mSv/yr, *GL* is WHO guidance level of nuclide in drinking water (Bq/L), and *q* is annual water intake (L).

It was assumed that: (1) a person consumes 730 L/yr (WHO, 2008), (2) the contaminated water is not diluted along the flow path due to 3D flow and mixing nor by mixing at the water intake, (3) there are no solubility limits and the entire pool of the nuclide in each waste type leaves the repository, (4) retardation due to sorption is not included, (5) concentration effects caused by drinking water treatment are not included, and (6) there are no solubility limits and the entire pool of the nuclide in each waste type leaves the repository. These assumptions are conservative and were used to exclude the least harmful nuclides from the reactive transport modeling, including all nuclides with a half-life x 10 less than 10 kyr. The threshold of a half-life x 10 less than 10 kyr was selected as (1) simulated concentration of the conservative tracer at the average abstraction depth is zero within the first 10 kyr (Section 6.2) and (2) nuclides activity after a period of half-life x 10 is below harmful levels. In the next step, a solubility constraint was added to select the most harmful nuclides from the remaining pool.

Nuclides where the half-life x 10 is less than 10 kyr, equivalent to 82 in total, were excluded from the reactive transport modeling. The reason is that their activity and dose from the annual water intake, calculated from Equations 8–14, after 10 kyr do not exceed WHO limits for nuclides activity in drinking water and annual doses, even under the conservative assumption that the released amount of nuclide is not limited by solubility. If the engineered barriers would fail on the first day after closure of the radioactive waste repository, the conservative tracer concentration is zero at the abstraction level after 10 kyr of simulation in the models set, as described in Section 6.2.

Based on the above solution, 18 nuclides remained (Figure 13). At this stage, their release was assumed to be constrained by solubility and changes in their amount, activity, and resulting dose from the annual water intake from the abstraction level throughout 1 Myr was calculated using Equations 8–14 under the assumption that there is no dilution caused by mixing during transport or at the abstraction level. Nuclide solubilities were assumed as in the assessment of the Callovio-Oxfordian claystone (ANDRA, 2005b) and an overview of

nuclides solubilities in the literature is given in Table 6. Since Ca-41 (total amount of 6 g) in the Danish waste is found in the concrete (200 t), only a fraction of Ca solubility (7×10^{-8}) was assigned to Ca-41. For the selected 18 nuclides, half-life (Be et al., 2016), selected solubilities (ANDRA, 2005b), WHO guidance levels, dose coefficients (WHO, 2008), and decay mode (Friedlander et al., 1981) are presented in Table 7.

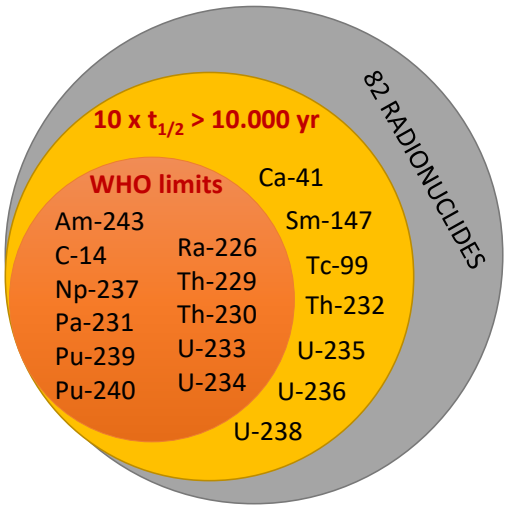

***Figure 13**. Nuclides selection for the reactive transport modeling. Nuclides in the two inner circles has a 10 × half-life above 10 kyr. WHO dose-limits from the annual water intake was exceeded within 1 Myr for 11 nuclides in the innermost circle.*

***Figur 13**. Nuklid udvælgelse for reaktiv transportmodellering. Nuklider i de to inderste ringe har en halveringstid x 10 større end 10.000 år. WHO grænseværdier for det årlige vandindtag blev overskredet inden for 1 M år for 11 nuklider i den inderste cirkel.*

Nuclides that do not exceed WHO limits (WHO, 2008) – the gross α activity of 0.5 Bq/L, gross β activity of 1 Bq/L and the dose of 0.1 mSv/yr from the annual drinking water intake from the water abstraction level, at any time within 1 Myr, either due to solubility limits or long half-life time preventing high activity and therefore dose exceedance – were also excluded from the reactive transport modeling. Consequently, the model was set up for 11 nuclides – Am-243, C-14, Np-237, Pa-231, Pu-239, Pu-240, Ra-226, Th-229, Th-230, U-233, and U-234 (Figure 13).

***Table 6**. Solubility (mol/m^3) of the selected 18 nuclides.*

***Tabel 6**. Opløselighed (mol/m^3) for de 18 udvalgte nuklider.*

Source:	1	2	3	4	5	6	7	8	9	10	11
Am-241	4.0E-4	7.7E-7 to 1.2E-4	1.0E-4 to 1.0E-2	1.0E-4			5.6E-5 to 9.2E-4	0.011	0.01		1.0E-7 to 1.0E-4
C-14	2.3			1			unlim-ited	unlim-ited	10		
Ca-41	2.3			10							
Np-237	4.0E-6	3.4E.13 to 3.4E-6	1.0E-5 to 1.0E-4	1.0E-6			7.2E-7 to 1.1E-6	1.1E-6	0.01	1.0E-12	1.0E-13 to 1.0E-6
Pa-231	1.0E-3		1.0E-4	1.0E-4			2.8E-4 to 3.2E-4	1.0E-5	0.001	3.0E-4	1.0E-7 to 1.0E-2
Pu-239	2.0E-4	1.4E-13 to 6.3E-8	1.0E-7 to 1.0E-3	1.0E-5			1.3E-7 to 1.1E-3				1.0E-13 to 1.0E-8
Pu-240	2.0E-4							6.3E-6	0.001	1.0E-6	
Ra-226	1.0E-4		1.0E-4 to 1.0E-3	1.0E-5	1.0E-5		2.2E-5 to 8.8E-4	6.7E-8	0.001		1.0E-3
Sm-151			1.0E-4 to 1.0E-2	1.0E-4			1.8E-6 to 7.5E-5	3.6E-4			
Tc-99	4.0E-6		1.0E-6 to 1.0E-5	1.0E-5	0.1		4.0E-6 to 4.5E-6	3.9E-6	0.1	1.0E-9	
Th-229	6.0E-4	6.1E-12 to 5.9E-6	1.0E-7 to 1.0E-6	1.0E-6		1.0E-5 to 1.0E-3	6.8E-7 to 6.3E-6				1.0E-12 to 1.0E-6
Th-230	6.0E-4							4.2E-6	0.001	1.0E-6	
Th-232	6.0E-4										
U-233	7.0E-4	9.7E-7 to 2.2E-3	1.0E-5 to 1.0E-4	1.0E-6	1.0E-3	1.0E-8 to 1.0E-4	6.2E-7 to 2.3E-6	2.4E-5	0.1	1.0E-5	1.0E-6 to 1.0E-2
U-234	7.0E-4									1.0E-5	
U-235	7.0E-4										
U-236	7.0E-4									1.0E-5	
U-238	7.0E-4									1.0E-5	

1 – ANDRA, 2005b; 2 – Baik et al., 2008; 3 – Bruno et al., 1997; 4 – COWI, 2011a; 5 – De Windt et al., 2004; 6 – Kim et al., 2009; 7 – Nykyri et al., 2008; 8 – Poteri et al., 2014; 9 – Schwartz, 2012; 10 – Schwartz, 2018; 11 – Stockman and Steinbarn, 2000.

***Table 7**. Half-life (yr), solubility (mol/L), WHO guidance levels (Bq/L), dose coefficients (mSv/Bq) and decay mode for the selected 18 nuclides.*

***Tabel 7**. Halveringstider (år), opløselighed (mol/L), WHO vejledende niveauer (Bq/L), dosis-koefficienter (mSv/Bq) og henfaldstype for de 18 udvalgte nuklider.*

	Half-life [yr]	Solubility [mol/L]	WHO guidance level [Bq/L]	Dose coefficient [mSv/Bq]	Decay mode
Am-241	7.4E3	4.0E-7	1	1.37E-4	Alpha
C-14	5.7E3	2.3E-3	100	1.37E-6	Beta
Ca-41	1.0E5	1.6E-10	100	1.37E-6	EC
Np-237	2.1E9	4.0E-9	1	1.37E-4	Alpha
Pa-231	3.2E4	1.0E-6	0.1	1.37E-3	Alpha
Pu-239	2.4E4	2.0E-7	1	1.37E-4	Alpha
Pu-240	6.6E3	2.0E-7	1	1.37E-4	Alpha
Ra-226	1.6E3	1.0E-7	1	1.37E-4	Alpha
Sm-147	1.1E11	3.6E-7	100	1.37E-6	Alpha
Tc-99	2.1E5	4.0E-9	100	1.37E-6	Beta
Th-229	7.9E3	6.0E-7	0.1	1.37E-3	Alpha
Th-230	7.5E4	6.0E-7	1	1.37E-4	Alpha
Th-232	1.4E10	6.0E-7	1	1.37E-4	Alpha
U-233	1.6E5	7.0E-7	1	1.37E-4	Beta
U-234	2.5E5	7.0E-7	1	1.37E-4	Alpha
U-235	7.0E8	7.0E-7	1	1.37E-4	Alpha
U-236	2.3E7	7.0E-7	1	1.37E-4	Alpha
U-238	4.5E9	7.0E-7	10	1.37E-5	Alpha

5.3.3 Reactive transport model

The conservative transport model (Section 5.3.1) was developed into reactive transport models for 11 nuclides (Section 5.3.2). The exact repository design is unknown at the present stage, so it was assumed that the total amount of each nuclide summed up for 21 waste types is released at 500 meters through a 1×1 m^2 cross-section. The nuclide source is either continuous or transient and limited by solubility. Temporal changes in nuclide release are estimated based on the total amount of nuclide in the waste changing over time due to the radioactive decay and volumes of water flushed through the source cell. Nuclide release is set at the solubility limit and changed to zero either when its total amount is flushed out from the waste or when the amount in the waste decreased below solubility due to the radioactive decay. Because of the difference in porewater flow velocity between chalk and claystone model, Am-243 is released until 2.6 kyr in the chalk model and 84 kyr in the claystone model. C-14 release stopped at 96 yr in the chalk model and 36 kyr in the claystone model. The remaining nuclides were constantly produced as daughter isotopes and therefore set as a continuous source.

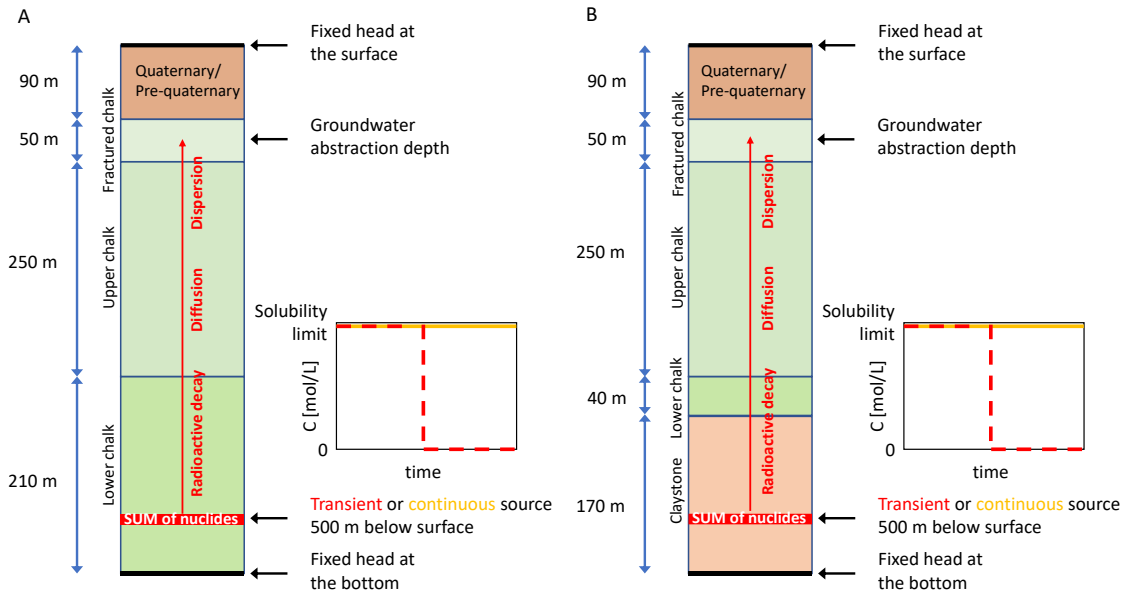

***Figure 14**. Conceptual reactive transport model for A) chalk as host rock formation, and B) claystone as host rock formation.*

***Figur 14**. Konceptuel reaktiv transportmodel for A) kalk som værtsbjergartsformation, og B) lersten som værtsbjergartsformation.*

The release concentrations are set at the solubility levels (Table 7), except for nuclides with more than one isotope (Pu, Th, U), where solubility was divided between isotopes proportionally to their fraction in the waste. The fraction of the isotopes was: 0.74 for Pu-239, 0.26 for Pu-240, nearly 1.0 for Th-230 and U-234, 6.6E-6 for Th-229, and 5.8E-5 for U-233. Radioactive decay was set as a first-order irreversible kinetic reaction with a decay constant λ estimated from Equation 9 and a half-life in Table 7. Sorption was not included in the model as the sorption coefficients are site-specific and related to the mineralogy and groundwater chemistry in both, engineered barriers and the host rock formation (Section 2.6.2). Conceptual reactive transport models for chalk and claystone are shown in Figure 14. Concentration BTCs for each nuclide was sampled at the groundwater abstraction depth. The models were used as an indication of the relative effects of the different geological settings and parameter sensitivities.

6. Results

6.1 Stochastic modeling

6.1.1 Chalk as host rock formation

The BTCs from all realizations of each ensemble for chalk as host rock formation (Table 4) are given in Appendix D. Here, the average from the ensembles is shown. In Figures 15 to 18, the average BTC from scenarios 1 to 4, 5 to 8, 9 to 12, and 13 to 16 are shown.

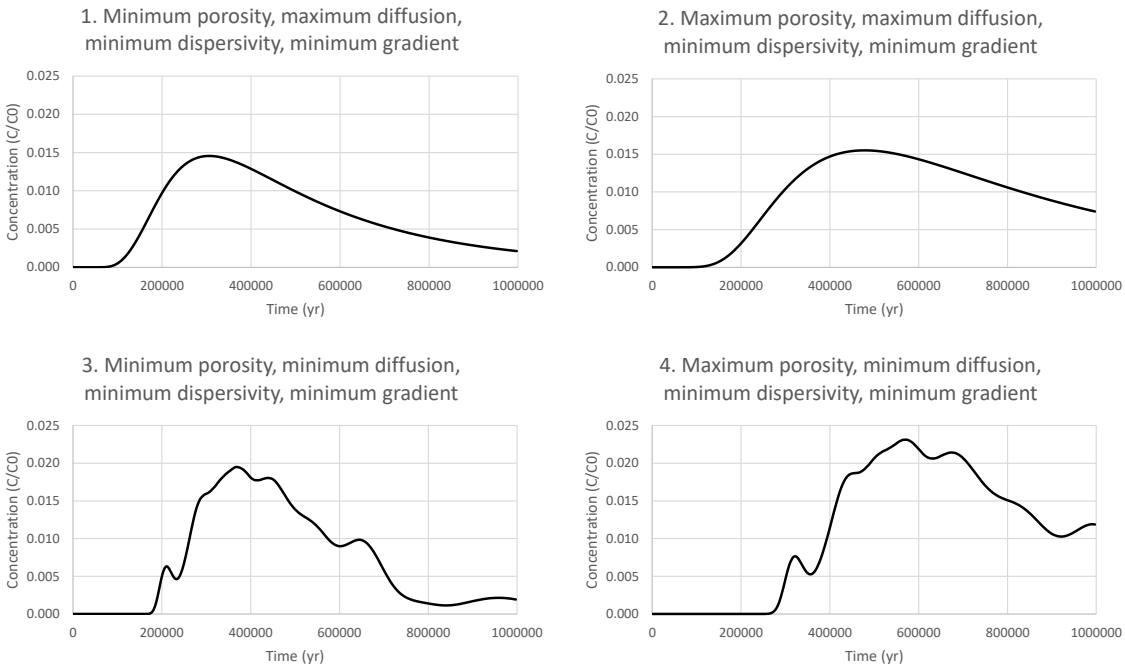

***Figure 15**. Average BTCs from scenarios 1 to 4 as relative concentration vs. time. The number in the heading of each plot refers to the ensembles listed in Table 4.*

***Figur 15**. Gennemsnitlige gennembrudskurver for scenarier 1 til 4 vist som relative koncentration mod tid. Numrene i figuroverskrifterne relaterer til ensemblerne angivet i Tabel 4.*

In ensembles 1 and 2, the difference was related to a change in effective porosity (Table 4), and the effect on the arrival time for the average peak concentration is clear. The increase in effective porosity and thus the porewater velocity led to a delay in average peak concentrations of around 170 kyr (Figure 15, Table 8). The difference between ensembles 1 and 3 was related to the diffusion coefficient. By changing the diffusion coefficient to the minimum in ensemble 3, the simulated BTCs became less skewed, and the average peak concentration breakthrough time was reduced by around 60 kyr (Figure D1, Table 8). The lower diffusion

coefficient also implies that the average of the ensemble is less smooth. This is a result of the simulated nuclide breakthrough becoming less dispersed with minimal tailing effects resulting in the higher average peak concentrations (Figure 15). I.e., the simulations with minimum diffusion coefficients yield BTCs that are relatively narrow with higher peak concentrations and therefore with the current number of realizations create a less smooth average. In ensembles 3 and 4, the porosity was different (Figure 15), and following the lower porewater velocities from increasing the porosity in ensemble 4, the breakthrough of the average peak concentration is delayed around 200 kyr compared to ensemble 3. In ensembles 2 and 4, two different diffusion coefficients were applied (Table 4) and the change to minimum diffusion coefficient in scenario 4 led to a delay in average peak concentrations of around 90 kyr. Similar to the observed change from scenario 1 to 3, where the diffusion coefficient was changed to the minimum in the latter, the patterns of less skewed BTCs were also observed in scenario 4 compared to scenario 3 (Figures 15 and D1).

***Table 8**. Summary of results from each ensemble within ensembles 1 to 19 based on average peak concentrations.*

***Tabel 8**. Opsummering af resultater for hvert ensemble inden for nummer 1 til 19 baseret på gennemsnitlige maksimale koncentrationer.*

Ensemble	Percentage of initial concentration in peak	Peak concentration time (kyr)	Average porewater velocity (m/d)
1	1.5%	306.8	3.44E-06
2	1.6%	478.5	2.20E-06
3	1.9%	368.9	2.86E-06
4	2.3%	569.8	1.85E-06
5	1.4%	306.8	3.44E-06
6	1.5%	478.5	2.20E-06
7	1.8%	368.9	2.86E-06
8	2.1%	569.8	1.85E-06
9	2.0%	32.9	3.20E-05
10	2.1%	54.8	1.92E-05
11	1.9%	36.5	2.89E-05
12	2.3%	58.4	1.80E-05
13	1.8%	32.9	3.20E-05
14	1.9%	54.8	1.92E-05
15	1.8%	36.5	2.89E-05
16	2.1%	58.4	1.80E-05
17	2.2%	347.0	3.04E-06
18	2.2%	343.3	3.07E-06
19	2.2%	303.2	3.48E-06

In terms of the maximum relative concentration within ensembles 1 to 4, the largest concentrations were simulated in ensemble 4 (Figures 15 and D1). Here, the maximum porosity was applied with the minimum diffusion coefficient and dispersivity. Comparing ensemble 4 to ensemble 2 where the only difference was the maximum diffusion coefficient, the maximum simulated concentration in ensemble 4 was around 2.3% of the initial concentration whereas

the maximum simulated concentration in ensemble 2 was around 1.6%. Likewise, comparing ensemble 3 to ensemble 1 which only differed in having maximum diffusion coefficient, the maximum simulated concentration was around 1.9% whereas the maximum simulated concentration in ensemble 1 was around 1.5%. Nevertheless, the average peak concentration of the ensembles within each of the ensembles, 1 to 4, showed comparable concentrations varying from 1.5 to 2.3% of the initial concentration. Only slight changes (<0.5%) in average peak concentrations were observed when changing the porosities from ensembles 1 to 2 and 3 to 4 (Table 8).

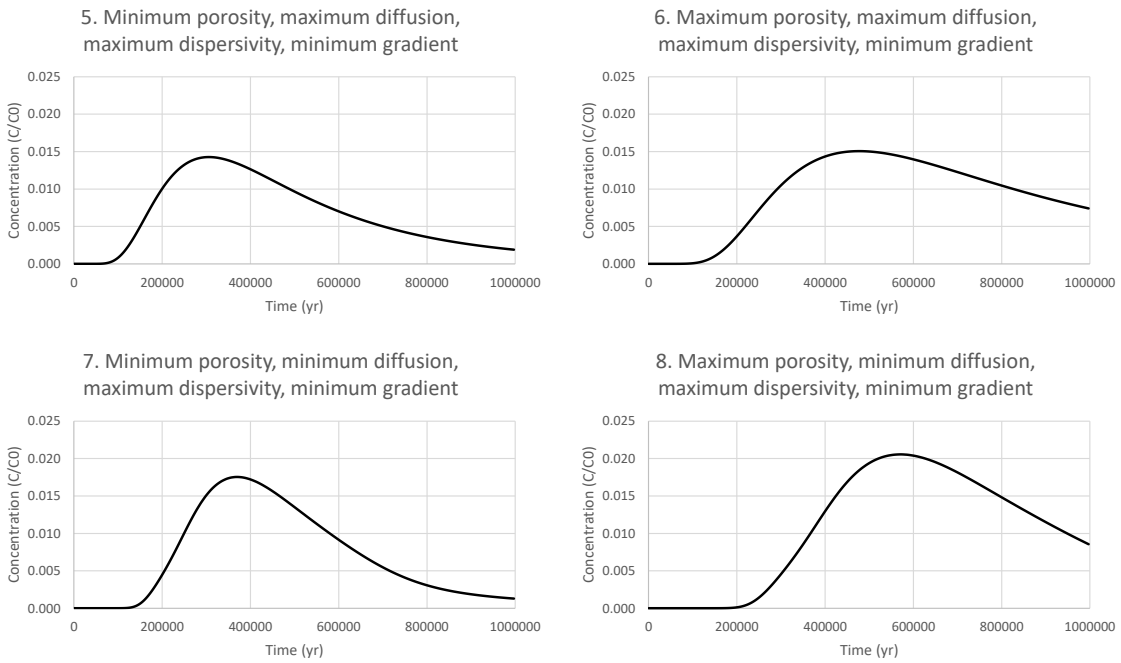

***Figure 16**. Average BTCs from ensembles 5 to 8 as relative concentration vs. time. The number in the heading of each plot refers to the ensembles listed in Table 4.*

***Figur 16**. Gennemsnitlige gennembrudskurver for scenarier 1 til 4 vist som relative koncentration mod tid. Numrene i figuroverskrifterne relaterer til ensemblerne angivet i Tabel 4.*

Compared to ensembles 1 to 4, ensembles 5 to 8 are only different with respect to the maximum dispersivity (Table 4). The changes in breakthrough times for the average peak concentrations as a result of changes in porosity and the diffusion coefficient among ensembles 5 to 8 (Figures 16 and D2) were similar to those described for ensembles 1 to 4 (Figures 15 and D1). As such, the changes in breakthrough times for average peak concentrations of ensembles 5 and 6 were similar to 1 and 2, ensembles 5 and 7 were similar to ensembles 1 and 3, ensembles 7 and 8 were similar to ensembles 3 and 4, and ensembles 6 and 8 were similar to ensembles 2 and 4. Though the breakthrough times for the average peak concentrations were similar, the peak average concentration in ensembles 5 to 8 was slightly lower, around 0.1%, compared to the average peak concentration in ensembles 1 to 4 (Table 8). This is a result of hydrodynamic dispersion (Equation 5a) increasing with an increased dispersivity (Table 9). It is noted that the calculated P_e numbers are all above 2 indicating the

relative importance of advection driven transport although the average calculated porewater velocities are in the order of 10^{-6} to 10^{-5} m/d.

Table 9. *Summary of results for transport regime in ensembles 1–16.*

Tabel 9. *Opsummering af resultater for transportvariabler i ensemble 1–16.*

Ensemble	Average porewater velocity (m/d)	Diffusion (m^2/d)	Hydrodynamic dispersion coefficient (m^2/d)	P_e
1	3.44E-06	8.00E-05	8.21E-05	> 2
2	2.20E-06	8.00E-05	8.13E-05	> 2
3	2.86E-06	2.60E-09	1.72E-06	> 2
4	1.85E-06	2.60E-09	1.11E-06	> 2
5	3.44E-06	8.00E-05	1.01E-04	> 2
6	2.20E-06	8.00E-05	9.32E-05	> 2
7	2.86E-06	2.60E-09	1.72E-05	> 2
8	1.85E-06	2.60E-09	1.11E-05	> 2
9	3.20E-05	8.00E-05	9.92E-05	> 2
10	1.92E-05	8.00E-05	9.15E-05	> 2
11	2.89E-05	2.60E-09	1.73E-05	> 2
12	1.80E-05	2.60E-09	1.08E-05	> 2
13	3.20E-05	8.00E-05	2.72E-04	> 2
14	1.92E-05	8.00E-05	1.95E-04	> 2
15	2.89E-05	2.60E-09	1.73E-04	> 2
16	1.80E-05	2.60E-09	1.08E-04	> 2

In ensembles 9 to 12, the maximum gradient was used compared to ensembles 1 to 4. Since the gradient was increased by a factor of 10, the simulated break-through time of average peak concentrations was also overall decreased by a factor of 10 compared to ensembles 1 to 4. This was also evident from the calculated average velocities (Table 8). With increasing gradient, leaving less time for diffusion, the tailing effect in the BTCs of ensembles 1 and 2 (Figure 15), was less pronounced in ensembles 9 and 10 (Figure 17) resulting in higher average peak concentration.

The results found for ensembles 1 to 2 and 3 to 4 showed that increasing the porosity led to a slower breakthrough time of the average peak concentration, which was also observed in ensembles 9 to 10 and 11 to 12 (Figure 17). Here, the delay caused by using maximum porosities was equivalent to around 22 kyr regardless of the changes in diffusion and dispersivity values. This contrasts with ensembles 1 to 2 and 3 to 4, where the breakthrough times increased by 170 and 200 Kyr, respectively (Table 8). Still, there are substantial differences in the shape of the BTCs when changing from maximum diffusion to minimum diffusion (Figure D3), and again causing the average to be less smooth.

In terms of the maximum relative concentration within ensembles 9 to 12, the largest concentrations were simulated in ensemble 12, where maximum porosity, minimum diffusion, and minimum dispersivity were applied (Figure D3). A general pattern of increasing average peak concentrations was observed when changing to maximum porosities (ensembles 9 and

10, ensembles 11 and 12). Changing the diffusion coefficient, the average peak concentration was similar in ensembles 9 (2%) and 11 (1.9%), while a slight increase occurred from ensemble 10 (2.1%) to 12 (2.3%).

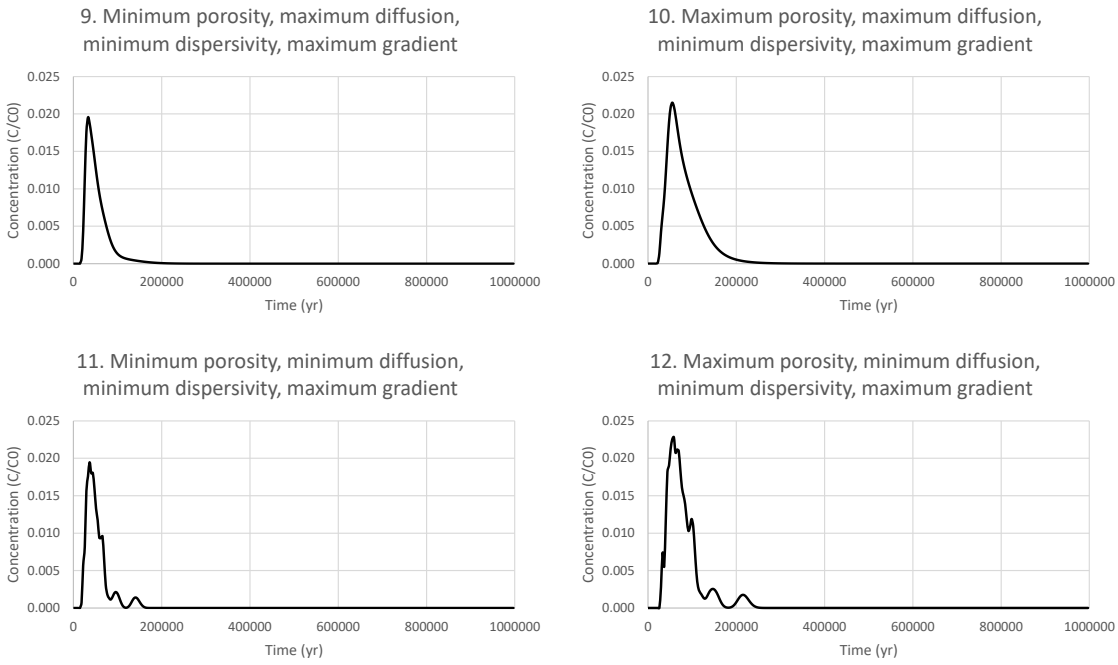

***Figure 17**. Average BTCs from ensembles 9 to 12 as relative concentration vs. time. The number in the heading of each plot refers to the ensembles listed in Table 4.*

***Figur 17**. Gennemsnitlige gennembrudskurver for scenarier 9 til 12 vist som relative koncentration mod tid. Numrene i figuroverskrifterne relaterer til ensemblerne angivet i Tabel 4.*

The changes in breakthrough times for the average peak concentrations from altering the porosity and the diffusion coefficient among ensembles 13 to 16 (Figures 18 and D4) were similar to those described for ensembles 9 to 12 (Figures 17 and D3). As such, the changes in breakthrough times for average peak concentrations of ensembles 13 and 14 were similar to 9 and 10, ensembles 13 and 15 were similar to ensembles 9 and 11, ensembles 15 and 16 were similar to ensembles 11 and 12, and ensembles 14 and 16 were similar to ensembles 10 and 12.

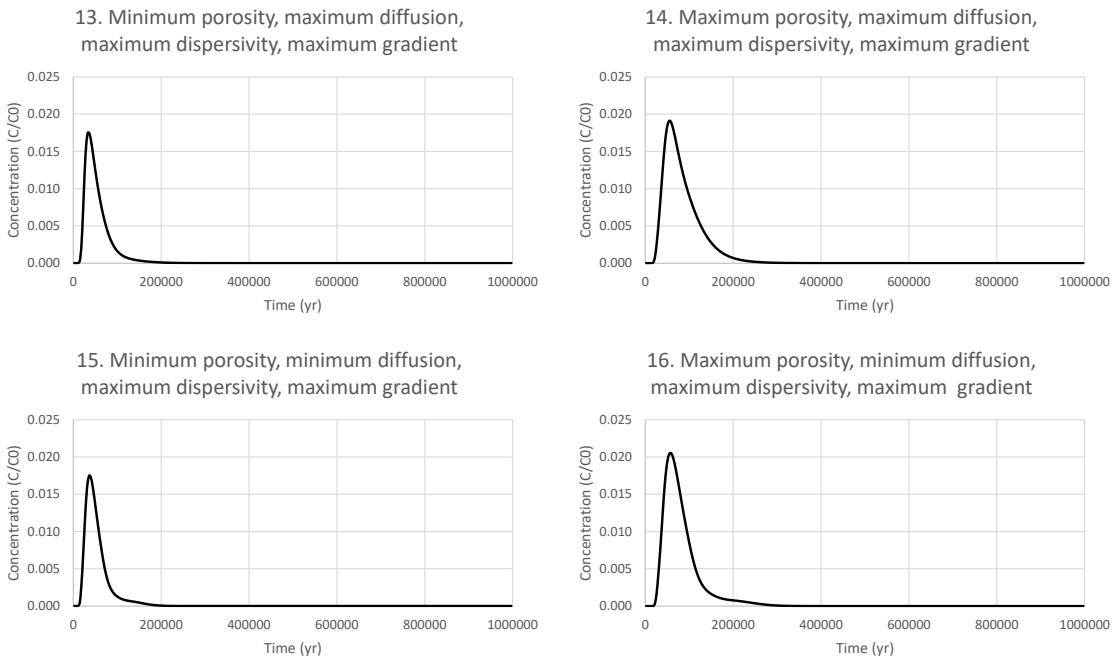

***Figure 18**. Average BTCs from ensembles 13 to 16 as relative concentration vs. time. The number in the heading of each plot refers to the ensembles listed in Table 4.*

***Figur 18**. Gennemsnitlige gennembrudskurver for scenarier 13 til 16 vist som relative koncentration mod tid. Numrene i figuroverskrifterne relaterer til ensemblerne angivet i Tabel 4.*

The changes in breakthrough times for the average peak concentrations from altering the porosity and the diffusion coefficient among ensembles 13 to 16 (Figures 18 and D4) were similar to those described for ensembles 9 to 12 (Figures 17 and D3). As such, the changes in breakthrough times for average peak concentrations of ensembles 13 and 14 were similar to 9 and 10, ensembles 13 and 15 were similar to ensembles 9 and 11, ensembles 15 and 16 were similar to ensembles 11 and 12, and ensembles 14 and 16 were similar to ensembles 10 and 12.

In summary, the 16 stochastic simulation ensembles where four variables were changed to their minimum and maximum value showed that when applying the minimum gradient, the fastest breakthrough time for an average peak concentration from an instantaneous source was achieved after around 300 kyr. At the fastest breakthrough time, the averaged peak concentration was around 1.5% of the initial concentration. When applying the maximum gradient, the fastest breakthrough time for an average peak concentration from an instantaneous source was achieved after around 30 kyr with peak concentrations reaching around 2% of the initial concentration.

6.1.2 Chalk as host rock formation with changing thicknesses

Changing the thickness of the host rock formation yielded differences of around 40 kyr when comparing the arrival time of peak concentrations using minimum and maximum thickness (Table 8). Comparing the maximum thickness in ensemble 18 with the base case thickness in ensemble 17, the peak concentration arrival occurs faster in ensemble 18 (Figures 19 and

D5). This is not expected as the thickness is increased in ensemble 18 compared to ensemble 17. However, when comparing results of ensemble 19 with ensembles 17 and 18, the expected faster arrival of the peak concentration is occurring in ensemble 19 with the minimum thickness of the host rock Lower Chalk. Apparently, also the average velocities are similar for ensembles 17 and 18 (Table 8).

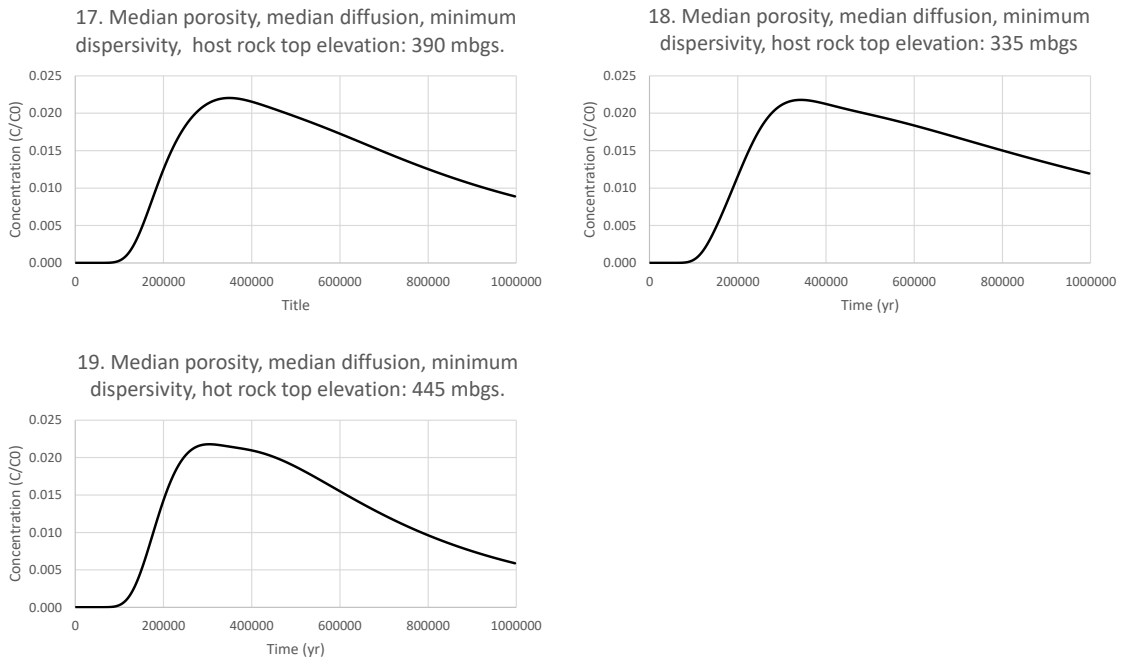

Figure 19*. Average BTCs from ensembles 17 to 19 as relative concentration vs. time. The number in the heading of each plot refers to the ensembles listed in Table 5.*

Figur 19*. Gennemsnitlige gennembrudskurver for ensemble 17 til 19 som relative koncentrationer mod tid. Numrene i figuroverskrifterne relaterer til ensemblerne angivet i Tabel 5.*

6.1.3 Claystone as host rock formation

The BTCs for claystone from the entire ensemble of each ensemble in Table 4 are given in Appendix E. Here, the average from the ensembles is shown. In Figures 20 to 23, the average BTC from scenarios 1 to 4, 5 to 8, 9 to 12, and 13 to 16 are shown.

In all ensembles, the maximum average peak concentrations were not reached within 1 Myr. The change in porosity between ensembles 1 and 2 (Table 4) affected the average BTC concentration and a clear difference is seen at 1 Myr (Figure 20). The increase in porosity and thus decrease in porewater velocity decreased dispersion (Equation 5a) and resulted in higher concentrations throughout time (Figure E1), and thus, a higher average maximum concentration after 1 Myr in ensemble 2 (Table 10). It also caused a delay in the BTC arrivals (Figure E1) with the earliest peak before 200 kyr in ensemble 1 and after 300 kyr in ensemble 2. The difference between ensembles 1 and 3 was related to the diffusion coefficient. The

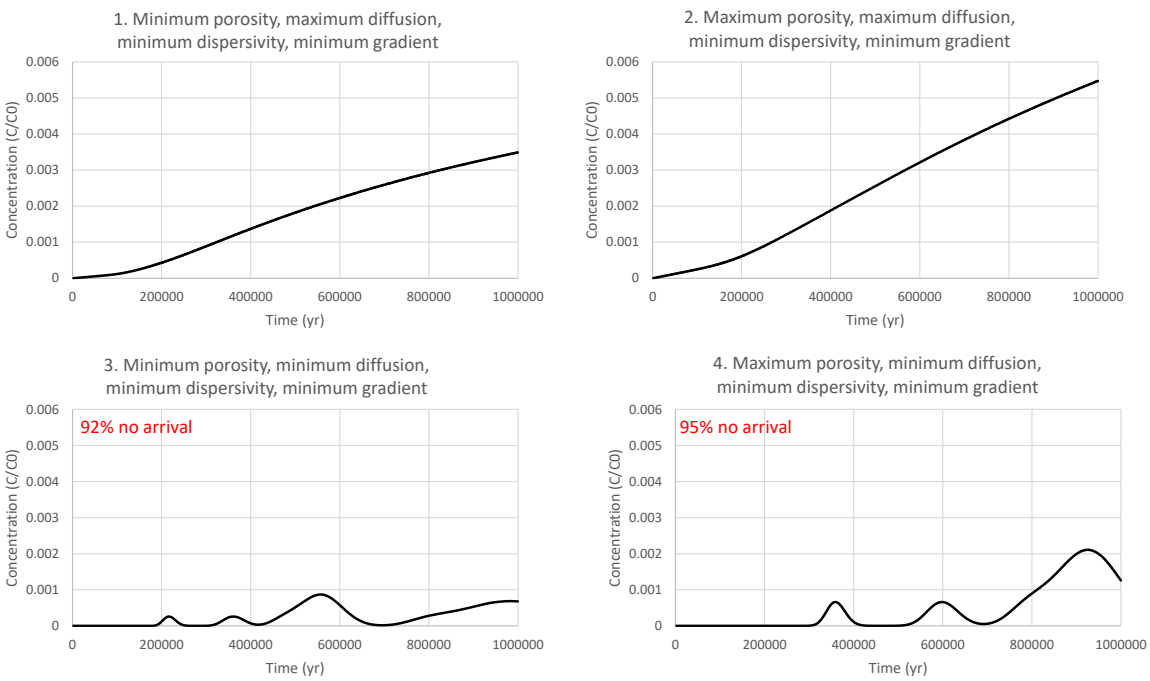

***Figure 20**. Average BTCs from ensembles 1 to 4 as relative concentration vs. time. The number in the heading of each plot refers to the ensembles listed in Table 4.*

***Figur 20**. Gennemsnitlige gennembrudskurver for scenarier 1 til 4 vist som relative koncentration mod tid. Numrene i figuroverskrifterne relaterer til ensemblerne angivet i Tabel 4.*

change of the diffusion coefficient to the minimum in ensemble 3 resulted in a delay of the BTCs arrival and 92% of the BTCs did not reach the abstraction depth within 1 Myr. The BTCs simulated with a minimum diffusion coefficient also became less skewed and had a more uniform peak concentration, around one order of magnitude higher than in ensemble 1. Less skewed BTCs with more uniform peaks are seen in the realizations yielding the average BTC (Figure E1), though the pattern is not pronounced in the depicted average BTC from the ensemble (Figure 20). While 8% of the realizations yield BTCs that have a concentration above zero using the minimum diffusion, the effect of the parameter changes on the average BTC is not pronounced (Figure 20). However, the pattern of less dispersed individual realization BTCs with minimal tailing effects observed in similar ensembles for chalk as host rock formation (Figure D1) is also represented in the current simulations with claystone as host rock formation (Figure E1).

The difference between ensembles 3 and 4 is found for the porosity (Figure 20, Table 4). The lower porewater velocities from increasing the porosity in ensemble 4 resulted in further delay of the BTCs arrival. In 95% of the realizations, the average concentration did not exceed zero within 1 Myr (Figures 20 and E1). The peak concentrations of realizations yielding the average BTC in ensemble 4 are doubled compared to ensemble 3 (Figure E1) because of the decreased dispersion (Equation 5a). An increase of the relative peak concentration when porosity was increased was also observed in chalk, although less distinctive (Figures 15 and D1). A change in the diffusion coefficient from a maximum in ensemble 2, to the minimum in ensemble 4 (Table 4) led to a delay in arrival time such that only 5% of the BTCs arrived before 1 Myr in ensemble 4 (Figures 20 and E1). Realization BTCs yielding an average BTC in ensemble 4 became less skewed compared to BTCs in ensemble 2 (Figure E1). Thus, an

average concentration at 1 Myr decreased in ensemble 4 compared to ensemble 2 (Figure 20). A similar change was observed between ensembles 1 and 3, where the diffusion coefficient was changed to the minimum in the latter and the pattern of less dispersed BTCs was also observed (Figure E1). It is noted that only a minor part of the realizations in ensemble 4 yielded BTCs within 1 Myr (5%), but for the simulated BTCs a similar pattern of less dispersed BTCs with minimal tailing effects was observed in the ensembles for chalk as host rock formation when changing from maximum diffusion to minimum diffusion (Figure D1).

***Table 10**. Summary of results from each ensemble with claystone as host rock formation based on average peak concentrations.*

***Tabel 10**. Opsummering af resultater fra hvert ensemble med lersten som værtsbjergartsformation baseret på gennemsnitlige maksimale koncentrationer.*

Ensemble	Percentage of initial concentration where concentration was highest	Observed concentration time (Myr)
1	0.35%	1
2	0.55%	1
3	0.07%	1
4	0.13%	1
5	0.18%	1
6	0.27%	1
7	0.02%	1
8	0.10%	1
9	0.19%	1
10	0.32%	1
11	0.03%	1
12	0.06%	1
13	0.19%	1
14	0.32%	1
15	0.05%	1
16	0.10%	1
17	0.14%	1
18	0.13%	1
19	0.17%	1
20	0.02%	1

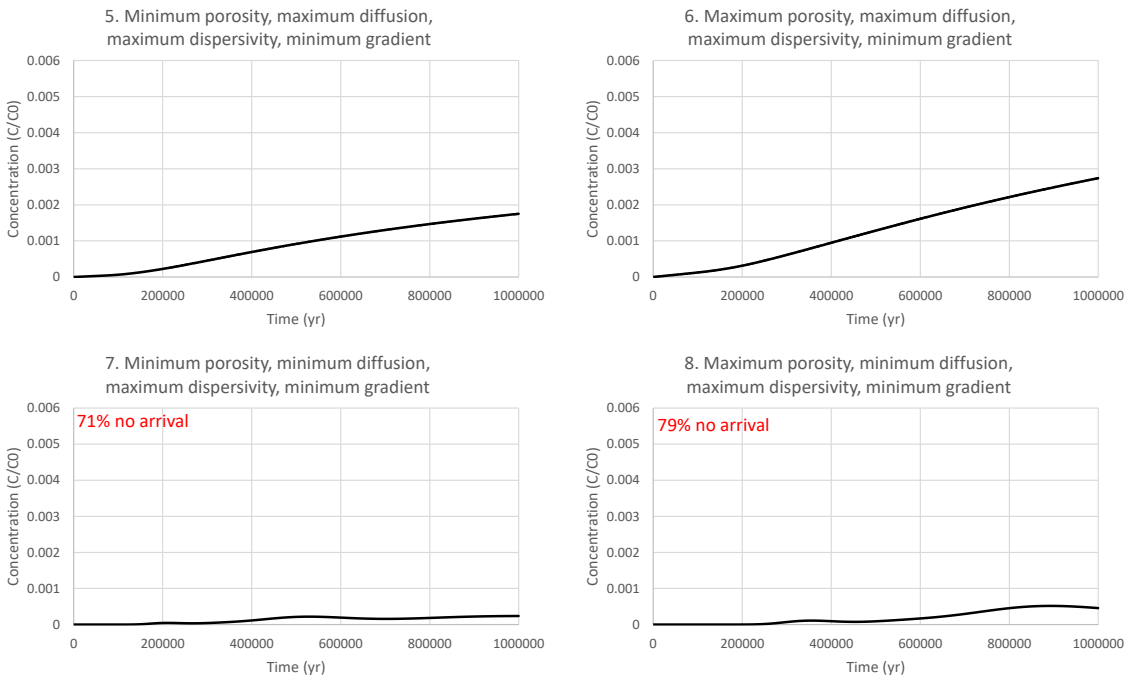

***Figure 21**. Average BTCs from ensembles 5 to 8 as relative concentration vs. time. The number in the heading of each plot refers to the ensembles listed in Table 4.*

***Figur 21**. Gennemsnitlige gennembrudskurver for scenarier 1 til 4 vist som relative koncentration mod tid. Numrene i figuroverskrifterne relaterer til ensemblerne angivet i Tabel 4.*

The largest relative concentration within the realizations of ensembles 1 to 4 was simulated in ensemble 4 (Figure E1) where the maximum porosity was applied with the minimum diffusion coefficient and dispersivity. The maximum simulated relative concentration of a single realization in ensemble 4 was around 16% of the initial concentration whereas the maximum simulated relative concentration of a single realization in ensemble 2, which only differed in having maximum diffusion coefficient, was around 2.5%, showing the importance of diffusion on long time scales (Figure E1). Likewise, a difference in diffusion coefficient between minimum in ensemble 3 and maximum in ensemble 1 resulted in a maximum realization concentration of around 6% and 1.3%, respectively (Figure E1). Contrary, the limited number of BTCs that reached the sampling depth within 1 Myr in ensembles 3 and 4 compared to ensembles 1 and 2 (Figure E1) resulted in lower average concentration at 1 Myr in ensembles 3 and 4 compared to ensembles 1 and 2 (Figure 20). In chalk ensembles, where the peak concentrations of all realization BTCs reached the sampling point, the average peak concentration in ensembles 3 and 4 was higher than in ensembles 1 and 2 (Table 8). A similar effect, because of the decreased dispersion (Equation 5a), could be observed in claystone if all realization BTCs would reach the sampling point. The highest average concentration at 1 Myr and nearly double of that in ensemble 1 was reached in ensemble 2 as a result of a change in the porosity from ensemble 1. Likewise, a nearly doubled average concentration was observed when changing the porosities from ensembles 3 to 4 (Table 10).

Ensembles 5 to 8 were different from ensembles 1 to 4 in the dispersivity which was set at the maximum in ensembles 5 to 8 (Table 4). The changes in the average relative BTC caused by changing the porosity and the diffusion coefficient in ensembles 5 to 8 (Figures 21 and

E2) were similar to those described for ensembles 1 to 4 (Figures 20 and E1). The average concentration at 1 Myr was higher in ensembles 5 and 6 (Figure 21), similar to changes observed in ensembles 1 and 2 (Figure 20), and a delay in BTCs arrival occurred in ensembles 7 and 8 (Figure 21), similar to ensembles 3 and 4 (Figure 20). The observed patterns were: (1) decrease in dispersion (Equation 5a) related to increasing porosity and therefore decreasing porewater velocity (ensemble 6 and 8, Figures 21 and E2), (2) delay in the arrival of the realization BTCs caused by a decrease of a diffusion coefficient (ensemble 7 and 8, Figures 21 and E2). Though the average breakthrough curves showed similar responses to variations in porosity and diffusion, the average concentration at 1 Myr in ensembles 5 to 8 was half of that in ensembles 1 to 4 (Table 10) and the number of realizations that reached the sampling depth within 1 Myr increased to 29% and 21% in ensembles 7 and 8, respectively (Figure E2), as a result of increased dispersivity.

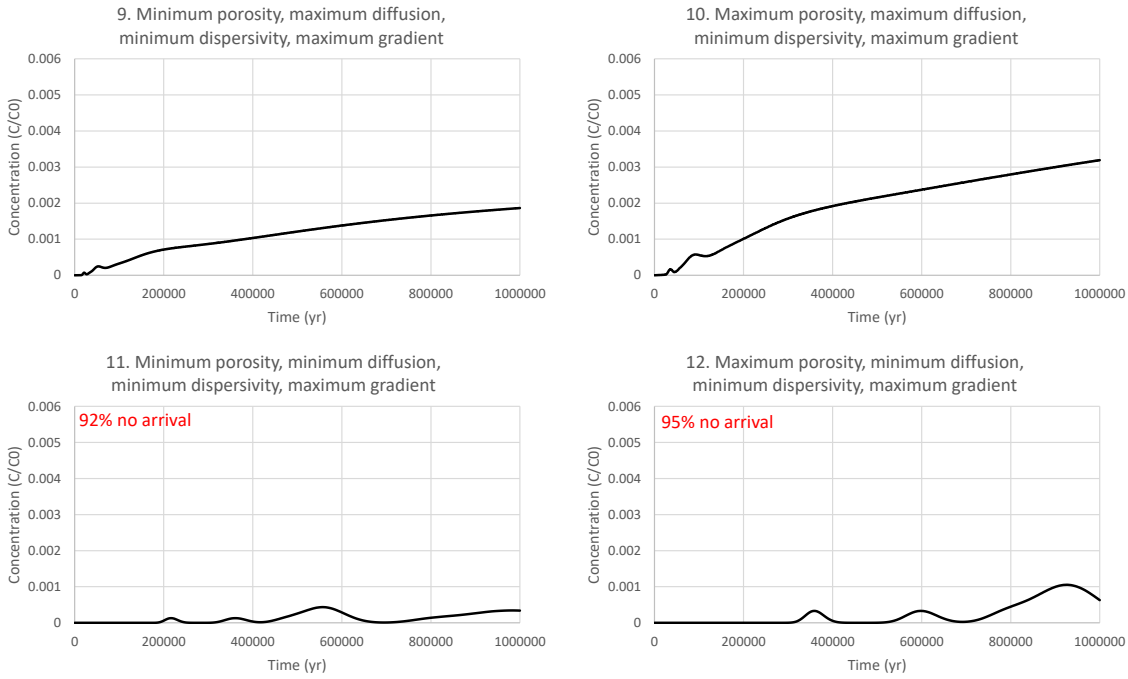

***Figure 22**. Average BTCs from ensembles 9 to 12 as relative concentration vs. time. The number in the heading of each plot refers to the ensembles listed in Table 4.*

***Figur 22**. Gennemsnitlige gennembrudskurver for scenarier 9 til 12 vist som relative koncentration mod tid. Numrene i figuroverskrifterne relaterer til ensemblerne angivet i Tabel 4.*

Compared to ensembles 1 to 4, ensembles 9 to 12 differed only in using the gradient that was increased by a factor of 10. An increase in the gradient led to faster arrivals in ensembles 9 and 10, where the diffusion coefficient was set to the maximum, while the change in gradient has essentially no influence on the arrival times in ensembles 11 and 12 with a minimum diffusion coefficient (Figure E3) compared to ensemble 3 and 4 (Figure E1). Changes in the hydraulic gradient influenced the shape of the BTCs. Ensembles 9 to 12 had less skewed realizations than ensembles 1 to 4 (Figures E1 and E3). Similar to ensembles 1 to 8, an increase in the porosity led to a delay in BTCs arrivals and a doubled average concentration in ensembles 10 and 12 compared to ensembles 9 and 11 (Figures 22 and E3).

The largest relative concentrations within 1 Myr from the realizations of ensembles 9 to 12 were simulated in ensemble 12, where maximum porosity, minimum diffusion, and minimum dispersivity were applied (Figure E3). Still, long transport times resulted in BTC concentration above zero for merely 5% of the realizations, ensemble 12 had a lower average concentration at 1 Myr than ensembles 9 and 10 (Figure 22). Ensembles with maximum porosities (10 and 12) had higher average concentrations compared to ensembles with minimum porosities (9 and 11), as a result of decrease in dispersion (Figure 22). Because of the limited number of realizations in ensembles with minimum diffusion coefficients (9 and 10), the effect of a decreased dispersion is not pronounced in the average relative concentrations (Figure 22). However, realization BTCs in ensembles 11 and 12 have higher peak concentrations than in ensembles 9 and 10 (Figure E3).

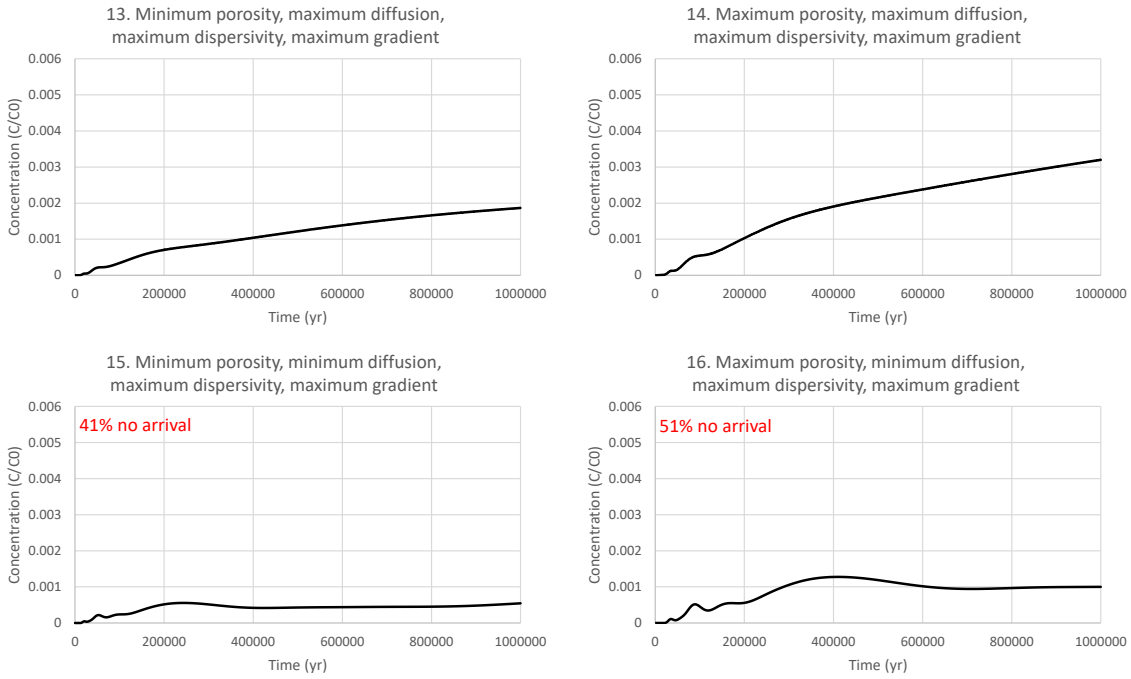

***Figure 23**. Average BTCs from ensembles 13 to 16 as relative concentration vs. time. The number in the heading of each plot refers to the ensembles listed in Table 4.*

***Figur 23**. Gennemsnitlige gennembrudskurver for scenarier 13 til 16 vist som relative koncentration mod tid. Numrene i figuroverskrifterne relaterer til ensemblerne angivet i Tabel 4.*

In ensembles 13 to 16, the dispersivity was set at the maximum compared to the minimum value applied in ensembles 9 to 12. The arrival times and average relative concentrations in ensembles 13 and 14 with maximum diffusion coefficient (Figures 23 and E4, Table 10) were similar to those in ensembles 9 and 10 (Figures 22 and E3, Table 10). Using the maximum dispersivity in ensembles 15 and 16 compared to ensembles 11 and 12 with minimum dispersivity led to a decrease in arrival times. In ensemble 15, a relative concentration above zero within 1 Myr was predicted for 59% of BTCs compared to 8% in ensemble 11, and 49% of BTCs arrived in ensemble 16, compared to 5% in ensemble 12 (Figures 23 and E4), because of an increase in dispersion (Equation 5a). Changes in an average concentration from altering the porosity and the diffusion coefficient among ensembles 13 to 16 (Figures 23 and

E4) were similar to those described for ensembles 9 to 12 (Figures 22 and E3). The average concentration at 1 Myr in ensembles 13 and 14 was equal to those in ensembles 9 and 10, while in ensembles 15 and 16 the average concentration was nearly double compared to ensembles 11 and 12 (Table 10). The concentrations in realizations of ensembles 13 to 16 (Figure E4) were decreased compared to realizations of ensembles 9 to 12 (Figure E3) due to an increase in dispersivity.

In summary, the 16 ensembles of stochastic simulations where four variables were changed to their minimum and maximum values showed that the earliest BTCs arrivals occur in ensembles with a maximum diffusion coefficient while in ensembles with a minimum diffusion coefficient only 5 to 59% of BTCs reached the sampling point within 1 Myr. The arrival times were also faster in ensembles with a maximum dispersivity and a minimum porosity, and thus maximum porewater velocity and dispersion. When applying the maximum gradient, the fastest realization BTCs arrival times were achieved. However, changes in the gradient in ensembles with the minimum diffusion did not significantly influence the arrival times of BTCs, and the number of BTCs with an average concentration of zero within 1 Myr was reduced only when applying maximum dispersivity.

6.1.4 Claystone as host rock formation with varied thickness and hydraulic conductivity

The BTCs from the entire ensemble of ensembles 17 to 20 for claystone with varied thickness are given in Appendix E. The average concentrations are presented in Figure 24.

Changes in the formation thickness in ensembles 17 to 19 did not significantly influence the average concentration at 1 Myr. The average relative concentration was 0.14% for the median formation thickness in ensemble 17, decreased to 0.13% when the formation thickness was increased by 50% in ensemble 18 and increased to 0.17% when the formation thickness was decreased by 50% in ensemble 19 (Figure 24, Table 10).

By changing the hydraulic conductivity from median to harmonic mean the average relative concentration at 1 Myr decreased from 0.14% in ensemble 17 to 0.02% in ensemble 20 (Figure 24, Table 10). Hydraulic conductivity set at the harmonic mean, representing the best-case scenario of a perfectly layered system, led to a pronounced delay of the arrival times in the ensemble of BTCs in ensemble 20 compared to ensemble 17 where a median was used (Figure E5).

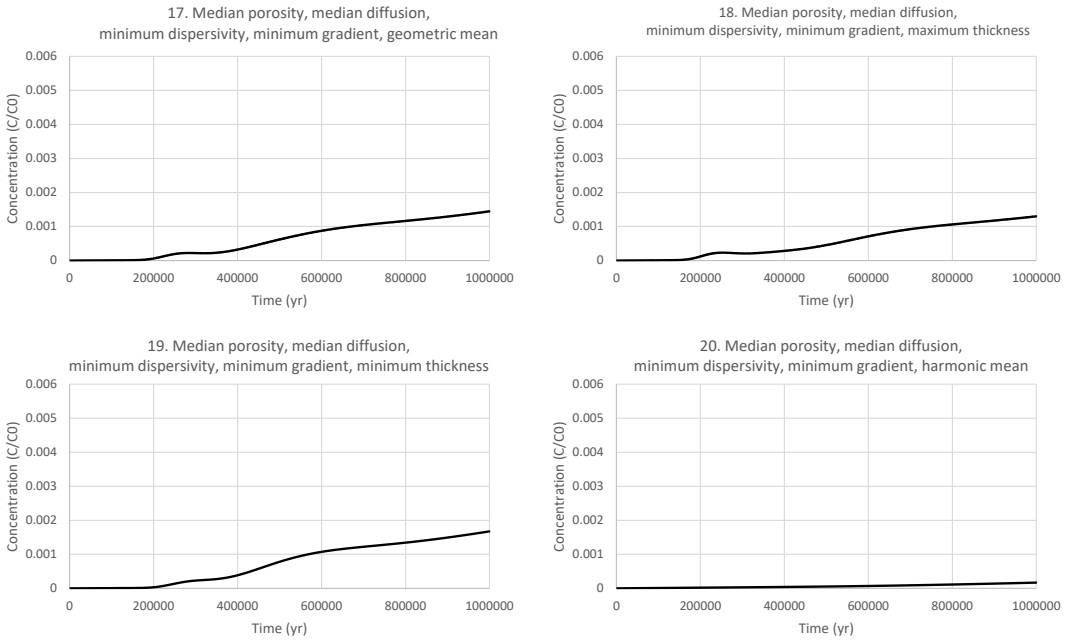

***Figure 24**. Average BTCs from ensembles 17 to 20 as relative concentration vs. time. The number in the heading of each plot refers to the ensembles listed in Table 5.*

***Figur 24**. Gennemsnitlige gennembrudskurver for ensemble 17 to 20 som relative koncentrationer mod tid. Numrene i figuroverskrifterne relaterer til ensemblerne angivet i Tabel 5.*

In summary, a claystone formation with a median thickness and perfectly layered clay and sand system represented in ensemble 20 has a substantially higher potential for delaying the nuclides transport than a claystone-sand layer of a much greater thickness and with median hydraulic properties, as shown in ensemble 18 (Figure 24, Table 10). However, the setting characterized in ensemble 20 does not represent average conditions expected at 500 meters depth in Denmark.

6.2 Reactive transport modeling

6.2.1 Chalk as host rock formation

The relative BTC for the conservative tracer using the parameters chosen for the reactive transport modeling (Section 5.3.1) is shown in Figure 25. Concentrations and relative concentrations of nuclides at the abstraction depth based on modeling including solubility (Table 6) and half-life (Table 7) are given in Figure 26.

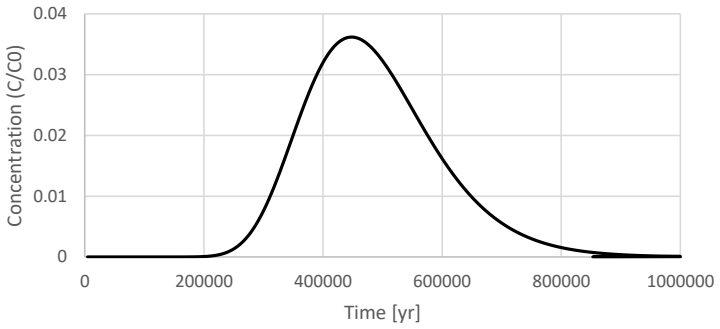

***Figure 25**. BTC of a conservative tracer as a relative concentration vs. time.*

***Figur 25**. Gennembrudskurver for konservativ tracere som relative koncentrationer mod tid.*

The peak of the relative concentration of a conservative tracer arrives at 450 kyr. Its maximum value is 3.6% of the starting concentration (Figure 25). It corresponds to the peak values of realization BTCs in chalk (Appendix D). The relative concentration of the conservative tracer is zero until 33.5 kyr (not visible in the figure). The relative concentrations of nuclides (Figure 26A), released at a continuous source, are substantially below 1‰, except for Np-237 that reaches a C/C0 concentration of 99% at 785 kyr, U-234 with a maximum C/C0 of 28% from 737 kyr, U-233 that reaches a C/C0 of 15% at 728 kyr and Th-230 with a maximum C/C0 of 2% after 507 kyr. The highest molar concentration was modeled for U-234 and equaled 1.97E-7 mol/L starting at 785 kyr (Figure 26B). Th-230 reached a maximum concentration of 1.31E-8 mol/L at 642 kyr, and Np-237 a maximum concentration of 4.0E-9 mol/L at 938 kyr.

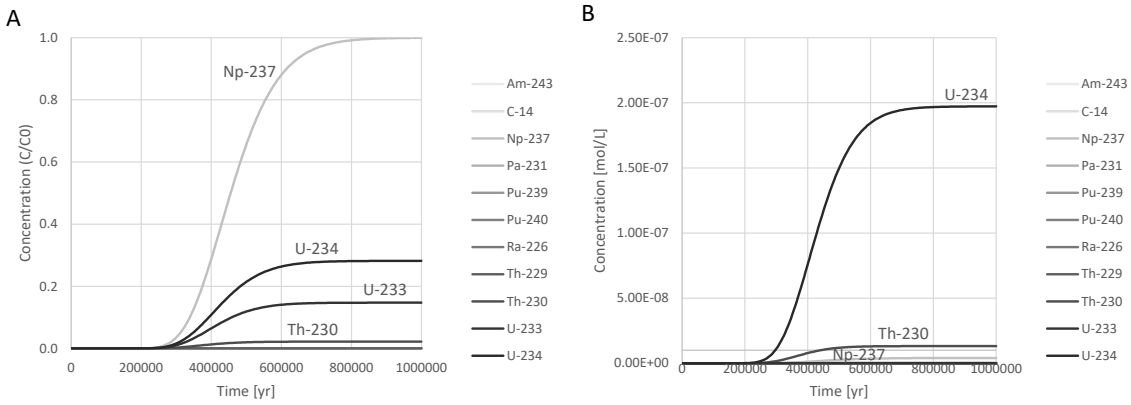

***Figure 26**. BTCs of the modeled nuclides as a relative concentration (A) and concentration (B) vs. time for a highly simplified model that does not include 3D effects, mixing at the well intake nor sorption, which would lower concentrations and delay the breakthrough.*

***Figure 26**. Gennembrudskurver for simulerede nuklider som relative koncentrationer (A) og koncentrationer (B) mod tid i en simplificeret modelopsætning, der ikke inkluderer 3D effekter, opblanding i indvindingsfilteret eller sorption, som vil mindske koncentrationerne og forsinke gennembrud.*

Figure 26 indicates an effect of solubility and half-life of nuclides on the concentration and relative concentration simulated at the abstraction depth. Only nuclides with a half-life above 100 kyr reached the abstraction depth (Figure 26A). The highest relative concentration was simulated for Np-237 (Figure 26A), which has a half-life of 2100 Myr (Table 7). However, the solubility of Np-237 is two orders of magnitude lower than the solubility of U-234 (Table 7). Therefore, the highest concentrations were simulated for U-234 (Figure 26B). Th-230 has solubility similar to the solubility of U-234, but a shorter half-life (Table 7). Therefore, the relative concentration and concentration of Th-230 at the abstraction depth are low (Figure 26).

6.2.2 Claystone as host rock formation

Relative BTC for the conservative tracer using the parameters chosen for the reactive transport modeling (Section 5.3.1) is shown in Figure 27. Concentrations and relative concentrations of nuclides at the abstraction depth, modeled including solubility (Table 6) and half-life (Table 7) but neither 3D and well intake dilution nor sorption effects, are given in Figure 28.

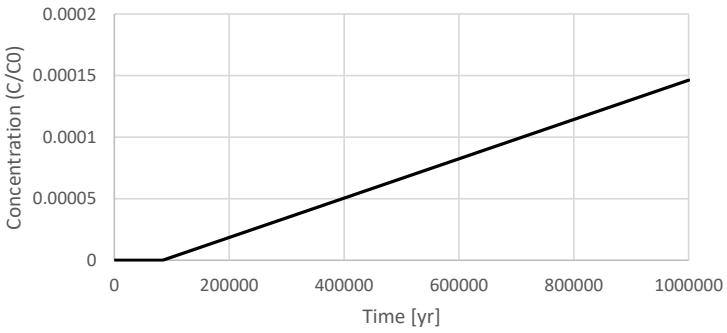

Figure 27*. BTC of a conservative tracer as a relative concentration vs. time.*

Figur 27*. Gennembrud af konservative tracere som relative koncentrationer mod tid.*

The peak of the relative concentration of a conservative tracer does not arrive within 1 Myr. The maximum value at 1 Myr is 0.15‰ of the starting concentration. The relative concentration of a conservative tracer is zero until 84 kyr (Figure 27). The relative concentrations of nuclides (Figure 28A) are negligible and substantially below 1‰, except for Np-237 that reaches C/C0 concentration of 1‰ at approximately 500 kyr and a maximum of 6‰ at 1 Myr, and U-234 that reaches C/C0 of 0.1‰ at 1 Myr. The highest molar concentration was modeled for U-234 and equaled 7.84E-11 mol/L at 1 Myr (Figure 28B). Np-237 reached a maximum concentration of 2.44E-11 mol/L at 1 Myr.

Similar to the chalk setting an effect of solubility and half-life is pronounced. Np-237 with longer half-life and lower solubility than U-234 (Table 7) has a higher relative concentration (Figure 28A) and lower total concentration at the abstraction depth than U-234.

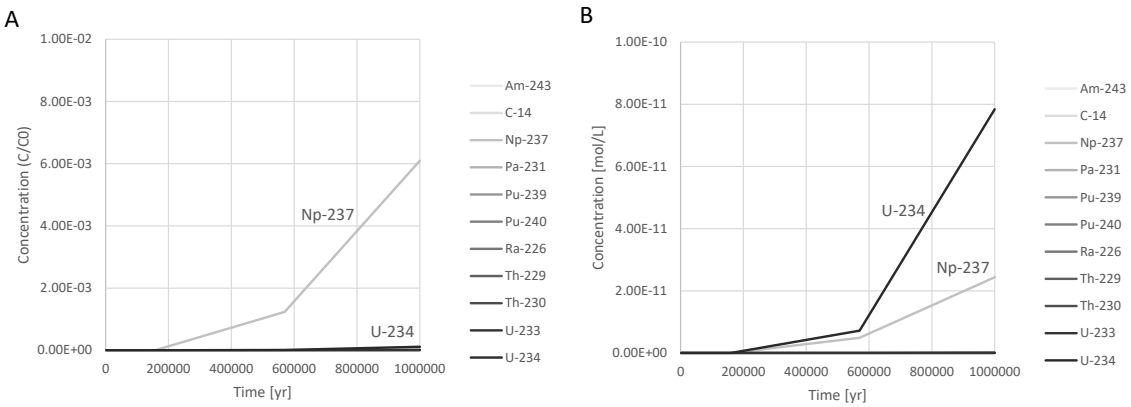

***Figure 28**. BTCs of the modeled nuclides as a relative concentration (A) and concentration (B) vs. time for a highly simplified model that does not include 3D effects, mixing at the well intake nor sorption which would lower concentrations and delay the breakthrough.*

***Figur 28**. Gennembrudskurver for simulerede nuklider som relative koncentrationer (A) og koncentrationer (B) mod tid i en simplificeret modelopsætning, der ikke inkluderer 3D effekter, opblanding i indvindingsfilteret eller sorption, som vil mindske koncentrationerne og forsinke gennembrud.*

7. Discussion

7.1 Stochastic modeling of chalk as host rock formation

7.1.1 The effect of changing the effective porosity, diffusion, and dispersivity

The effect of changes in effective porosity is evident for all ensembles with chalk as a host rock, where an increase in effective porosity leads to delays in the BTCs and vice versa for a decrease in effective porosity (e.g., Figure 15, Table 8). While there is certainly an effect from changing the effective porosity, the effect on the resulting BTCs is less apparent in comparison to changing the diffusion coefficient. The highest average peak concentrations are simulated in ensembles 4, 8, 12, and 16 having minimum diffusion and maximum effective porosity (Figures 15–18 and D1–D4). This is a consequence of the hydrodynamic dispersion coefficient being the lowest in these ensembles (Table 9). Compared to ensembles 4, 8, 12, and 16, ensembles 2, 6, 10, and 14 only differ by having the maximum diffusion (Table 4) resulting in lower average peak concentration and faster average breakthrough (Figures D1–D4, Table 8). The reason is that the magnitude of the mechanical dispersion (Equation 5a) in ensembles 2, 6, 10, and 14 is mainly governed by the diffusion coefficient (Table 9). Hence, the maximum applied diffusion in these ensembles is governing for the BTC rather than the average porewater velocities. In contrast, in ensembles 4, 8, 12, and 16 where the diffusion coefficient is at a minimum, the magnitude of the mechanical dispersion is substantial compared to the diffusion coefficient (Table 9). Consequently, the advective flow and mechanical dispersion control transport in these ensembles, even though the breakthrough occurs at a later stage compared to ensembles with maximum diffusion. The applied maximum and minimum diffusion coefficients are in the order of 10^{-5} and 10^{-9} m^2/d, respectively. Therefore, with the average porewater velocities in the order of 10^{-6} m/d and dispersivity values of 0.6 or 6 meters in ensembles 1–8 (Table 8), the magnitude of the hydrodynamic dispersion coefficient is dependent on the applied diffusion coefficient being set to the maximum or minimum value.

Increasing the dispersivity from ensembles 1–4 (dispersivity of 0.6 m) to 5–8 (dispersivity of 6 m) and similarly from ensembles 9–12 to 13–16 show minor reductions of the average peak concentrations resulting in average peak concentrations of around 0.1% (Figures 15–18 and D1–D4). Again, this is related to the hydrodynamic dispersion coefficient being dependent on the magnitude of the applied diffusion coefficient. With the increase in dispersivity by a factor of 10 in ensembles 5–8 and 13–16, the increase in mechanical dispersion coefficient is proportional. Hence, with the maximum and minimum applied diffusion coefficient, respectively, the increase in the hydrodynamic dispersion coefficients affects only the average peak concentrations slightly. However, when comparing the individual realizations within ensembles 4 and 8 and 5 and 16, where the diffusion is at a minimum, the magnitude of the peak concentrations is reduced substantially (Table 8). Due to the increase in the dispersivity and

the relatively small effect of the diffusion coefficient on the hydrodynamic dispersion coefficient, the magnitude of the relative concentration decreases from around 0.14% in ensembles 4 and 12 to 0.05% in ensembles 8 and 16 (Figures D1–D4). In contrast, when comparing the individual realizations within ensembles 2 and 6, where the diffusion is at a maximum, the magnitude of the peak concentrations is similar with minimum and maximum dispersivity values. This indicates again that the hydrodynamic dispersion coefficient is governed by the applied diffusion coefficient.

Using the maximum gradient ensembles 9 to 16 show similar patterns compared to ensembles 1 to 8 in terms of the effects related to changing the effective porosity, diffusion coefficient, and dispersivity values. Hence, with the deduced average velocity range from the ensembles in the order of 10^{-6} to 10^{-5} m/d, the average time for the peak breakthrough is dependent on the hydrodynamic dispersion coefficient, which in turn is dependent on the magnitude of the applied diffusion coefficient. It is noted that the calculated P_e for all ensembles is >2 (Table 9), and therefore relative importance of advective transport is greater. However, the simulated ensembles also show that diffusion is the rate-limiting step in terms of the hydrodynamic dispersion coefficient. Nevertheless, in the simulated ensembles, the range of probable K-values for chalk yields porewater velocities which cause average peak concentrations to arrive within 33 to 570 kyr. Obviously, further investigations are needed in terms of 3D flow and transport simulations also including preferential flow paths, as well as host rock formation property characterization to better describe the breakthrough in chalk formations. As an example, retardation of nuclides due to adsorption on clay minerals or the chalk itself as well as addition of density effects would result in a much later breakthrough, as observed in claystone studies (e.g. ANDRA, 2005b). Thus, in a French study Hubert et al. (2006) suggested retardation factors of 10–35 for U and Th in chalk, meaning that average peak concentration arrival would be delayed by a factor of 10–35 compared to predicted arrival calculated without sorption.

7.1.2 The effect of changing the hydraulic gradient

The effect of changing the hydraulic gradient is evident comparing the peak concentration arrival time in ensembles 1–8 to ensembles 9–16 (Table 8). With the applied porosities, the porewater velocities are proportional to the hydraulic gradient (Equation 1). I.e., by increasing the hydraulic gradient by a factor of 10, the porewater velocities increase by a factor of 10. From the current knowledge of vertical hydraulic gradients within the chalk, it has been shown that relatively large gradients can be present (Bonnesen et al., 2009). However, these gradients were measured across a chalk-marl sequence within the chalk unit and porewater velocity calculations showed that velocities were within a few centimeters per year. Thus, the large hydraulic gradients most likely indicate the low hydraulic conductivity of the marl layers rather than fast advective transport. In line with this, Bonnesen et al. (2009) showed that the diffusive transport was governing within the chalk.

With the hydraulic gradient being the driving force for groundwater flow, it is important to note that the current 1D conceptualization is simple and therefore not representative for groundwater flow paths in chalk deposits or any deposits that may be influenced by fracture flow or

preferential flows along faults as illustrated in Figure 29. For example, the regional groundwater flow system in claystone and chalk sediments in Switzerland was mainly controlled by the regional fault system implemented in the sensitivity studies as hydraulic barriers or conductors (Luo et al., 2014a, b). BTC arrival times for the repository in basalt were decreased from 200 kyr to 20 kyr when vertical fractures were included in the model, although the peak dose concentration at 1 Myr remained unchanged (Schwartz, 2018). Therefore, when numerically assessing the host rock formation potential in detail at a later stage, it is critical to gather site-specific information on the hydraulic gradients as well as hydrogeological data representing groundwater movement in 3D.

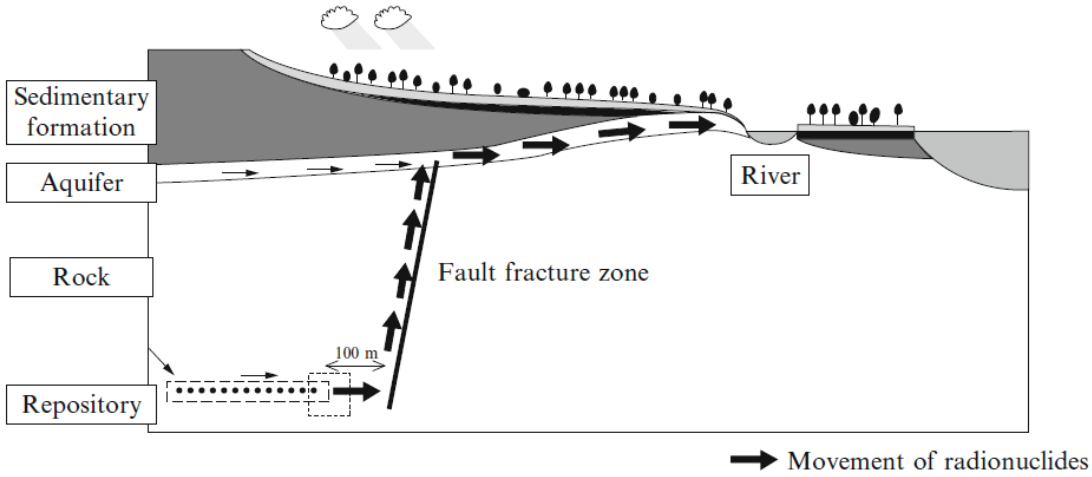

***Figure 29**. Depiction of groundwater flow movement (Nagasaki and Nakayama, 2015).*

***Figure 29**. Skildring af grundvandstrømninger (Nagasaki and Nakayama, 2015).*

7.1.3 Changes in thickness of chalk as host rock formation

The changes in thickness of the host rock formation tested in the present modeling study do not yield substantial changes in average flow velocity (based on the breakthrough of the average peak concentration) with the increase in thickness from ensemble 17 to 18 of 55 meters (Table 8). In fact, the arrival time of the average peak concentration is around 4 kyr faster changing from 347 kyr to 343 kyr, where slower arrival time was expected since the thickness of the host rock formation was larger in ensemble 18. When decreasing the thickness of the host rock formation in ensemble 19, as expected a faster breakthrough is observed compared to the base case of ensemble 17. The reason for the faster average peak movement in ensemble 18 compared to ensemble 17 is likely related to the randomization of K-values contributing to some realizations yielding faster porewater velocities. Since the hydrogeological properties of the lower chalk host rock formation and the upper chalk barrier rock (ECZ) are only different within the same order of magnitude (cf. Table 2), this seems like a reasonable explanation. Another explanation could be that the changes in hydraulic heads are minor with a 55 meters increase in thickness and therefore gradients within the host rock formation remain similar. Hence, the increase of 55 meters in chalk thickness (corresponding to an increase of median chalk thickness by 50%) does not yield substantial changes in the arrival time of the average peak concentration. In contrast, the difference

between the minimum and maximum thickness of the host rock formation corresponding to 110 meters yielded a delay of around 40 kyr for the arrival time of average peak concentration in ensemble 18 (maximum chalk thickness) compared to ensemble 19 (minimum chalk thickness). This indicates that depending on the K values of the host rock formation, the sufficient thickness for a repository should be evaluated.

7.2 Stochastic modeling of the claystone host rock formation

7.2.1 The effect of changing the effective porosity, diffusion, and dispersivity

In all claystone ensembles, the average peak concentration of the BTCs is not attained at the groundwater abstraction depth of 115 meters (Figures 20–23). However, a fraction of realizations reaches a peak concentration within each ensemble (Figures E1–E4). In contrast, also for some ensembles, only a fraction of the realizations shows BTC (relative concentration above zero) within 1 Myr of simulation time at the groundwater abstraction depth. In ensembles 3–4, 7–8, 11–12, and 15–16, the fraction of realizations, where the nuclide reaches (relative concentration above zero) the groundwater abstraction depth within 1 Myr ranges from 5 to 59% (Figures E1–E4). In the remaining ensembles (1–2, 5–6, 9–10, 13–14), the nuclide reaches a peak concentration at the groundwater abstraction depth in only a few realizations. The nuclide concentrations in the remaining realizations are not peaking within 1 Myr, but still rising towards a peak (e.g., Figures 20 and E1). Overall, these large differences illustrate the large uncertainties related to the present knowledge available for parameterization of the numerical models. Still, the effect of changing the different parameters is apparent. Changes in effective porosity from minimum to maximum in all cases resulted in a delay of the transport (Figures E1–E4) and higher average concentrations at 1 Myr in ensembles with maximum porosity compared to the ensembles with minimum porosity. The reason is that the mechanical dispersion (Equation 5a) is decreased because of lower porewater velocities and therefore does not add to hydrodynamic dispersion relative to the ensembles with minimum effective porosities. Increasing the effective porosity in e.g. ensemble 2 compared to ensemble 1 increases the maximum average concentration arriving within 1 Myr (Table 10). Hence, due to less dispersion following the decrease in porewater velocity, the simulated maximum concentration within 1 Myr is less dispersed. A similar pattern is evident for all ensembles where the diffusion coefficient is at a maximum, and the porosity is decreased (ensembles 1–2, 5–6, 9–10, and 13–14).

From the simulated ensembles with claystone as host rock formation, it is clear that diffusion is the governing transport in this rock type, and the advective transport is minimal in the claystone formation with the generated realizations. Only in the ensembles where the diffusion coefficient is set to the maximum, the nuclide reaches the groundwater abstraction depth for all realizations within 1 Myr (Figures E1–E4). In the ensembles with the minimum diffusion coefficient, nuclide reaches the groundwater abstraction depth in only a fraction of the realizations (Figures E1–E4). . This corroborates with ANDRA (2005b) where diffusion was also reported as a major transport factor in Callovo-Oxfordian claystone.

In the ensembles with the minimum diffusion coefficient (10^{-9} m^2/d), a fraction of the realizations that show concentration above zero within 1 Myr substantially increases by varying the dispersivity from minimum to maximum. The fraction of realizations where nuclide reached the groundwater abstraction depth within 1 Myr increases by 16% between ensembles 4 and 8, and by 51% between ensembles 11 and 15 (Figures E1–E4). Thus, the increase of the mechanical dispersion (Equation 5a) apparently results in faster arrivals.

7.2.2 The effect of changing the hydraulic gradient

The effect of an increase in the hydraulic gradient is seen for all cases, and most clearly on the arrival time of individual realizations in the cases where maximum diffusion is assigned, and all realizations reach the groundwater abstraction depth within 1 Myr. For the BTC in ensembles 3, 4, 11, and 12 with minimum diffusion and minimum dispersivity values and varying hydraulic gradient (Figures E1 and E3) a negligible difference is observed in the peak arrival times. However, the maximum average concentration at 1 Myr in the ensembles with maximum dispersivity and minimum diffusion changes from 0.02 to 0.05% by varying the hydraulic gradient between ensembles 7 and 15 and equals 0.1% both for ensemble 8 and 16 despite the hydraulic gradient variation (Table 10).

Though the average peak concentration is not simulated in any of the ensembles, it is noted that there are realizations within each ensemble simulating a peak concentration. In fact, some of the peak BTC concentrations arrive within 20 kyr (e.g., Figure E4) representing the most conservative realizations within the ensembles. These realizations are within ensembles with the maximum hydraulic gradient.

Further, in the ensembles with minimum diffusion, it is evident that more realizations simulate relative concentrations above zero within 1 Myr with a higher gradient compared to the ensembles with minimum diffusion and lower gradient. For instance, in ensemble 7–8 representing low gradient ensembles with minimum diffusion, the fraction of realizations simulating relative concentrations above zero within 1 Myr ranges from 21 to 29%. In comparison, in ensemble 15–16 representing the same variables as ensemble 7–8 but with a hydraulic gradient increased by a factor of 10, between 49 to 59% of realizations reach relative concentrations above zero within 1 Myr. As it was also noted in the simulations with chalk as host rock formation, the proportionality between porewater velocity and hydraulic gradient is pronounced. Thus, information to represent hydraulic gradients is essential when numerically assessing the host rock formation potential in detail at a later stage.

7.2.3 Hydraulic conductivity as harmonic mean and altered host rock formation thickness

Obviously, the K-value in claystone has a high influence on the arrival times of the simulated BTCs. In ensemble 17, where the K-value of the claystone was represented by the arithmetic mean, the maximum average concentration after 1 Myr at the groundwater abstraction depth is 0.14% of the initial concentration. When implementing a K-value represented by the harmonic mean in ensemble 20, the maximum average simulated concentration at 1 Myr decreased to 0.02% of the initial concentration (Table 10). Since the harmonic mean may be used to describe the average hydraulic properties in the orthogonal direction to stratification, in this case in the vertical direction, it is expected that the simulated concentrations decrease when using the harmonic mean. The different results obtained using the arithmetic versus harmonic mean of the K-value accentuate the importance of representing the hydrogeological regime at a sufficient detail and proportion. Here, the groundwater flow and transport simulated in 1D and the K-value within the units are assumed isotropic and homogenous, and thus anisotropy is not considered. This gives reason to large uncertainties in the calculated breakthrough curves and is representative to the conceptual case only. As noted in the simulations with chalk as host rock formation, an improved characterization of the 3D groundwater flow and transport system, and host rock formation properties are critical in the next phase of the geological project to determine the effectiveness of the host rock formation at specific sites.

The sensitivity of the conservative tracer transport to changes in the claystone host rock formation thickness is not pronounced. Average relative concentrations at 1 Myr for the claystone thickness of 70 meters above the repository were 0.14% and only decreased to 0.13% if the host rock thickness was increased by 50% and increased to 0.17% if the host rock thickness was decreased by 50% (Figure 24, Table 10). This is contrary to the findings of ANDRA (2005b) who showed that an increase of thickness of the Callovo-Oxfordian clay by 10 meters had a significant influence on the transport of the nuclides in terms of arrival times and peak concentrations (Section 2.5.2). However, in the present simulations, the conceptualization of the model domain is simplified into 1D compared to ANDRA (2005b), where the simulations represented a 3D flow and transport system. Further, the present simulation time is restricted to 1 Myr meaning that the entire BTC of each realization is not captured in the calculation of the average maximum peak concentration within the ensembles. Therefore, it is likely that the arrival time of the average peak concentration is increased with the maximum thickness of claystone and vice versa as the case was for the French study (ANDRA, 2005b).

7.3 Comparison of properties influencing the host rock formation potential

7.3.1 Effect of changing parameters

For both model conceptualizations with chalk and claystone as host rock formations, it is evident that the hydraulic gradient is governing the transport of nuclides and that the modeling results are most sensitive to changes in the hydraulic gradient compared to the remaining hydrodynamic variables included in the modeling exercise. For the ensembles with chalk as host rock formation, where the average peak concentration occurs within the simulated time frame, the proportionality between the hydraulic gradient and the porewater velocity is exemplified when increasing the hydraulic gradient, a factor of ten in ensembles 9–16 from 1–8 (Table 8). The factor ten increase of the hydraulic gradient results in a factor ten increase in the average porewater velocities and thereby generally in 10 times faster breakthrough. In the ensembles with the claystone as host rock formation, the effect of increasing the hydraulic gradient is apparent comparing ensembles 7–8 (Figure 21) with 15–16 (Figure 23). Here, the fraction of realizations with simulated relative concentrations above zero increases to 49% and 59% from 21% and 29% although diffusion is considered as the controlling transport mechanism in the claystone host rock in all ensembles.

The main difference in the host rock formation conceptualization with chalk versus claystone is related to the arrival of the average peak concentrations and the magnitude of the relative concentrations. The earliest simulated average peak concentration within the ensembles is around 33 kyr in the chalk conceptualization, whereas average peak concentrations are not attained within the ensembles in the claystone conceptualization. Still, in both host rock formation conceptualizations, realizations with average peak concentration arriving within 20 kyr are simulated in cases representing the most conservative estimates of the hydraulic variables (e.g., Figures D3 and E3). Further, there are differences related to the magnitude of the relative concentration arriving within 1 Myr, which in turn are influenced by the porewater velocity and dispersion of which the conservative tracers are transported. In the two model conceptualizations, the boundary conditions, and variation in minimum and maximum value for diffusion coefficients and dispersivities are similar. Therefore, it is evident that the differences in arrival of peak concentration and their magnitude is related to the K value of the host rock formation. This highlights the importance of investigating and determining the K values of the host rock formation in Phase 2 of the geological repository project.

Since the conceptualizations are simplified in terms of representing generic hydrogeological settings for the host rock formations, and flow and transport are represented in 1D, it is acknowledged that representativeness is limited compared to a natural setting with a 3D flow and transport system. Nevertheless, the presented simplified approach does elucidate the host rock potential for chalk and claystone, as the conceptualizations are comparable and regarded as conservative; (1) The effects of 3D dispersion are not accounted for in the models and therefore the simulated BTC's are overestimated as the effects of solute dispersion in the 3D space is not represented. (2) The hydraulic gradient is upward while in natural settings a more complex flow pattern will be present. The hydraulic gradient may essentially be absent in deeper parts or be a mix of upward/downward and horizontal components in a

given groundwater system (Luo et al., 2014b). Upward flow occurs in the system of multiple aquifers isolated by confining units, e.g., karst limestone aquifers isolated by claystone layers (Luo et al., 2014a, b). Similar flow patterns can be expected in the claystone-sandstone systems in Denmark, however, further data on the hydraulic gradients in the deep subsurface need to be collected for more advanced conceptualizations to be made. In the Danish chalk, hydraulic conductivity and fracturing intensity decrease with the depth. Thus, it is likely that the flow gradient at 500 meters in chalk settings is low and diffusion is the governing transport process (Bonnesen et al., 2009). Though a hydraulic gradient of up to 0.14 was observed in the chalk layers separated by a marl layer at the Stevns-1 borehole at a depth of 300 meters (Jakobsen et al., 2021) this merely reflects buildup of a high gradient due to lower hydraulic conductivity of marl rather than the ability to transmit water at fast velocities. Further, in the current study, density effects were not considered. With increasing depth, the salinity of groundwater increases and for instance Bonnesen et al. (2009) showed that the chloride concentration reached almost 0.9 mol/L at about 450 meters depth. With higher salinity and thus higher density, the gradient needed to transport saline water from larger depths must be higher compared to transporting freshwater. Therefore, the simulated BTC arrival and concentration magnitude in the present conceptualization are likely over-estimated in many cases and merely highlight the sensitivity of the system to hydraulic gradient changes rather than the actual conditions in the chalk and claystone at a given repository site. Whether the applied hydraulic gradient of 0.001 or 0.01 is representative of groundwater flow is site-specific. With the earliest simulated arrival of peak concentrations being around 300 kyr or 30 kyr, depending on the gradient, the potential for chalk as host rock formation evident and should be further explored when more data becomes available for specific sites in Phase 2 of the geological project. In this context, it should be emphasized that the calculations presented here., in addition to the discussion above regarding density effects and 3D representation of the flow regime, do not take into account sorption which would likely delay the BTC arrival by a factor of 10-35.

With the relatively slower arrival time simulated for claystone as host rock, its potential should also be further explored. Though preferential flow and transport are not explicitly represented in the conceptualization, other studies suggest that these should be investigated site-specifically (Luo et al., 2014a, b). Presently, the fractured chalk is represented with K-values based on the latest calibration of the national DK-model (Section 5.2.2), in which the fractured chalk is represented as an equivalent porous medium. Here, in both model conceptualizations of host rock formation, the fractured chalk is represented similarly and therefore the models are comparable. However, in Phase 2, the effect on fracture flow above the different barrier formations should be explored in detail.

In both host rock model conceptualizations, the arrival and shape of the peak BTCs seemed related to the hydrodynamic dispersion coefficient (Equation 5a). The magnitude and arrival of the peak concentration are dependent on whether the maximum or minimum diffusion coefficient is applied. Regardless of the simulated porewater velocities in both host rock conceptualizations, the magnitude of the diffusion coefficient is to some extend governing the BTCs. Hence, when the maximum diffusion coefficient is applied, the arrival of the maximum concentration is faster and the magnitude lower compared to using the minimum diffusion coefficient (for chalk see e.g., ensembles 2 and 4 in Figure D1, and for claystone ensemble 2 and 4 in Figure E1). Further, in chalk, in contrast to the claystone ensembles, using the

maximum diffusion coefficient affected the magnitude of the maximum peak concentration only slightly when increasing the dispersivity value from the minimum in ensemble 2 to the maximum in ensemble 6 (Figures D1 and D2, Table 8). In claystone, the effect of changing the dispersivity from a minimum to a maximum using the maximum diffusion coefficient yielded a relatively larger change in the magnitude of the maximum relative concentrations (Figures E1 and E2, Table 10). Diffusion was reported as a dominant process in the Callovo-Oxfordian clay and the models were highly sensitive to changes in the diffusion coefficient compared to the sensitivity to changes in the host rock formation permeability (ANDRA, 2005b; Enssle et al., 2014). It is thus critical that diffusion properties of potential host rock sites are investigated in the coming next phase.

7.3.2 Changes in hydraulic barrier thickness

The simulations where the thicknesses of the host rock formations were changed are not conclusive with the applied conceptualizations. In the chalk and claystone, the relative change of thickness above the repository does not yield any substantial changes in the magnitude of the average peak concentration. In terms of the arrival time, here the effects of increasing the thickness of the host rock formation in chalk are minimal, while faster arrival of average peak concentrations are obtained with a decrease in thickness (Table 8). The effects of increasing the thickness of the claystone as host rock formation are also minimal with only a -0.01%-point change in the relative maximum concentration at 1 Myr, while higher average maximum concentrations at 1 Myr are reached with a decrease in thickness (Table 10). From the individual realizations within the ensembles, the arrival times appear faster in the ensembles for scenario 18 with a maximum thickness compared to ensembles 17 with the base case thickness (Figures D5 and E5). This is due to the conceptualization of the realizations in which the K-values are randomized sometimes resulting in higher K-values and therefore a higher flow velocity in the host rock formation than in the overlying deposits in part of the realizations. In cases of hydraulic conductivity decreasing with depth, the increase in the host rock thickness results in delayed arrival times. A change in hydraulic barrier thickness is expected to influence the arrival times and magnitudes of nuclide compounds but as shown here, the effect is dependent on the K-values. Still, it is pertinent to investigate the host rock thickness as different hydraulic flow and transport regimes could call for conditions that would make thickness less than 100 meters sufficient for delaying nuclides transport.

7.4 Reactive transport modeling

The reactive transport modeling was performed for the median values of hydraulic parameters known for the Danish geological formations (Table 2), a hydraulic gradient of 0.001, and minimum dispersivity. The results of this modeling shows that both chalk and claystone have a good potential for comprising an effective geological barrier in nuclides transport. Only few radionuclides with a long half-life reach the sampling point in the groundwater, even though modeled in 1D with conservative assumptions on parameter values. In the current model conceptualization (1) no sorption was included, (2) all nuclides were released into one model flow tube, i.e. a single point, (3) no dilution or mixing of contaminated water took place along the flow path or at the depth of groundwater abstraction, and (4) density effects were not

considered. Including these parameters/factors would all decrease the simulated nuclide concentration at the sampling point compared to the results presented in the present report.

Sorption of nuclides to clay minerals delays their transport to the surface, leaving more time for the nuclide decay in the geological barriers, and thus decreases nuclide concentration at the groundwater abstraction depth (ANDRA, 2005b, c; Baeyens et al., 2014). Clay minerals are abundant in claystone and the marl layers of the chalk. Therefore, future investigation of the Danish host rock formations will include analyses of the amount and types of clay minerals for a more precise evaluation. Further, the future work in Phase 2 of the geological repository project will include estimates of sorption capacities of various geological formations at specific sites.

The nuclide concentration at the groundwater abstraction depth is expected to decrease considerably if the site-specific hydrogeological conditions are modeled in 3D. Another crucial parameter in the evaluation of nuclides transport in 3D is a detailed design of the engineered barriers and geometry of the repository (ANDRA, 2005c; COWI, 2011b, Ström et al., 2008). The detailed information on the design of the engineered barriers is not available at present.

Based on the current simplistic approach with a 1D conceptualization, it is indicated that both, the Danish claystone and chalk, based on the median hydrogeological properties, have a high potential for retention of both long-lived parents and produced daughter isotopes, assuming that the used rock properties interpreted from very limited information are representative. Nuclide concentrations simulated at the sampling point would further decrease or increase, if a different set of hydrogeological parameters comprising hydraulic conductivity, porosity, hydraulic gradient, diffusion, and dispersivity, is applied, as shown in the changes of the relative concentrations of a conservative tracer while varying these variables (Section 6.1). Changes in simulated nuclides concentration are also expected by varying nuclides solubility that is linked to hydrochemical conditions and design of the engineered barriers at the repository.

Ovrerall, the reactive transport model results – and specifically the large uncertainties associated with these – emphasize that collection of data describing the host rock formation mineralogy and groundwater chemistry at 500 meters depth, as well as detailed description of the engineered barriers and sorption capacities are crucial for an improved evaluation of nuclides transport at the further modeling stages.

8. Summary and conclusions

This report describes the results of the numerical model calculations performed in the first phase of the geological repository project. The purpose of the model calculations is to contribute to an initial assessment of the possibilities for deep geological storage of the Danish radioactive waste in low-permeable rocks in Denmark.

At present, there is limited knowledge about rock properties and hydrogeological conditions at 500 meters depth in the Danish subsurface. Therefore, assessments of possible transport of radioactive nuclides from layers at a depth of 500 meters to the fresh groundwater currently need to be based on a number of assumptions and conceptual considerations. This means that model calculations, such as those presented in this report, are not very accurate in terms of describing e.g. transport times from a depth of 500 meters to the fresh groundwater. The knowledge needed to increase the accuracy the numerical solute transport models – and thereby increase the certainty on evaluations of specific rocks' host rock and ECZ potential – include knowledge of the physical/chemical rock properties, the mineralogical rock composition, the hydrogeological properties, the groundwater chemical composition, and specific geochemical properties in relation to the radioactive substances found in the Danish waste. Much of this knowledge will be related to local, site-specific conditions.

Currently, there are three low-permeability rock types in Denmark that could potentially be used as host rocks of a geological repository: crystalline bedrock, chalk, and claystone. Several studies, including studies from Scandinavia, have shown that crystalline rocks can constitute a geological repository. Therefore, crystalline rocks are not included in the present model study, as the existing data base cannot further qualify this assessment in a Danish context. Based on the current knowledge and level of knowledge about the Danish subsurface, it was therefore considered relevant to set up conceptual numerical models for the low-permeable sedimentary rocks, chalk and clay.

As mentioned, in the present work it has been chosen to carry out a number of conceptual model studies. This means that the models do not represent specific localities in Denmark, but rather a general consideration of the geological record, in which relevant low-permeable rocks under different assumptions are included. The assumptions relate to hydrogeological conditions and parameter values that, as far as possible, represent the current knowledge in Denmark. The modeling has been carried out with the aim to: (1) evaluate the barrier efficiency of the low-permeable sedimentary rocks, and (2) identify which geological, hydrogeological and geochemical parameters have the greatest significance for the transport of nuclides in the subsurface. This will provide guidelines for data collection and the design of further modelling studies in the subsequent phases of the geological repository project.

The model study is divided into two parts, where the barrier properties of the rocks are assessed in Part 1 on the basis of conservative solute transport simulations. Thus, in these models, it is assumed as a conservative scenario that the leakage from a possible final repository occurs immediately and the effects of degradation, retardation/sorption, density flow, and/or dispersion in a 2D/3D domain are not included. The results of the models therefore represent a situation with an expected greater risk of impact on the fresh groundwater than will actually be the case with future final deposition in chalk or claystone. Several scenarios

with different parameter values and boundary conditions are assessed in Part 1 by stochastically generating values for the hydraulic conductivity within a parameter value space, which is based on the existing data available for chalk and claystone in Denmark (described in Report no. 3 and 4, see Chapter 9.1 for reference). That is, a number of equally probable values for the hydraulic conductivity are generated for the different geological units in the models, assuming different boundary conditions and solute transport parameter values. Boundary conditions and parameter values are also based on the available knowledge.

In Part 2, the barrier properties are assessed on the basis of solute transport simulations of radioactive nuclides, where the effects of decay and solubility are included. The reason why other transport mechanisms, e.g. sorption and density effects, are not included, and that only 1D representations of the subsurface have been developed is partly because of the lack of data, and partly because many of these mechanisms will be solute and site specific, which is not possible to take into account at present. The hydrogeological parameters used in the models in Part 2 are based on median values for the existing data sets for chalk and claystone, respectively.

It is important to note that the simulated breakthrough times, and derived assessments presented in this report, represent one specific conceptual geological model for each host rock and at the same time, as mentioned, a situation with expected greater risk of impact on fresh groundwater than will actually be the case if a repository is placed in chalk or claystone. Therefore, it is expected that new, multi-dimensional models based on site-specific data in the next phase of the geological repository project will result in significantly longer breakthrough times than presented in this report. The simulated breakthrough times and concentrations in this first phase of the final repository project should therefore only be used for an initial qualification of chalk and claystone as host rocks, respectively - as well as to assess which parameters are important for solute transport from 500 meters to the fresh groundwater.

The results for Part 1, where modeling is performed with simple conservative solute transport, show that:

- In the case where a final repository is placed in chalk at a depth of 500 meters, simulated breakthroughs of the average maximum concentration in the abstraction depth of groundwater occurs within 33,000 to 530,000 years.
- In the case where a final repository is placed in the claystone at a depth of 500 meters, none of the simulations result in breakthrough of the average maximum concentration in the abstraction depth within 1 million years.
- It is crucial for the accuracy of the simulated transport time and the maximum concentrations that the following site-specific parameters are determined as accurately as possible, as these can naturally vary by several orders of magnitude:
  - The hydraulic conductivity of the rocks, including variations within a specific rock.
  - The hydraulic gradient.
  - The diffusion coefficient, which will also be solute specific.
- It is less crucial for the accuracy of the simulated transport time and the maximum concentrations to have an accurate determination of e.g. the porosity and geological boundaries of the rocks, as these often vary less than an order of magnitude.

The results for Part 2, which include decay and solubility of specific radioactive nuclides in the models, show that:

- The time that elapses until the first breakthrough of nuclide in groundwater is seen when transported from a repository at a depth of 500 meters is more than twice as long when the clay is host rock compared to chalk as host rock.
- The concentration of nuclides in the groundwater, which is caused by transport from a geological repository at a depth of 500 meters, will largely depend on the half-lives and solubility of the nuclides. With the hydraulic properties used, and 1D conceptual representations of the subsurface, it is seen, for example, that for the scenario with chalk as the host rock, only nuclides with half-lives over 100,000 years, and the greatest solubility, will reach the groundwater within a period of 1 million year. Similar results are obtained with claystone as host rock, but with breakthroughs of only the most soluble and slowly decaying nuclides - and in lower concentrations than with limestone as host rock.

Overall, the results show that both chalk and claystone can potentially constitute a host rock for a geological repository, as for both types of host rock long breakthrough times are seen for the conservative substance transport simulations. The results also show that clay as a host rock gives a greater retention of nuclides than chalk as a host rock. Chalk, however, already in the simple 1D conceptual models provides a significant retention of nuclides, and factors that are not included in the conceptual models, such as degradation, sorption, density effects and dispersion in 3D, will mean that nuclides are actually retained significantly more in both types of host rocks.

It should be noted that the model scenarios with claystone as the host rock for the sake of simplicity are based on a conceptual model with 170 meters of homogeneous clay and a repository located 70 meters below the top of this claystone. As described in Report no. 4 (cf. Chapter 9.1 for reference), the claystones found at a depth of 500 meters in Denmark are often heterogeneous with frequent, several meters thick, interbedded sand layers. The effect of these sand layers on the solute transport from a depth of 500 meters to the groundwater has not been assessed in this first phase of the geological repository project, but it is expected that such an assessment will be included in the more advanced 3D numerical models set up in the next phase.

In addition, the repository concept and the constructed barriers in a final repository will contribute to further retention of the nuclides in the radioactive waste.The model calculations show a large spread in the calculated breakthrough times. To reduce this uncertainty, it is necessary for the forthcoming modeling in Phase 2 of the geological repository project to collect site-specific hydrogeological and geochemical data to determine the above-mentioned governing parameters, including parameters not included in the current models. Finally, a good determination of the hydraulic system is also important in relation to the assessment of 3D flow.

9. References

ANDRA, 2005a: Evaluation of the feasibility of a geological repository in an argillaceous formation. The geological medium: the Meuse/Haute-Mare site. Dossier 2005 Argile, 57-105. pp.238.

ANDRA, 2005b: Dosier 2005 Argile – Safety evaluation of a geological repository. pp.782.

ANDRA, 2005c: Dossier 2005 Granite – Safety analysis of a geological repository. pp.221.

Appelo, C.A.J., Postma, D., 2005: Geochemistry, groundwater and pollution. 2nd edition. A.A. Balkema Publishers, Amsterdam, Netherlands. pp.649.

Bagtzoglou, A.C., Ababou, R., Nedungadi, A., Sagar B., 2009: Fuzzy rule-based hydrologic models for performance assessment of nuclear waste disposal sites. *J. Hydrol. Eng.* 14: 1240–1248.

Baik, M.H., Lee, S.Y., Lee, J.K., Kim, S.S., Park, C.K., Choi, J.W., 2008: Review and compilation of data on radionuclide migration and retardation for the performance assessment of a HLW repository in Korea. *Nucl. Eng. Technol* 40(7): 593–606.

Baeyens, B., Thoenen, T., Bradbury, M.H., Fernandes, M.M., 2014: Sorption data bases for argillaceous rocks and bentonite for the provisional safety analyses for SGT-E2. NAGRA Technical Report 12-04. pp.76.

Be, M.M., Chiste, V., Dulieu, M.A., Kellett, M.A., Mougeot, X., Arinc, A., Chechev, V.P., Kuzmenko, N.K., Kibedi, T., Luca, A., Nichols, A.L., 2016: Table of radionuclides (vol. 8 – A=41 to 198). pp.258.

Blechschmidt, I., Frieg, B., Vomvoris, S., Turner, J. & Tweed, C. 2021: Geological siting project on disposal of the Danish radioactive waste. Review of: Phase 1, report no. 8. Criteria and requirements for identification of suitable disposal sites. pp.17.

Bonnesen, E.P., Larsen, F., Sonnenborg, T.O., Klitten, K., Stemmerik, L., 2009: Deep saltwater in chalk of North-West Europe: origin, interface characteristics and development over geological time. *Hydrogeol. J.* 17(7): 1643–1663.

Bourgeat, A., Kern, M., Schumacher, S., Talandier, J., 2004: The COUPLEX test cases: nuclear waste disposal simulation. *Comput. Geosci.* 8: 83–98.

Brommundt, J., Kaempfer, U., Enssle, C.P., Mayer, G., Wendling, J., 2014: Full-scale 3D modelling of a nuclear waste repository in the Callovo-Oxfordian clay. Part 1: thermo-hydraulic two-phase transport of water and hydrogen. *Clays in Natural and Engineered Barriers for Radioactive Waste Confinement* 400: 443–467.

Bruno, J., Cera, E., de Pablo, J., Duro, L., Jordana, S., Savage, D., 1997: Determination of radionuclide solubility limits to be used in SR 97 uncertainties associated to calculated solubilities. Swedish Nuclear Fuel and Waste Management CO, SKB, TR 97-33, pp.184.

Cliffe, K.A., Kelly, M., 2006: COMP23 version 1.2.2 user's manual. SKB R-04-643, Swedish Nuclear Fuel and Waste Management Co., Stockholm. pp.76.

COVRA, 2017: Opera Safety Case. Covra. pp.146.

COWI, 2011a: Pre-feasibility study for final disposal of radioactive waste. Working Report 3. Nuclides in the waste. pp.74.

COWI, 2011b: Pre-feasibility study for final disposal of radioactive waste. Working Report 5. Groundwater modelling. pp.45.

COWI, 2011c: Pre-feasibility study for final disposal of radioactive waste. Working Report 8. Repository groundwater model. pp.119.

COWI, 2011d: Pre-feasibility study for final disposal of radioactive waste. Working Report 9. Overall groundwater model incl. results. pp.70.

Danish Parliament, 2018: Parliamentary resolution B 90. Proposal for parliamentary resolution on a long-term solution for Denmark´s radioactive waste. Ministry for Higher Education and Science. Adapted by the Danish Parliament 15 March 2018. pp.11.

Danish Health Authority, 2020: Responsible and Safe Management of Radioactive waste, Denmark. pp.68.

Dansk Dekommissionering, 2021: Notat om mulige koncepter for dyb geologisk slutdeponering i Danmark.

De Windt, L., Pellegrini, D., van der Lee, J., 2004: Coupled modeling of cement/claystone interactions and radionuclide migration. *J. Contam. Hydrol.* 68: 165–182.

De Windt, L., Spycher, N.F., 2019: Reactive transport modeling: a key performance assessment tool for the geologic disposal of nuclear waste. *Elements* 15: 99–102.

Enssle, C.P., Brommundt, J., Kaempfer, U., Mayer, G., Wendling, J., 2014: Full-scale 3D modelling of a nuclear waste repository in the Callovo-Oxfordian clay. Part 1: thermo-hydraulic two-phase transport of water, hydrogen, ^{14}C and ^{129}I. *Clays in Natural and Engineered Barriers for Radioactive Waste Confinement* 400: 469–481.

EU, 2011: Rådets Direktiv 2011/70/EURATOM af 19. juli 2011 om fastsættelse af en fællesramme for ansvarlig og sikker håndtering af brugt nukleart brændsel og radioaktivt affald, L 199, 48–56.

Fetter, C.W., 2001: Applied Hydrogeology. Upper Saddle River, N.J.: Prentice Hall. pp.620.

Follin, S., Hartley, L., Jackson, P., Roberts, D., Marsic, N., 2008: Hydrogeological conceptual model development and numerical modelling using CONNECTFLOW, Forsmark modelling stage 2.3. R-08-23. pp.139.

Friedlander, G., Kennedy, J.W., Macias, E.S., Miller, J.M., 1981: Nuclear and radiochemistry. 3rd edition. Canada. pp.684.

Gelhar, L.W., Welty, C. and Rehfeldt, K.R., 1992: A critical review of data on field-scale dispersion in aquifers. *Water Resour. Res.* 28(7): 1955–1974.

Grambow, B., Landesman, C., Ribet, S., 2014: Nuclear waste disposal: I. Laboratory simulation of repository properties. *Appl. Geochem.* 49: 237–246.

Gravesen, P., 2016: De geologiske forhold i ca. 500 m´s dybde. Foreløbig redegørelse udarbejdet på eksisterende data. GEUS-NOTAT nr. 05-VA-16-08. Til: Uddannelses- og Forskningsministeriet V/ Merete Storr-Hansen og Ole Kastbjerg Nielsen. pp.24.

Gravesen, P., Jakobsen, P. R., Nilsson, B., Pedersen, S.A.S., Midtgaard, H. H., 2021: Studies of geological properties and conditions for deep disposal of radioactive waste, Denmark. Report no. 5. Precambrian crystalline basement distribution and properties. GEUS Report no. 2021/56. 97pp .

Hadgu, T., Karra, S., Kalinina, E., Makedonska, N., Hyman, J.D., Klise, K., Viswanathan, H.S., Wang, Y., 2017: A comparative study of discrete fracture network and equivalent continuum models for simulating flow and transport in the far field of a hypothetical nuclear waste repository in crystalline host rock. *J. Hydrol.* 553: 59–70.

Harbaugh, A.W., Banta, E.R., Hill, M.C., McDonald, M.G., 2000: MODFLOW-2000, the U.S. Geological Survey modular ground-water model. User guide to modularization concepts and the ground-water flow process. Open File Rep. 00-92, USGS, Denver, CO, pp.121.

Hubert, A., Bourdon, B., Pili, E., Meynadier, L., 2006: Transport of radionuclides in an unconfined chalk aquifer inferred from U-series disequilibria. *Geochim. Cosmochim. Acta* 70(22): 5437–5454.

Hughes, J.D., Sanford, W.E., 2004: SUTRA-MS: a version of SUTRA modified to simulate

heat and multiple-solute transport. USGS Open-File Rep 2004-1207. pp.141.
IAEA, 2011: Geological Disposal Facilities for Radioactive Waste. IAEA Safety Standards. Specific Safety Guide No. SSG-14. pp.101.
IAEA, 2018a: Roadmap for Developing a Geological Disposal Programme, IAEA NUCLEAR ENERGY SERIES; Draft. pp.83.
IAEA, 2018b: The Management of Site Investigations for Radioactive Waste Disposal Facilities. IAEA NUCLEAR ENERGY SERIES; Draft. pp.263.
Jakobsen, P.R., Frykman, P., Jakobsen, R. 2021: Studies of geological properties and conditions for deep disposal of radioactive waste, Denmark. Report no. 3. Upper Cretaceous chalk and Paleocene limestone distribution and properties. GEUS Report no. 2021/54. 76 pp.
Johnson, P.J., Otto, S., Weaver, D.J., Dozier, B., Miller, T.A., Jordan, A.B., Hayes-Rich, N.G., Stauffer, P.H., 2019: Heat-generating nuclear waste in salt: field testing and simulation. *Vadose Zone J.* 18: 1–14.
Joyce, S., Hartley, L., Applegate, D., Hock, J., Jackson, P., 2014: Multi-scale groundwater flow modeling during temperate climate conditions for the safety assessment of the proposed high-level nuclear waste repository site at Forsmark, Sweden. *Hydrogeol. J.* 22: 1233–1249.
Kim, S.S., Baik, M.H., Kang, K.C., 2009: Solubility of neptunium oxide in the KURT (KAERI Underground Research Tunnel) groundwater. *J. Radioanal. Nucl.* 280: 577–583.
Konikow, L.F., 2011: The secret to successful solute-transport modelling. *Groundwater*, 49(2): 144–159.
Lanteri, S., Raffourt, C., 2004: Strategies for reducing computing time of nuclear waste management simulations using the PORFLOW™ software. *Computat. Geosci.* 8: 203–2015.
La Venue, A.M., Cauffman, T.L., Pickens, J.F., 1990: Groundwater flow modeling of the Culebra Dolomite. pp.260.
Lichtner, P.C., 2007: FLOTRAN user's manual: two-phase non-isothermal coupled thermal-hydrologic-chemical (THC) reactive flow & transport code, version 2.0. Report LAUR-01-2349, Los Alamos National Laboratory, Los Alamos, NM. pp.168.
Lim, D.H., 2006: Numerical study of nuclides migration in a nonuniform horizontal flow field of a high level radioactive waste repository with multiple canisters. *Nucl. Technol.* 156: 222–245.
Luo, J., Monninkhoff, B., Schatz, P., Seifert, S., Becker, J.K., Gmunder, C., Jordan, P., 2013: Elaboration of groundwater models for deep geological repository sites by using FEFLOW. Modflow and More 2013: Translating Science Into Practice – Conference Proceedings: 381–389.
Luo, J., Monninkhoff, J., Becker, J.K., 2014a: Hydrogeological model Jura Ost. NAGRA, Arbeitsbericht NAB 13-26. pp.108.
Luo, J., Monninkhoff, J., Becker, J.K., 2014b: Hydrogeological model Jura Südfuss. NAGRA, Arbeitsbericht NAB 13-27. pp.98.
Mathiesen, A., Midtgaard, H. H., Hjelm, L., 2021: Studies of geological properties and conditions for deep disposal of radioactive waste, Denmark. Report no. 6. Subsurface distribution of Jurassic and Cretaceous fine-grained formations based on seismic mapping. GEUS Report no. 2021/57. 48 pp.
Mbia, E.N., Fabricius, I.L., Krogsbøll, A., Frykman, P., Dalhoff, F., 2014: Permeability, compressibility and porosity of Jurassic shale from the Norwegian-Danish Basin. *Pet. Geosci.* 20: 257–281.

Mills, R.T., Lu, C., Lichtner, P.C., Hammond, G.E., 2007: Simulating subsurface flow and transport on ultrascale computers using PFLOTRAN. *J. Phys. Conf. Ser.* 78: 1–7.

Muskat, M., Meres, M.W., 1936: The flow of heterogeneous fluids through porous media. *J. Appl. Phys.* 7: 346–363.

Nagasaki, S. and Nakayama, S. eds., 2015. Radioactive waste engineering and management. Tokyo: Springer Japan.

NAGRA, 2005: Darstellung und Beurteilung der aus sicherheitstechnisch-geologischer Sicht möglichen Wirtgesteine und Gebiete. Techniser Bericht 05-02. pp.3.

NAGRA; 2008: Derlegung der Anforderunger, des Vorgehens und der Ergebnisse. Technischer Bericht 08-03. pp.30.

NAGRA, 2017: Technical Reports. www.nagra.ch/en/cat/publikationen. (Switzerland).

NEA (Nuclear Energy Agency, OECD), 2005: Clay Club Catalogue of Characteristics of Argillaceous Rocks, No. 4436. pp.71.

NEA, 2006: Safety of Geological Disposal of High-level and Long-lived Radioactive Waste in France. An International Peer review of the “Dossier 2005 Argile” Concerning Disposal in the Callovo-Oxfordian Formation. NEA No. 6178, OECD. pp.76.

NEA, 2008: Moving Forward with Geological Disposal of Radioactive waste. A Collective Statement by the NEA Radioactive Waste Management Committee (RWMC). OECD, NEA No. 6433. pp.21.

NEA, 2012: Geological Disposal of Radioactive Wastes: National Commitment, Local and Regional Involvement. A collective Statement of the OECD Nuclear Energy Agency” Radioactive Waste Management Committee”, Adopted March 2011, NEA/RWM(2011)16. pp.17.

Nielsen, L., Boldreel, L.O., Hansen, T.M., Lykke-Andersen, H., Stemmerik, L., Surlyk, F., Thybo, H., 2011: Integrated seismic analysis of the Chalk Group in eastern Denmark — Implications for estimates of maximum palaeo-burial in southwest Scandinavia. *Tectonophysics* 511(1-2): 14–26.

Nilsson B., Gravesen P. 2018. Karst Geology and Regional Hydrogeology in Denmark. In: White W., Herman J., Herman E., Rutigliano M. (eds) Karst Groundwater Contamination and Public Health. Advances in Karst Science. Springer, Cham. https://doi.org/10.1007/978-3-319-51070-5_34

Norman, S., Kjelbert, N., 1990: FARF31: a far field radionuclide migration code for use with the PROPER package. SKB TR 90-01, Swedish Nuclear Fuel and Waste Management Co., Stockholm. pp.61.

Norris, 2012: An introduction to geosphere research studies for the UK geological disposal program. *Mineral. Mag.* 76 (8): 3105–3114.

Nykyri, M., Nordmann, H., Marcos, N., Löfman, J., Poteri, A., Hautojărvi, A., 2008: Radionuclide release and transport – RNT 2008. POSIVA 2008-6. pp.170.

Odorowski, M., Christophe, J., De Windt, L., Broudic, V., Jouan, G., Peuget, S., Martin, C., 2017: Effect of metallic iron on the oxidative dissolution of UO2 doped with a radioactive alpha emitter in synthetic Callovian-Oxfordian groundwater. *Geochim. Cosmochim. Acta* 219: 1–21.

ONDRAF/NIRAS, ANDRA (eds.) 2015: Clays in geological disposal systems. Brochure published on occasion of the 6th international conference “Clays in Natural and Engineered Barriers for Radioactive Waste Confinements”, Brussels, Belgium. pp.8.

Painter, S., Mancillas, J., 2009: MARFA version 3.2.2 user’s manual: migration analysis of radionuclides in the far field. SKB R-09-56, Swedish Nuclear Fuel and Waste Management Co., Stockholm. pp.62.

Pedersen, G. K, Lauridsen, B., Sheldon, E., Midtgaard, H. H, 2021: Studies of geological properties and conditions for deep disposal of radioactive waste, Denmark. Report no. 4. Jurassic and Lower Cretaceous claystone distribution, sedimentology, and properties. GEUS Report no. 2021/55. pp.107.

POSIVA, 2017a: Final Disposal. Selecting the Site: The Final Disposal at Olkiluoto. www.posiva.fi/en/final_Disposal. (Finland).

POSIVA, 2017b: Geologic disposal of spent nuclear fuel in Olkiluoto. pp.12.

Poteri, A., Nordman, H., Pulkkanen, V.M., Smith, P., 2014: Radionuclide transport in the repository near-field and far-field. POSIVA 2014-02, Finland. pp.336.

Rausch, R., Schäfer, W., Therrien, R., Wagner, C., 2005: Solute transport modelling. An introduction to models and solution strategies. Borntraeger Science Publishers, Berlin. pp.205.

Sawada, A., Saegusa, H., Ijiri, Y., 2005: Uncertainty in groundwater flow simulations caused by multiple modeling approaches, at the Mizunami Underground Research Laboratory, Japan. *Geophys. Monogr.* 162: 91–101.

Sawada, A., Saegusa, H., Takeuchi, S., Sakamato, K., Dershowitz, W.S., 2015: Äspö Task Force on modelling groundwater flow and transport of solutes. Task 7 – Groundwater flow and transport modelling of fracture system at regional, block, and single-fracture scale flow and transport, Olkiluoto. P-13-46. pp.82.

Schwartz, M., 2012: Modelling groundwater contamination above a nuclear waste repository at Gorleben, Germany. *Hydrogeol. J.* 20: 533–546.

Schwartz, M., 2018: Modelling groundwater contamination above a potential nuclear waste repository in the Columbia River Basalt, USA. *Environ. Earth Sci.* 77:451: 1–12.

Selroos, J.O., Painter, S.L., 2012: Effect of transport-pathway simplifications on projected releases of radionuclides from a nuclear waste repository (Sweden). *Hydrogeol. J.* 20: 1467–1481.

Selroos, J.O., Follin, S., 2014: Overview of hydrogeological site-descriptive modeling con ducted for the proposed high-level nuclear waste repository site at Forsmark, Sweden. *Hydrogeol. J.* 22: 295–298.

Serco, 2003: NAMMU 7.2 user guide. Serco, Didcot, UK. pp.262.

Serco, 2008: ConnectFlow Release 9.6 Technical Summary Document. SA/ENV/CON NECTFLOW/15, Serco Asuurance, Hampshire, UK. pp.27.

SFOE, 2008: Sectoral plan for deep geological repositories. Conceptual Part. Department of the Environment, Transport, Energy and Communications DETEC. Swiss Federal Office of Energy SFOE. pp.89.

SKB (Svensk Kärnbränslehantering AB), 2007: RD&D Programme 2007. Programme for research, development and demonstration of methods for the management and disposal of nuclear waste. pp.510.

Sonnenborg, T.O., Henriksen, H.J., 2005: Håndbog i grundvandsmodellering. GEUS Rapport 2005/80. pp.316.

Springer, N., Dideriksen, K., Holmslykke, H.D., Kjøller, K., Olivarius, M., Schovsbo, N., 2020: Capture, storage and Use of CO2 (CCUS). Danmarks of Grønlands Geologiske Undersøgelse Rapport 2020/30. pp.44.

Spycher, N.F., Sonnenthal, E.L., Apps, J.A., 2003: Fluid flow and reactive transport around potential nuclear waste emplacement tunnels at Yucca Mountain, Nevada. *J. Contam. Hydrol.* 62-63: 653–673.

Steefel, C.L., Lichtner, P.C., 1998: Multicomponent reactive transport in discrete fractures: II: infiltration of hyperalkaline groundwater at Maqarin, Jordan, a natural analogue site. *J. Hydrol.* 209: 200–224.

Stisen, S., Ondracek, M., Troldborg, L., Schneider, R.J.M., van Til, M.J., 2019: National Vandressource Model. Modelopstilling og kalibrering af DK-model 2019. GEUS Rapport 2019/31. pp.125.

Stockman, C., Steinborn, T., 2000: Pure phases solubility limits – LANL. Office of Civilian Radioactive Waste Management Analysis/Model Revision Record. pp.42.

Ström, A., Andersson, J., Skagius, K., Winberg, A., 2008: Site descriptive modelling during characterization for a geological repository for nuclear waste in Sweden. *Appl. Geochem.* 23: 1747–1760.

Sundhedsstyrelsen, 2015: Statusrapport for den nukleare sikkerhed.

Svensson, U., Kuylenstierna, H.O., Ferry, M., 2010: DarcyTools version 3.4: concepts, methods and equations. SKB R-07-38, Stockholm. pp.144.

Tournassat, C., Steefel, C., 2015: Ionic transport in nano-porous clays with consideration of electrostatic effects. *Rev. Mineral. Geochem.* 80: 287–329.

Trinchero, P., Iraola, A., 2020: Models for the assessment of transport pf naturally-occuring nuclides in fractured media. *J. Hydrol.* 580: 1–11.

Trujillo, D., 2004: Mixed primal-dual method for nuclear waste disposal far field simulation. *Computat. Geosci.* 8: 173–185.

Tsang, C.F., Neretnieks, I., Tsang, Y., 2015: Hydrologic issues associated with nuclear waste repositories. *Water Resour. Res.* 51: 6923–6972.

UFM, 2021: Notat om roller og ansvar.

Verma, A.K., Gautam, P., Singh, T.N., Bajpai, R.K., 2015: Discrete element modelling of conceptual deep geological repository for high-level nuclear waste disposal. *Arab. J. Geosci.* 8: 8027–8038.

Vidstrand, P., Follin, S., Selroos, J.O., Naslund, J.O., 2014: Groundwater flow modeling of periods with periglacial and glacial climate conditions for the safety assessment of the proposed high-level nuclear waste repository site at Forsmark, Sweden. *Hydrogeol. J.* 22: 1251–1267.

Vidstrand, P., Ahokas, H., Bockgård, N., Holton, D., Lanyon, B., Poteri, A., Koskinen, L., 2015: SKB Task Force GWFTS – Task 7 Descriptions for hydrogeological modelling of Olkiluoto, Finland. Compilation of all task descriptions assessed within the Task 7 of the SKB Task Force on modelling of groundwater flow and transport of solutes. P-12-21. pp.97.

WHO, 2008. Guidelines for drinking-water quality. Geneva. pp.515.

Yoshida, H., Metcalfe, R., Ishibashi, M., Minami, M., 2013: Long-term stability of fracture systems and their behaviour as flow paths in uplifting granitic rocks from the Japanese orogenic field. *Geofluids* 13: 45–55.

Zhang, Y., Pinder, G., 2003: Latin hypercube lattice sample selection strategy for correlated random hydraulic conductivity fields. *Water Resour. Res.* 39(8): 1–11.

Zheng, C., Wang, P.P., 1999: MT3DMS: A modular three-dimensional multispecies transport model for simulation of advection, dispersion, and chemical reactions of contaminants in groundwater system. Documentation and user's guide. US Army Corps of Engineers, Engineers Research and Development Center. pp.230.

Zheng, C., Bennett, G.D., 2002: Applied contaminant transport modeling. Second edition. Wiley Interscience, Canada, pp.621.

Zyvoloski, G.A., Robinson, B.A., Dash, Z.V., Kelkar, S., Viswanathan, H.S., Pawar, R.J., Stauffer, P.H., Miller, T.A., Chu, S., 2012: Software users manual (UM) for the FEHM

Application Version 3.1-3.X LANL Rep. LA-UR-12-24493. Los Alamos Natl. Lab., Los Alamos, NM. pp.212.

9.1 Literature from the project on deep geological disposal

Title of the report series:

Studies of geological properties and conditions for deep disposal of radioactive waste, Denmark

1. Requirements and criteria for initial evaluation of geological properties and conditions (Midtgaard, H.H., Hjelm, L., Jakobsen, R., Karan, S., Kjøller, C., Nilsson, B. & Poulsen, M.L.K.). GEUS Report no. 2021/52 51 pp.

2. Geological setting and structural framework of Danish onshore areas (Gravesen, P., Pedersen, S. A. S. & Midtgaard, H. H.). GEUS Report no. 2021/53 72 pp.

3. Upper Cretaceous chalk and Paleocene limestone distribution and properties (Jakobsen, P.R., Frykman, P. & Jakobsen, R.) GEUS Report no. 2021/54 76 pp.

4. Jurassic and Lower Cretaceous claystone distribution, sedimentology, and properties (Pedersen, G. K, Lauridsen, B., Sheldon, E. & Midtgaard, H. H.) GEUS Report no. 2021/55 107 pp.

5. Precambrian crystalline basement distribution and properties (Gravesen, P., Jakobsen, P. R., Nilsson, B., Pedersen, S.A.S. & Midtgaard, H. H.) GEUS Report no. 2021/56 97 pp.

6. Subsurface distribution of Jurassic and Cretaceous fine-grained formations based on seismic mapping (Mathiesen, A., Midtgaard, H. H. & Hjelm, L.) GEUS Report no. 2021/57 48 pp.

7. Evaluation of long-term stability related to glaciations, climate and sea level, groundwater, and earthquakes (Sandersen, P., Binderup, M., Larsen, T. & Nilsson, B.). GEUS Report no. 2021/58 113 pp.

8. Conceptual 1D modeling of nuclides transport in low permeable formations (Kazmierczak, J., Karan, S. & Jakobsen, R.) GEUS Report no. 2021/59 103 pp.

9. Karakterisering og evaluering af geologiske egenskaber og forhold i 500 meters dybde (Midtgaard, H.H., Hjelm, L., Jakobsen, R., Karan, S., Kjøller, C., Nilsson, B. & Poulsen, M.L.K.) GEUS Report no. 2021/60 186 pp.

10. *(Translation of report no. 9): Characterization and evaluation of geological properties and conditions at 500 meters depth (Midtgaard, H.H., Hjelm, L., Jakobsen, R., Karan, S., Kjøller, C., Nilsson, B. & Poulsen, M.L.K.) GEUS Report no. 2021/61, in prep.*

9.2 Literature from previous projects on the Danish radioactive waste

Low- and intermediate level radioactive waste from Risø, Denmark. Location studies for potential disposal areas. Published in GEUS Report Series.

Report No. 1. Gravesen, P., Nilsson, B., Pedersen, S.A.S. & Binderup, M., 2010: Data, maps, models and methods used for selection of potential areas. GEUS Report no. 2010/122, 47 pages.

Report No. 2. Gravesen, P., Nilsson, B., Pedersen, S.A.S. & Binderup, M., 2010: Characterization of low permeable and fractured sediments and rocks in Denmark. GEUS Report no. 2010/123, 78 pages.

Report No. 3. Pedersen, S.A.S. & Gravesen, P.., 2010: Geological setting and tectonic framework in Denmark. GEUS Report no. 2010/124, 51 pages.

Report No. 4. Gravesen, P., Nilsson, B., Pedersen, S.A.S. & Binderup, M., 2011: Characterization and description of areas. Bornholm. GEUS Report no. 2011/44, 85 pages.

Report No. 5. Gravesen, P., Nilsson, B., Pedersen, S.A.S. & Binderup, M., 2011: Characterization and description of areas. Falster and Lolland. GEUS Report no, 2011/45, 76 pages.

Report No. 6. Gravesen, P., Nilsson, B., Pedersen, S.A.S. & Binderup, M., 2011: Characterization and description of areas. Sjælland. GEUS Report no. 2011/46, 85 pages.

Report No. 7. Gravesen, P., Nilsson, B., Pedersen, S.A.S. & Binderup, M., 2011: Characterization and description of areas. Langeland, Tåsinge and Fyn. GEUS Report no. 2011/47, 119 pages.

Report No. 8. Gravesen, P., Nilsson, B., Pedersen, S.A.S. & Binderup, M., 2011: Characterization and description of Areas. Eastern Jylland. GEUS Report no. 2011/ 48, 117 pages.

Report No. 9. Gravesen, P., Nilsson, B., Pedersen, S.A.S. & Binderup, M., 2011: Characterization and description of areas. Limfjorden. GEUS Report 2011/49, 138 pages.

Report No. 10. Gravesen, P., Nilsson, B., Pedersen, S.A.S. & Binderup, M., 2011: Characterization and description of areas. Nordjylland. GEUS Report 2011/50, 51 pages.

Report No. 11. Gravesen, P., Nilsson, B., Pedersen, S.A.S. & Binderup, M., 2011: Dansk og engelsk resume. Danish and English resume. GEUS Report no. 2011/51, 64 pages.

Low- and intermediate level radioactive waste from Risø, Denmark. Studies of the six sites (Omegnsstudier). Published in GEUS Report Series.

Rapport nr. 1. Gravesen, P., Nilsson, B., Binderup, M. Larsen, T. & Pedersen, S.A.S., 2012: Lav- og mellem radioaktivt affald fra Risø, Danmark. Omegnsstudier. Rapport nr. 1. Område Østermarie-Paradisbakkerne, Bornholms Regionskommune, GEUS Rapport 2012/123, 100 pages.

Rapport nr. 2. Gravesen, P., Nilsson, B., Binderup, M. Larsen, T. & Pedersen, S.A.S., 2012: Lav- og mellem radioaktivt affald fra Risø, Danmark. Omegnsstudier. Rapport nr. 2. Område Rødbyhavn, Lolland Kommune, GEUS Rapport 2012/124, 55 pages.

Rapport nr. 3. Gravesen, P., Nilsson, B., Binderup, M. Larsen, T. & Pedersen, S.A.S., 2012: Lav- og mellem radioaktivt affald fra Risø, Danmark. Omegnsstudier. Rapport nr. 3. Område Kertinge Mark, Kerteminde Kommune, GEUS Rapport 2012/125, 68 pages.

Rapport nr. 4. Gravesen, P., Nilsson, B., Binderup, M. Larsen, T. & Pedersen, S.A.S., 2012: Lav- og mellem radioaktivt affald fra Risø, Danmark. Omegnsstudier. Rapport nr. 4. Område Hvidbjerg, Thyholm, Struer Kommune, GEUS Rapport 2012/126, 61 pages.

Rapport nr. 5. Gravesen, P., Nilsson, B., Binderup, M. Larsen, T. & Pedersen, S.A.S., 2012: Lav- og mellem radioaktivt affald fra Risø, Danmark. Omegnsstudier. Rapport nr. 5. Område Thise, Skive Kommune, GEUS Rapport 2012/127, 83 pages.

Rapport nr. 6. Gravesen, P., Nilsson, B., Binderup, M. Larsen, T. & Pedersen, S.A.S., 2012: Lav- og mellem radioaktivt affald fra Risø, Danmark. Omegnsstudier. Rapport nr. 6. Område Skive vest, Skive Kommune, GEUS Rapport 2012/128, 91 pages.

Low- and intermediate level radioactive waste from Risø, Denmark. Studies of interim storage (Mellemlagerstudier).

DD & GEUS, 2016: Supplerende mellemlagerstudier-sammenfatning. Udarbejdet af Dansk Dekommissionering og de Nationale Geologiske Undersøgelser for Danmark og Grønland for en tværministeriel arbejdsgruppe under Uddannelses- og Forskningsministeriet, 30 pages.

GEUS og DD, 2015: BESLUTNINGSGRUNDLAG for et dansk mellemlager for lav- og mellemaktivt affald. Udarbejdet af GEUS og DD for en Tværministeriel arbejdsgruppe under Ministeriet for Sundhed og Forebyggelse, februar 2015, 128 pages.

Gravesen, P., Binderup, M., Nilsson, B. & Pedersen, S.A.S., 2016: Kriterier og proces for lokalisering af et mellemlager for det lav – og mellemaktive affald fra Risø. De Nationale Geologiske Undersøgelser for Danmark og Grønland (GEUS), 99 pages.

Appendix A. Modeling of nuclides transport in granite

Factors governing flow and transport in granite

Detailed studies of granite as a host rock were conducted in Finland, France, Sweden, and Switzerland (E.g. ANDRA 2005; Follin et al., 2008; Sawada et al., 2015). Transport of nuclides in granite is more complex than in unfractured sedimentary rocks and governed by effective porosity and permeability of the solid host rock and fracture network, heterogeneity in hydraulic properties and its changes with depth, hydraulic gradients in fractured and unfractured zones, conducting or sealing properties of the major fractures, connectivity between minor and major fracture networks, fracture dipping, aperture, length, and wetness, spatial characteristics of the major fault zones and their behavior at the model boundaries, diffusion between fractured zone and unfractured rock matrix, and sorption at the fractured surfaces (Sections 2.5 and 2.6). Various conceptualization of the fractured media may lead to a couple of orders of magnitude variations in travel times and flow path lengths (ANDRA, 2005; Sawada et al., 2005).

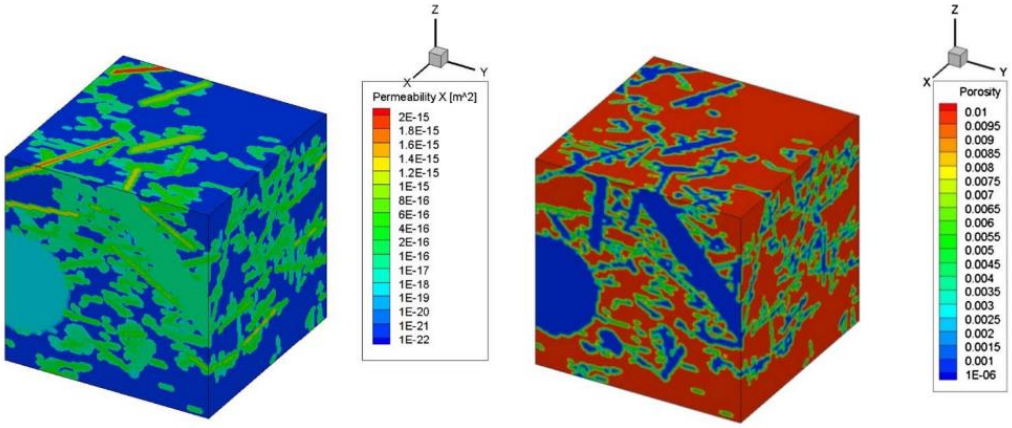

***Figure A1**. Permeability and porosity in the ECPM model obtained from the DFN model (Hadgu et al., 2017).*

***Figur A1**. Permeabilitet og porøsitet i ECPM modellen udviklet fra DFN modellen (Hadgu et al., 2017).*

Conceptualization of flow and transport in fractured granite

Groundwater flow and nuclides transport in fractured systems are most adequately reflected in numerical models implementing a Discrete Fracture Network (DFN) approach (Hartley and Joyce, 2013; Sawada et al., 2015). DFN models are used on the site-scale, in the far field and near field models to trace detailed paths of nuclides transport (ANDRA, 2005; Selroos and Painter, 2012). The DFN approach uses a highly detailed representation of geometry, connectivity, and hydraulic properties of fractures in the vicinity of the radioactive waste repositories, where the release of nuclides, and provides a detailed description of nuclides

transport in the near field models and the well-recognized areas of the far field (ANDRA, 2005; Hadgu et al., 2017; Hartley and Joyce, 2013). The advective flow in the unfractured rock matrix is neglected in the DFN models (Follin et al., 2014). DFN models consist of fractures modeled as 2D planes. The downstream movement of the particles at the fracture intersections is assigned in a stochastic manner (Selroos and Painter, 2012). In the fractured formations, tests are run for different scenarios of discrete fractures network distribution.

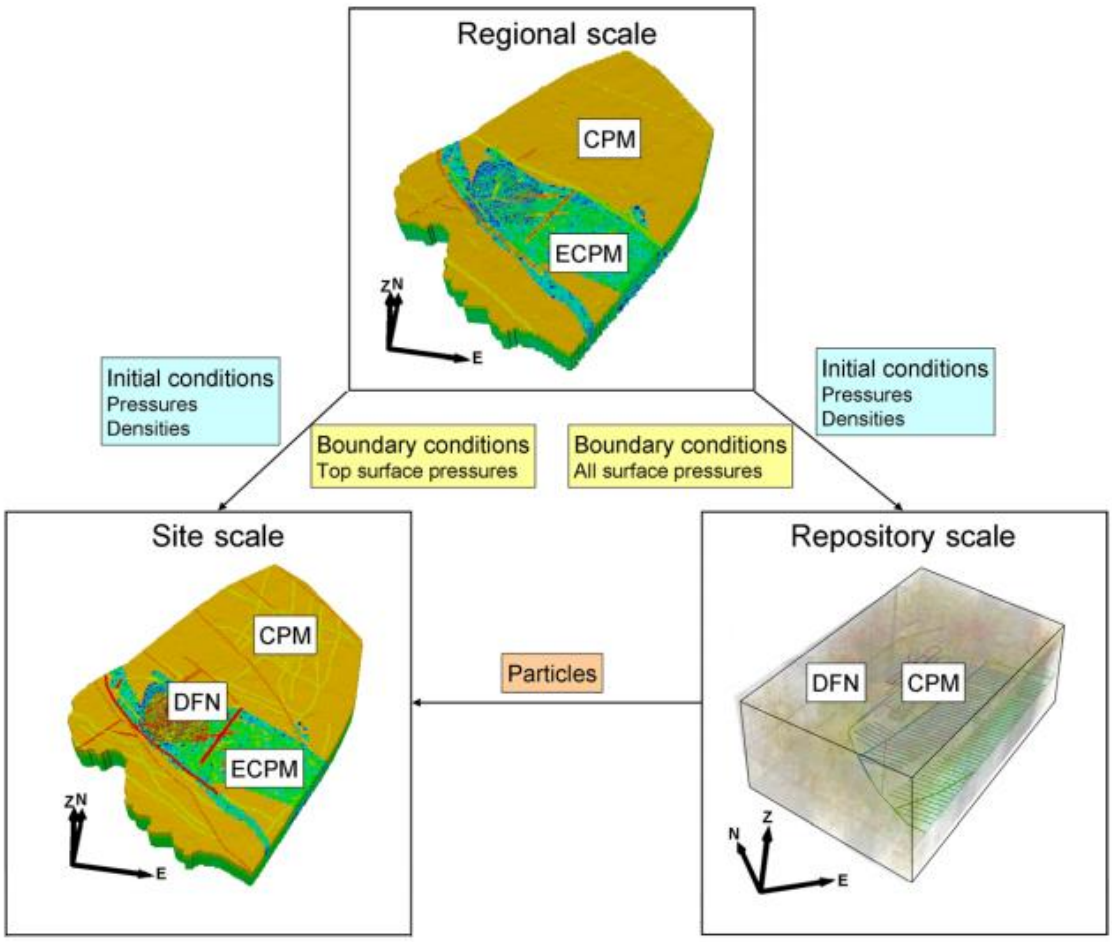

***Figure A2**. Concept of models embedding and enabling data transfer between Discrete Fracture Network (DFN), equivalent continuous porous medium (ECPM), and continuous porous medium (CPM), Joyce et al. (2014).*

***Figur A2**. Koncept for modeller som inkluderer Discrete Fracture Network (DFN), equivalent continuous porous medium (ECPM), og continuous porous medium (CPM), og muliggøre dataoverførsel imellem disse, Joyce et al. (2014).*

The detailed information on the fracture networks is not available at the far field and regional scales, where Continuous Porous Medium (CPM) models are used instead to simulate nuclides transport from the repository location to the surface (ANDRA, 2005; Follin et al., 2008; Selroos and Painter, 2012; Hartley and Joyce, 2013).

Far field models include fractured rocks as a CPM either based on the hydraulic characteristics of the area or hydraulic characteristics of the fracture networks (Sawada et al., 2005; Hadgu et al., 2017). Flow and transport in DFN models can be upscaled to equivalent CPM models (ECPM) if the unfractured rock matrix is relatively tight and the model discretization allows for the definition of heterogeneities in the fracture network distribution (Hartley and Joyce, 2013). ECPM models upscale fracture flow properties to bulk flow properties (Sawada et al., 2005; Follin et al., 2014). DFN are transformed into ECPM models by assigning a permeability value to each cell based on the volumetric amount of fractures and undisturbed rock matrix in the cell (Vidstrand et al., 2014; Hadgu et al., 2017). Flow magnitude and direction, pressure, and groundwater density simulated with the use of ECPM models must be consistent with the output of the DFN model at a cell scale (Hartley and Joyce, 2013; Joyce et al., 2014). The consistency between the models is achieved by assigning hydraulic properties (equivalent hydraulic conductivity tensor and kinematic porosity; Figure A1) to each cell of the ECPM model determined from a combination of the hydraulic properties of the unfractured rock matrix and the fracture network based on their volumetric proportion within the cell (ANDRA, 2005; Follin and Hartley, 2014; Joyce et al., 2014; Hadgu et al., 2017). Thus, the resulting ECPM model takes into account the anisotropies within the DFN model and has heterogeneous hydraulic properties at a model discretization scale (Joyce et al., 2014; Finsterle et al., 2018). ECPM models constructed by direct upscaling of DFN networks can reproduce the flow predicted in the DFN models while in the independently set ECPM models, the nuclides arrival times are delayed due to the differences in fractures connectivity (Hadgu et al., 2017). Further simplification of the complex flow system in the fracture networks into homogeneous CPM model leads to unreasonable solutions (Finsterle et al., 2018), although a homogeneous CPM approach is used in the areas without sufficient borehole information or in the studies focusing at the regional scales (Follin and Hartley, 2014; Selroos and Follin, 2014). In the case of multiple, stochastic realizations of the DFN models, ECPM models are also stochastic (Follin et al., 2014; Hadgu et al., 2017).

DFN models are often embedded into CPM models (Figure A2), which are used to track model particles from the canister location or the boundaries of the near field repository model to the surface. In the embedded models consisting of fractures cutting through deposition holes (DFN model) and the far field host rock and overlying deposits (CPM model), the particles move freely between DFN and CPM domains (ANDRA, 2005; Joyce et al., 2014; Sawada et al., 2015; Finsterle et al., 2018). The release of the nuclides in the ECPM model cells is equivalent to the release rates (mol/yr) calculated in the complex near field models (ANDRA, 2005; Selroos and Painter, 2012).

ECPM models, without embedded DFN models, can be used to model the evolution of groundwater composition over time (Follin and Hartley, 2014) or to trace particles and nuclide transport in the equivalent of the fracture network (Hadgu et al., 2017). In the three-dimensional domain, a comparison of transport in DFN and ECPM models is made by deactivation of the unfractured rock matrix cells in the ECPM models (Hadgu et al., 2017).

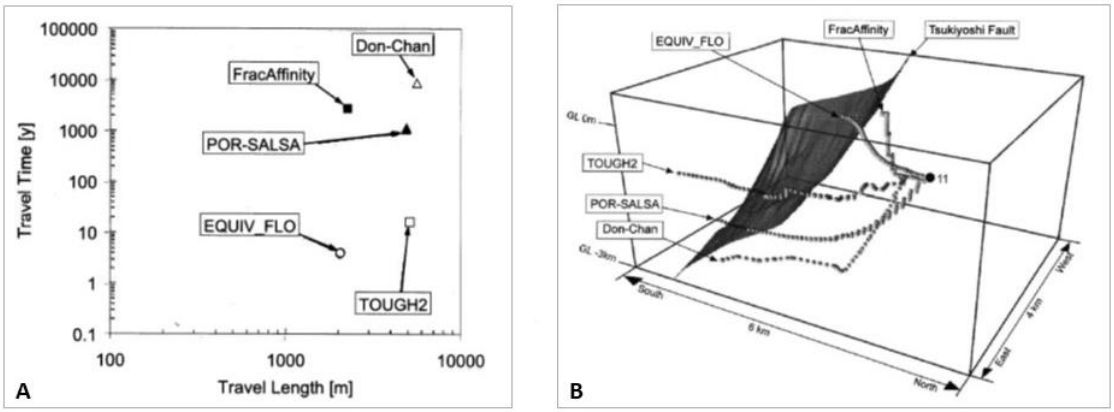

***Figure A3**. Influence of the different conceptualizations of granite as a host rock on the modeling results. A. Particle travel time from the same starting point (shown in panel B as point 11) obtained using different modeling codes and conceptualizations. The names in the boxes depict the applied modeling code. B. Simulated groundwater travel paths from the starting point 11 using different modeling codes and conceptualizations (Sawada et al., 2005).*

***Figur A3**. Effekt af forskellige konceptualiseringer af granit som værtsbjergargt på modelresultaterne. A. Partikelopholdstid fra den same start lokalitet (vist i B som punkt 11) simuleret med forskellige modelleringskoder og konceptualiseringer. Navnene i tekstboksene refererer til de anvendte modelleringskoder. B. Simulerede partikelbaner fra startpunktet 11 ved brug af forskellige modelleringskoder og konceptualiseringer (Sawada et al., 2005).*

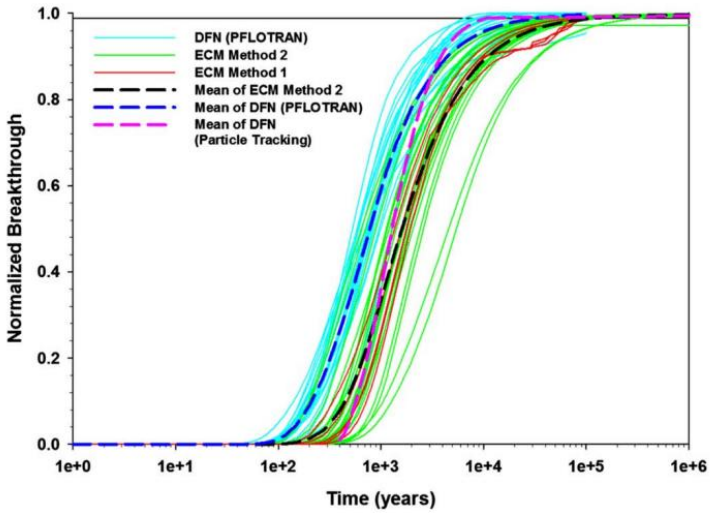

***Figure A4**. Breakthrough curves for the DFN model and corresponding ECPM model (Hadgu et al., 2017).*

***Figur A4**. Gennembrudskurver for DFN modellen og tilhørende ECPM model (Hadgu et al., 2017).*

Influence of various conceptualizations of flow in granite on nuclides transport is shown in Figures A3 and A4. Application of various hydrogeological parameter sets for granite as a host rock and variations in conceptualization of fractures led to high variation in the travel time and travel path length at the repository site in Japan (Sawada et al., 2005; Figure A3). Influence of different conceptualization of fracture networks on the simulation results was also tested at the theoretical site by Hadgu et al. (2017). The arrival times of nuclides in the ECPM models are delayed compared to DFN models due to the differences in hydraulic properties (Hadgu et al., 2017; Figure A4). The inclusion of matrix diffusion in ECPM models further delays the nuclide arrivals (Hadgu et al., 2017; Figure A5).

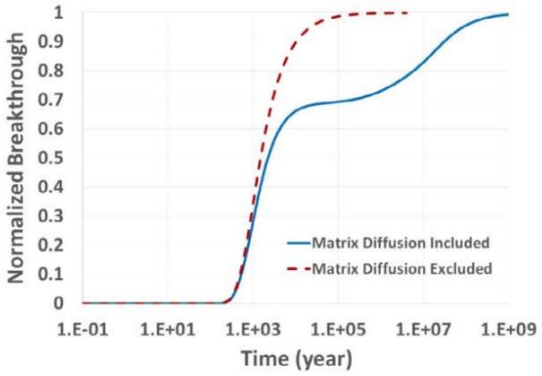

***Figure A5**. Breakthrough curves for ECPM model with and without matrix diffusion (Hadgu et al., 2017).*

***Figur A5**. Gennembrudskurver for ECPM model med og uden matrix diffusion (Hadgu et al., 2017).*

Modeling of flow and transport in Danish granite

There is no data on the geological, hydrogeological, and chemical conditions in the Danish granite at 500 meters depth and only scarce data exist to 100 meters depth (Gravesen et al., 2021). As mentioned above and in Section 2, the transport of nuclides in granite is site-specific and highly related to the characteristics of the fracture networks. As no relevant data exist for Danish granite, it is not justified to carry out preliminary modeling for assessment of the granite potential as a host rock prior to the collection of the additional data at the depth of interest. Nevertheless, as shown in detailed studies from Sweden and Finland, granite of the Fenno-Scandian shield at a depth of 500 meters has a host rock potential. As the granite and gneiss occurring on Bornholm constitute the southernmost extension of the Fenno-Scandian shield these studies are expected to be representative for the Danish granites.

References

ANDRA, 2005: Dossier 2005 Granite – Safety analysis of a geological repository. pp.782.

Finsterle, S., Lanyon, B., Åkesson, M., Baxter, S., Bergström, M., Bockgård, N., Dershowitz, W., Dessirier, B., Frampton, A., Fransson, Å., Gens, A., Gylling, B., Hancilova, I., Holton, D., Jarsjö, J., Kim, J.S., Kröhn, K.P., Malmberg, D., Pulkkanen, M., Sawada, A., Sjöland, A., Svensson, U., Vidstrand, P., Visvanathan, H., 2018: Conceptual uncertainties in modelling the interaction between engineered and natural barriers of nuclear waste repositories in crystalline rocks. In: Multiple roles of clays in radioactive waste confinement. Norris S., Neeft E.A.C., Geet V. (eds). Geological Society, London.

Follin, S., Hartley, L., Jackson, P., Roberts, D., Marsic, N., 2008: Hydrogeological conceptual model development and numerical modelling using CONNECTFLOW, Forsmark modelling stage 2.3. R-08-23. pp.139.

Follin, S., Hartley, L., 2014: Approaches to confirmatory testing of a groundwater flow model for sparsely fractured crystalline rock, exemplified by data from the proposed high-level nuclear waste repository site at Forsmark, Sweden. *Hydrogeol. J.* 22: 333–349.

Follin, S., Hartley, L., Rhen, I., Jackson, P., Joyce, S., Roberts, D., Swift, B., 2014: A methodology to constrain the parameters of a hydrogeological discrete fracture network model for sparsely fractured crystalline rock, exemplified by data from the proposed high-level nuclear waste repository site at Forsmark, Sweden. *Hydrogeol. J.* 22: 313–331.

Gravesen, P., Jakobsen, P. R., Nilsson, B., Pedersen, S.A.S., Midtgaard, H. H., 2021: Studies of geological properties and conditions for deep disposal of radioactive waste, Denmark. Report no. 5. Precambrian crystalline basement distribution and properties. GEUS Report no. 2021/56. 97 pp.

Hadgu, T., Karra, S., Kalinina, E., Makedonska, N., Hyman, J.D., Klise, K., Viswanathan, H.S., Wang, Y., 2017: A comparative study of discrete fracture network and equivalent continuum models for simulating flow and transport in the far field of a hypothetical nuclear waste repository in crystalline host rock. *J. Hydrol.* 553: 59–70.

Hartley, L., Joyce, S., 2013: Approaches and algorithms for groundwater flow modelling in support of site investigations and safety assessment of the Forsmark site, Sweden. *Hydrogeol. J.* 500: 200–216.

Joyce, S., Hatley, L., Applegate, D., Hock, J., Jackson, P., 2014: Multi-scale groundwater flow modeling during temperate climate conditions for the safety assessment of the proposed high-level nuclear waste repository site at Forsmark, Sweden. *Hydrogeol. J.* 22: 1233–1249.

Sawada, A., Saegusa, H., Ijiri, Y., 2005: Uncertainty in groundwater flow simulations caused by multiple modeling approaches, at the Mizunami Underground Research Laboratory, Japan. Geophysical Monograph Series 162: 91–101.

Sawada, A., Saegusa, H., Takeuchi, S., Sakamato, K., Dershowitz, W.S., 2015: Äspö Task Force on modelling groundwater flow and transport of solutes. Task 7 – Groundwater flow and transport modelling of fracture system at regional, block, and single-fracture scale flow and transport, Olkiluoto. P-13-46. pp.82.

Selroos, J.O., Painter, S.L., 2012: Effect of transport-pathway simplifications on projected releases of radionuclides from a nuclear waste repository (Sweden). *Hydrogeol. J.* 20: 1467–1481.

Selroos, J.O., Follin, S., 2014: Overview of hydrogeological site-descriptive modelling conducted for the proposed high-level nuclear waste repository site at Forsmark, Sweden. *Hydrogeol. J.* 22: 295–298.

Vidstrand, P., Follin, S., Selroos, J.O., Naslund, J.O., 2014: Groundwater flow modeling of periods with periglacial and glacial climate conditions for the safety assessment of the proposed high-level nuclear waste repository site at Forsmark, Sweden. *Hydrogeol. J.* 22: 1251–1267.

Appendix B. Porosity and permeability statistics of the chalk/limestone

Peter Frykman

Data background

The present report summarises statistics of the porosity and permeability of the chalk package as known from a few wells penetrating to 500–600 meters below surface, having available core plug measurements and a few supplementary hydraulic test interpreted permeabilities.

The data used is the same data as incorporated in the main report on the geological characterisation of chalk (Jakobsen et al., 2021), and a brief summary of their origin is given here.

***Table B1**. List of wells with data from core material or hydraulic tests in the chalk/limestone sequence. Data from hydraulic tests from depths at 500 meters is available only from the ES1–ES4 wells.*

***Tabel B1**. Liste over boringer med data fra kerne materiale eller hydrauliske test i kalkpakken. Data fra hydrauliske test fra 500 meters dybde findes kun fra ES1–ES4 boringerne.*

Table for depth of wells with chalk/limestone		
	Well name	Total depth
		m.
	E1S	561
	E2S	551
	E3S	551
	E4S	553
	Rørdal-1	100
	Dalbyover-1	350
	Skælskør-1	263
	Stevns-1	450
	Stevns-2	350
	Brøndby	19
	Karlstrup	31
	Karlslunde-1	269
	Tune-1	50
	Tuba-13	125

The data background includes 1) core material from wells, 2) outcrop material from surface, and 3) hydraulic tests in wells at variable depths. The wells with available data are listed in Table B1, they are shown on the map (Figure B1) and in the well panel (Figure B2) from west to east across the Danish onshore area. Most of the data have been collected in connection with studies on groundwater flow and transport and mainly focussing on production of water

***Figure B1**. Map showing the wells and outcrops with data available for the present study.*

***Figur B1**. Kort der viser placering af boringer og blotninger hvorfra data er tilgængelige.*

from the uppermost 50–100 meters. The retardation of flow and the sealing properties of the chalk has therefore not been studied at the same detail, which significantly limits the interpretation of seal capacity of the chalk. Only few wells penetrate down to a depth around 500 meters, which limits the data background for this section.

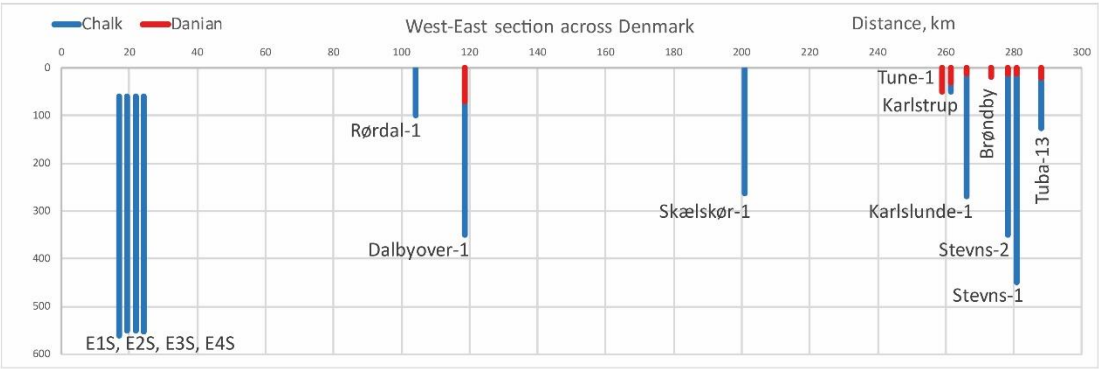

***Figure B2**. Well panel showing the penetration of the chalk/limestone in a West – East section where data have been available for the present study.*

***Figur B2**. Brøndpanel fra vest til øst som viser, hvor data er tilgængelige fra den gennemborede kalkpakke.*

Petrophysical properties of the chalk/limestone package

The hydraulic behaviour of chalk and limestones is controlled by the matrix properties and the presence of open fractures. The amount of open fractures fully determines the potential for extracting groundwater which is generally restricted to the upper 50 meters of the chalk/limestone formations. This is due to the glacial deformation history with fracturing of the upper layer, whereas deeper levels were left relatively undisturbed.

Data availability

Only few detailed investigations of porosity and hydraulic conductivity have been carried out in the deeper parts of the chalk and limestone sediments that are of interest here. The matrix properties have been sampled and analyzed extensively in wells, where drill cores are available and where formations are exposed at surface or in quarries.

The two wells Stevns-1 and Stevns-2 were drilled as scientific wells during 2005, reaching depths of 450 and 350 meters. The oldest strata recovered were dated as Late Campanian (Stemmerik et al., 2006; Surlyk et al., 2013). Outcrops at Stevns have supplied data for the uppermost parts of the sequence for both the Danian bryozoan limestones and the uppermost Maastrichtian chalk (Frykman, 2001). The core plug measured porosity and permeability from material in the deepest of the two wells, Stevns-1, is used in this report as representative material for most of the chalk package.

The well Skælskør-1 (263 meters total depth) penetrated down into Late Campanian limestone (Thibault et al., 2015). The well Dalbyover-1 penetrates a special lithology in the Danian of lime mudstone which is specific for this central part of the Danish Basin. This lime mudstone has a thickness of more than 60 meters in the well. The underlying Maastrichtian chalk is also cored. For investigating the sealing properties of the chalk overlying the Mors Salt Dome, 4 wells (E1S, E2S, E3S, E4S) were drilled to a depth of 550 meters., and a summary was reported (Gosk et al., 1981).

Matrix porosity and permeability of chalk and limestone

Matrix investigations have been carried out in two main material sources: 1) outcrops or shallow pits of different formations and 2) core material from wells drilled through various parts of the sequence. Most of the available data on porosity and permeability originates from core measurements in the laboratory, and the standard measurements of gas permeability is sometimes supplemented with Klinkenberg corrected measurements, and rarely with a few fluid permeability measurements. The measured gas permeability values obtained for this report have been recalculated to a proxy for fluid permeability with a generally applied function for low permeability chalk (Mortensen et al. 1998):

$$k_{fluid} = 0.52 \cdot k_{gas}^{1.083}$$

The porosity and permeability data clearly show two main populations (Figure B3) that can be linked to either the Danian limestones/bryozoan limestones, or to the more fine grained and less permeable chalk or lime mudstones. The separation of the data from the Erslev

wells at even lower permeabilities is probably due to diagenetic effects linked to the location immediately above a salt dome induced structure.

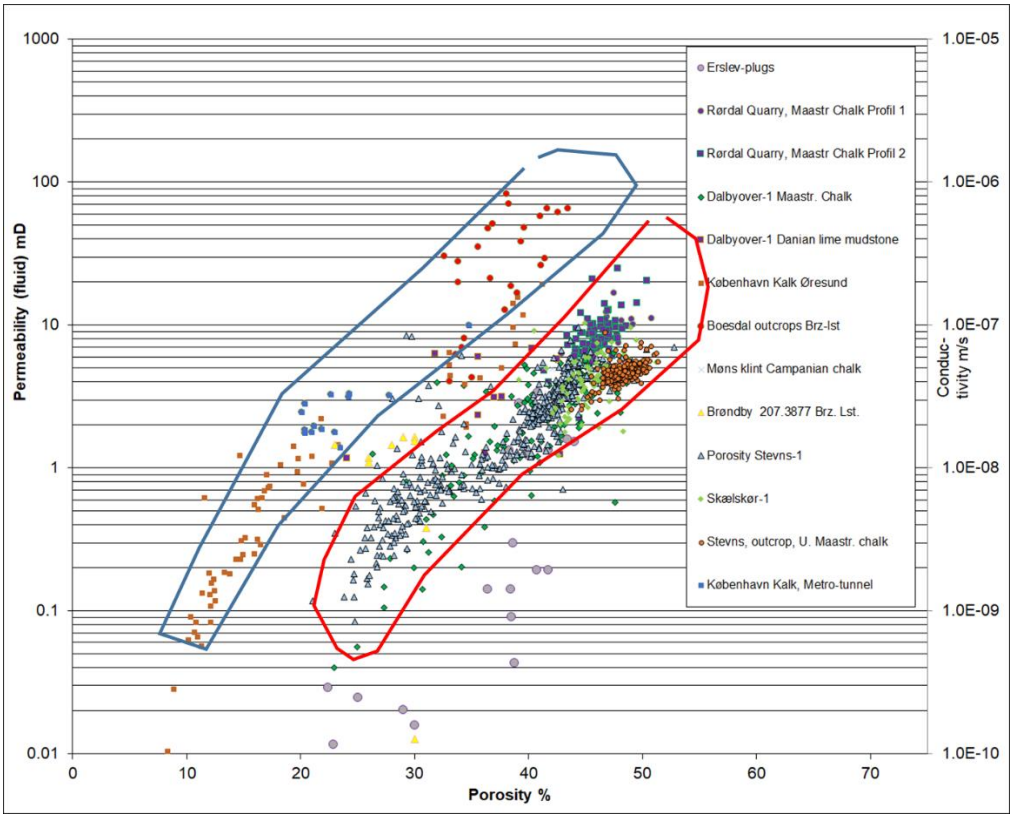

***Figure B3**. Crossplot of the porosity and permeability from different formations. The two main populations are the Danian limestones (blue) and the Upper Cretaceous chalks (red).*

***Figur B3**. Figuren viser relationen mellem porøsitet og permeabilitet for de forskellige dele af kalkpakken og illustrerer opdelingen i to hovedpopulationer der knytter sig til henholdsvis Danien kalksten/bryozokalk (blå) samt til den mere finkornede kridt bjergart (rød) med mindre permeabiliteter.*

Hydraulic parameters from deep well tests on Mors, North Jylland

Extensive hydraulic testing was carried out in wells in the 500 meters thick chalk package directly overlying the salt dome in a project investigating the potential for a storage facility for radioactive waste in a salt dome on the island of Mors in Northern Jylland.

Laboratory measurements of permeability and porosity on core plugs of the chalk formation from the wells E1-2-3-4S were carried out by DGU, Risø and Institute of Geological Sciences Wallingford, England. The core plug permeabilities were measured with gas permeameter and the values have been converted to fluid permeability with an empirical relation (Mortensen, 1998) to enable comparison to the hydraulic test results (Figure B4).

The similarity in permeability levels for matrix measurements and pumping tests indicates that fractures play a very limited role in the inflow to the wells during test pumping. The permeability of 1 mD is equal to conductivity $1*10^{-8}$ m/sec.

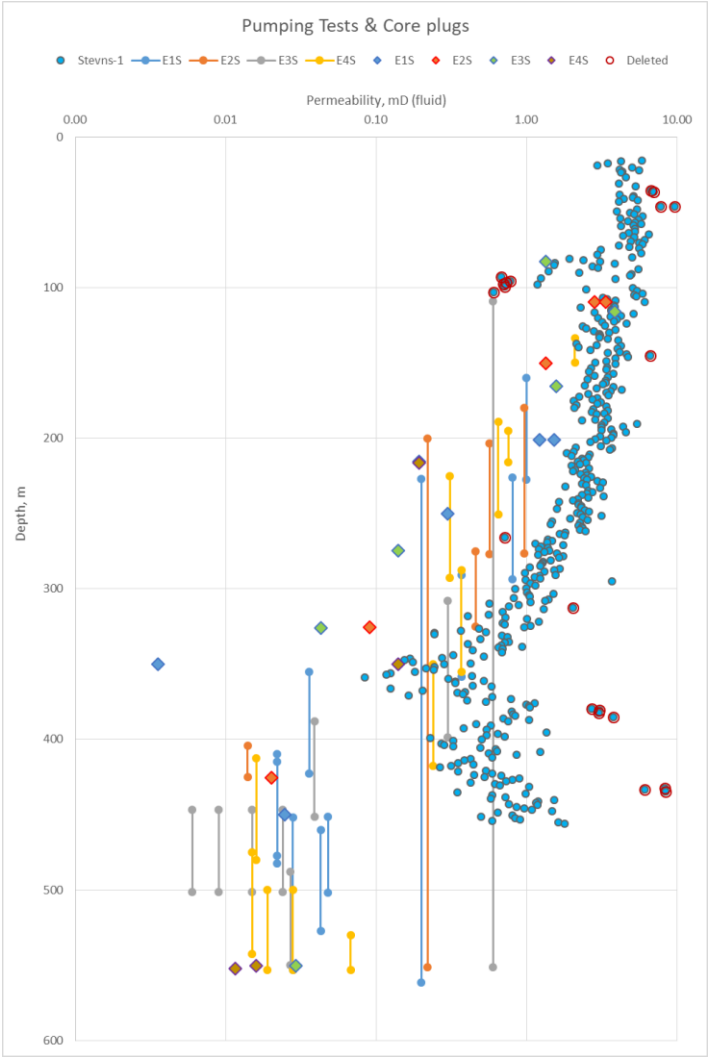

***Figure B4**. Figure showing permeability/depth comparison of the matrix measured permebilities in Stevns-1 and from core material from the Erslev wells and pumping test interpretations of interval permeabilities. The core measured gas permeabilities have been converted to fluid permeability for this comparison. Permeability of 1 mD equals a conductivity of $1*10^{-8}$ m/sec.*

***Figur B4**. Sammenligning af permeabilitets data fra Stevns-1 og matrix målte permeabiliteter fra kerne materiale fra Erslev boringerne og interval permeabiliteter tolkede fra pumpetest. De kerne målte gas permeabiliteter er blevet omregnet til væske permeabilitet til denne sammenligning. En permeabilitet på 1 mD svarer til en konduktivitet $1*10^{-8}$ m/sec.*

Porosity and permeability depth trends

The compaction and cementation processes have modified the primary high porosity of the various carbonates. The effect of the processes is slightly depending on the primary lithology, i.e. grainsize, mineralogy, clay content etc. but the figure shows overall decrease of porosity with depth trends for several data sets (Figure B5). A decrease with depth is also obvious for the matrix permeability and for the well tests available from the Erslev wells (Figure B4). The matrix permeabilities measured in the lowest part of the section in the Erslev wells might be anomalous since the chalk is directly overlying a salt diapir and have under-gone late uplift from previous deeper levels.

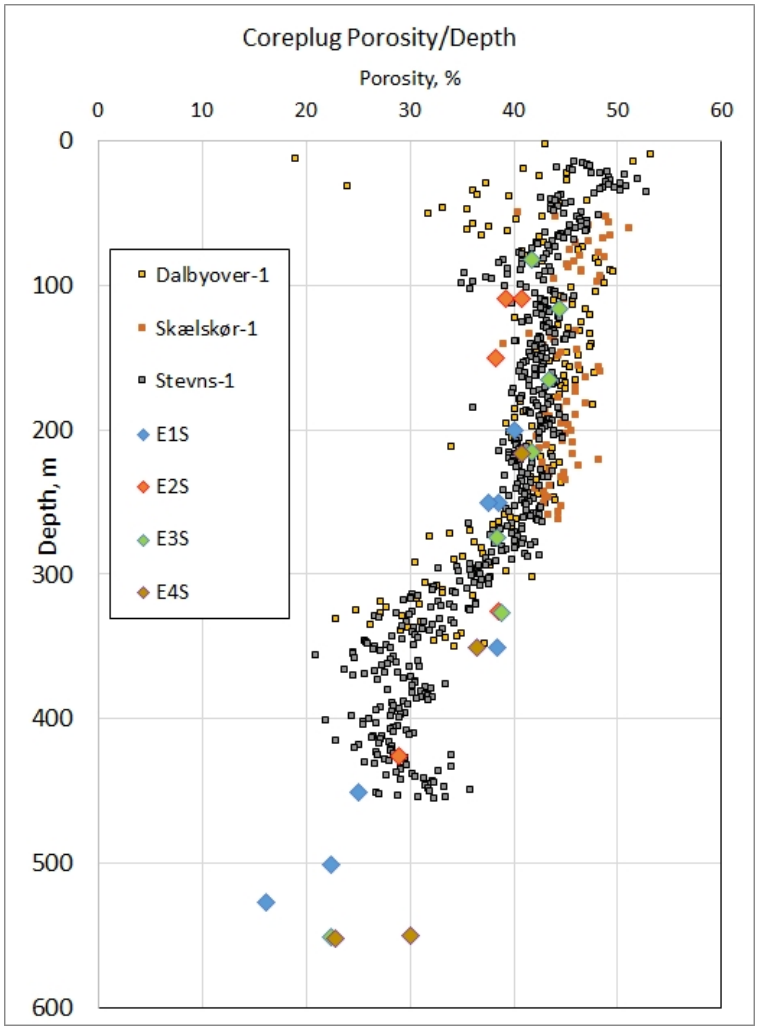

***Figure B5**. Porosity/depth trend for core measurements in selected wells is shown. The deviation towards low porosity at around 100 meters depth in the Stevns-1 well is caused by high clay content in the chalk at this level.*

***Figur B5**. Porøsitet mod dybde vist for kerne målte data fra udvalgte boringer. De lave porøsitetsværdier ved ca. 100 meters dybde for Stevns-1 skyldes tilstedeværelse af ler i dette niveau.*

Porosity and permeability distributions for modeling

For the purpose of modeling flow and diffusion the distribution of porosity and permeability has been simplified by subdividing the section into two main parts. For each part the distribution of the parameters has been analysed by calculating min/max, mean and standard deviation, and for permeability also a harmonic average. The subdivision is chosen at 300 meters depth, separating two slightly different trends in both porosity and permeability (Figure B6).

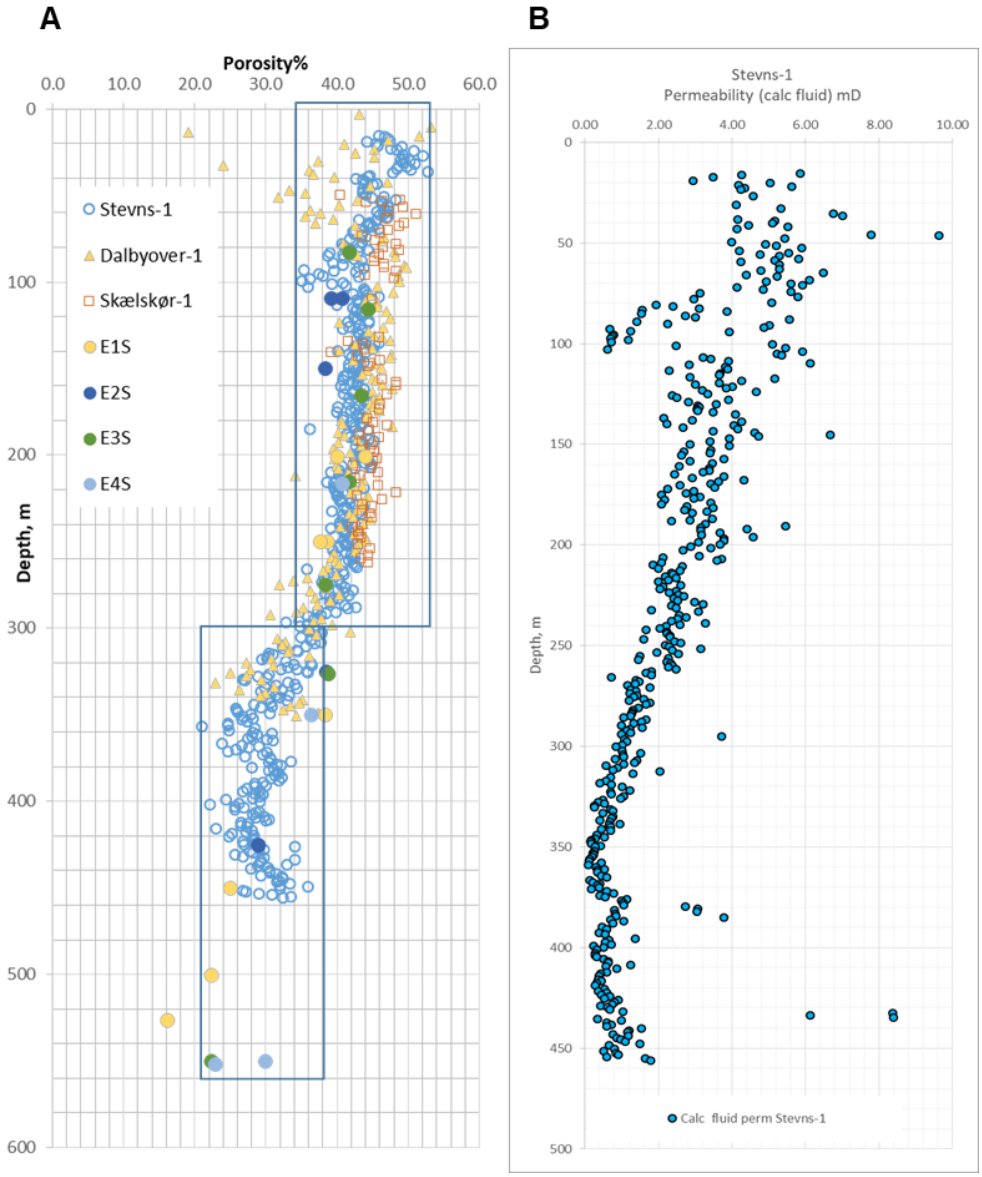

***Figure B6**. A: Porosity with depth including data from both the Erslev wells and three other wells (Stevns-1, Skælskør-1, Dalbyover-1). B: Permeability data for Stevns-1 only, showing the depth relation.*

***Figur B6**. A. Sammenligning af porøsitet mod dybde for Erslev boringerne og 3 andre boringer (Stevns-1, Skælskør-1, Dalbyover-1). B: Stevns-1 permeabilitets data viser dybde fordelingen.*

The min/max values for porosity have been selected as: Upper 34/53, Lower 21/38. A few permeability datapoints from the original dataset have been excluded in some of the cases investigated, as the very high values have been evaluated to be deviating measurements caused by small fractures artificially induced in the plug samples. The exotic low-permeability samples caused by high clay content at depths around 100 meters can also be evaluated. The points in question are indicated on the permeability plots (Figure B7).

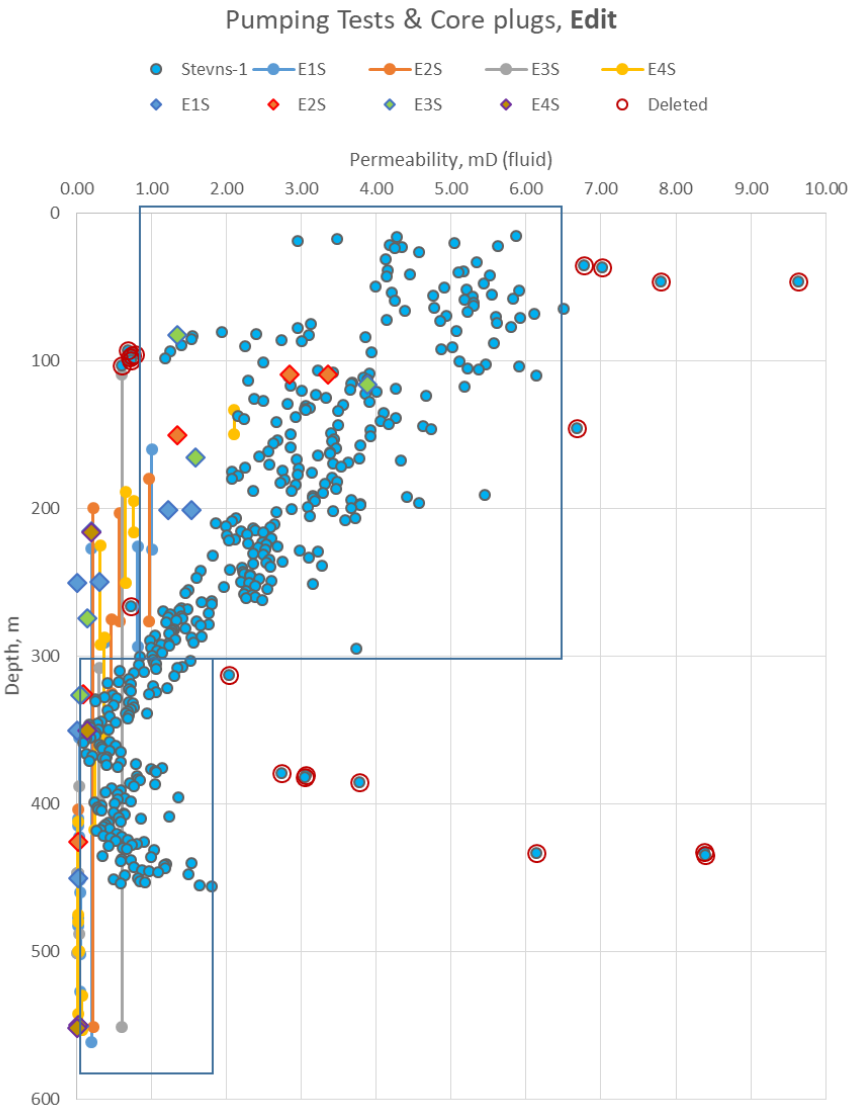

***Figure B7**. Permeability with depth including data from both the Erslev wells and the Stevns-1 well. The deviation towards low permeability at around 100 meters depth in the Stevns-1 well is caused by a high clay content in the chalk at that level. Data points undergoing exclusion are shown with red ring.*

***Figur B7**. Sammenligning af permeabilitet mod dybde for Erslev boringerne og Stevns-1 boringen. Afvigelse mod lav permeabilitet ved ca. 100 meters dybde for Stevns-1 data skyldes ler-indhold i dette niveau. Udeladte data punkter er vist med rød ring.*

For a better view of the distribution in the low permeabilities, a plot with log-scale for permeability is also supplied (Figure B8).

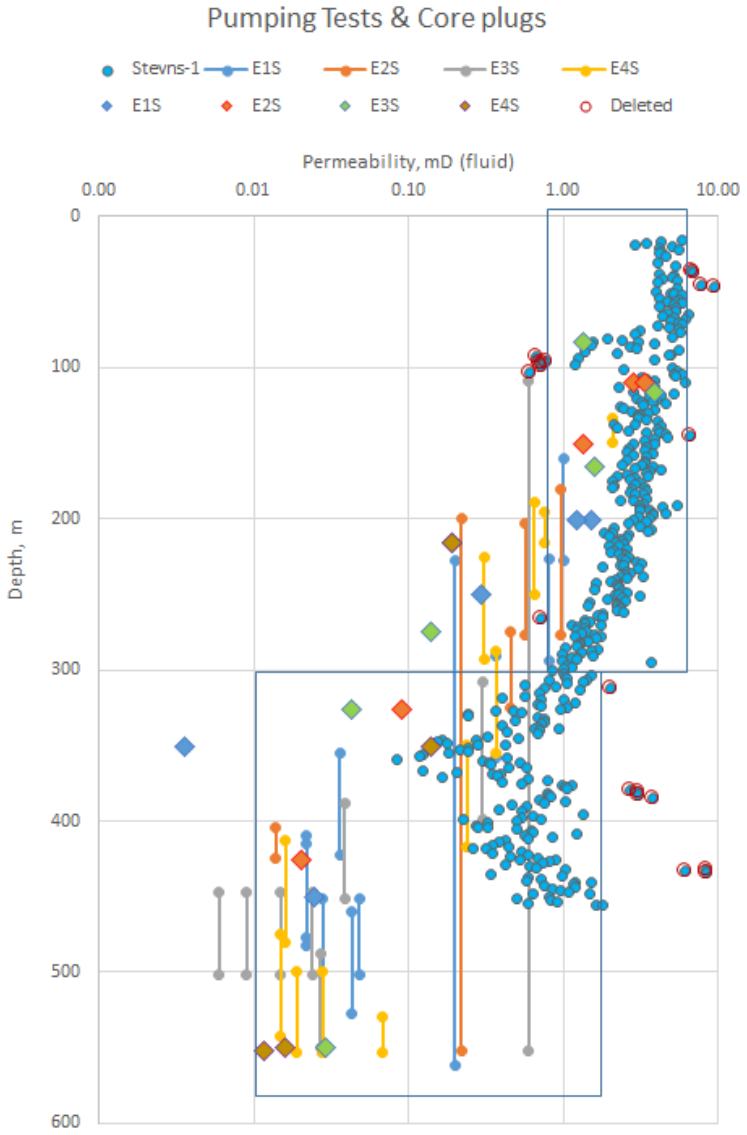

***Figure B8**. Permeability with depth including data from both the Erslev wells and the Stevns-1 well. The deviation towards low permeability at around 100 meters and 350 meters depth in the Stevns-1 well is caused by a high clay content in the chalk at those levels. Excluded data points shown with red ring.*

***Figur B8**. Sammenligning af permeabilitet mod dybde for Erslev boringerne og Stevns-1 boringen. Afvigelse mod lav permeabilitet ved cirka 100 og 350 meters dybde for Stevns-1 data skyldes ler-indhold i disse niveauer. Udeladte data punkter er vist med rød ring.*

As mentioned, the permeability min/max is selected as: Upper 0.8/6.5, Lower 0.01/1.8. The selection of the minimum range for the lower part as shown in Figure B8 can be questioned since only the data from the Erslev wells cover the range from 0.01 to 0.1, and these wells could have anomalous low values in this lower part due to influence from fluids connected to the underlying salt diaper. The marly chalk around 100 meters depth is also a deviation from

the normal chalk depth trend and requires extra analysis. Therefore, the developed statistical distributions include the following alternative cases:

1. Distribution based on the Stevns-1 data only (excluding the marl samples), establishing the lower bound for the lower part at 0.1 mD (fluid permeability).
2. Distribution based on the Stevns-1 data including the marly interval around 100 meters depth.
3. Distribution based on the merged Erslev well and Stevns-1 (excluding marl) data.
4. Distribution based on the merged Erslev well and Stevns-1 (including marl) data.

Statistics for porosity and permeability distributions

A combined plotting and calculation is performed with a histogram plotting routine from the GSLib software library, showing the histogram and box-plot with mean value added as box-point. The derived statistics for the four cases are summarized in Table B2.

***Table B2**. Calculated statistics for 4 cases.*

***Tabel B2**. Calculated statistics for 4 cases.*

Case 1	Porosity					Porosity				
Stevns-1 data,	Upper (<300 m)					Lower (>300 m)				
excluding the marl	Mean	Std	min	max		Mean	Std	min	max	
interval around 100 m depth	42.50	2.98	34.70	52.80		30.00	3.32	21.00	37.80	
	Permeability					Permeability				
	Upper (<300 m)					Lower (>300 m)				
	Mean	Std	min	max	Harmonic mean	Mean	Std	min	max	Harmonic mean
	3.15	1.30	0.98	6.49	2.58	0.66	0.35	0.08	1.79	0.46
Case 2	Permeability					Permeability				
Stevns-1 data,	Upper (<300 m)					Lower (>300 m)				
including the marl	Mean	Std	min	max	Harmonic mean	Mean	Std	min	max	Harmonic mean
interval around 100 m depth	3.09	1.34	0.61	6.49	2.44	0.66	0.35	0.08	1.79	0.46
Case 3	Permeability					Permeability				
Merged Erslev and Stevns-1 data,	Upper (<300 m)					Lower (>300 m)				
excluding the marl	Mean	Std	min	max	Harmonic mean	Mean	Std	min	max	Harmonic mean
interval around 100 m depth	3.07	1.35	0.14	6.49	2.16	0.62	0.37	0.04	1.79	0.17
Case 4	Permeability					Permeability				
Merged Erslev and Stevns-1 data,	Upper (<300 m)					Lower (>300 m)				
including the marl	Mean	Std	min	max	Harmonic mean	Mean	Std	min	max	Harmonic mean
interval around 100 m depth	3.02	1.37	0.14	6.49	2.07	0.62	0.37	0.04	1.79	0.17

Porosity statistics

The porosity distribution is analysed from the data set of Stevns-1 (including the marly chalk around depth of 100 meters, see Figure B6). The four cases have very similar porosity distributions, so the distributions shown in Figure B9 for the two depth intervals are taken as representative for all four cases studied and the summary statistics are given in Table B2.

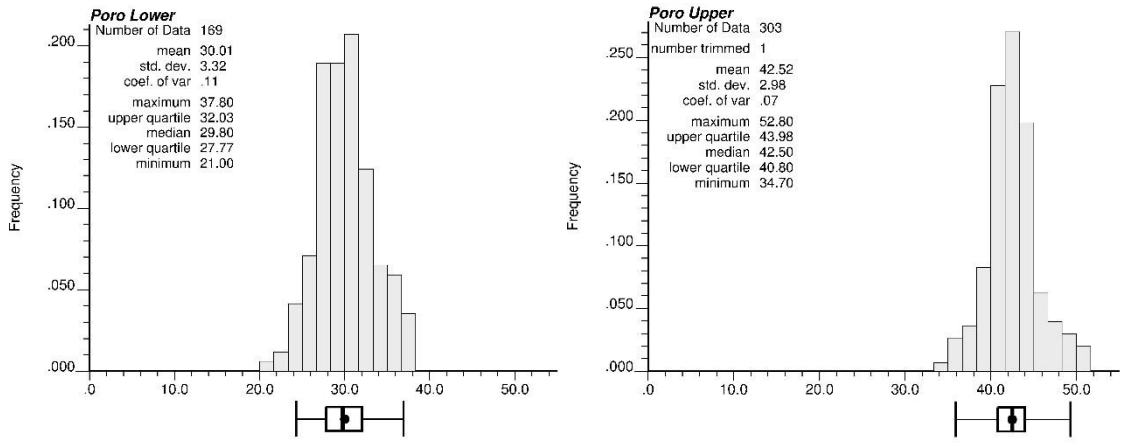

A B

Figure B9*. Histogram for porosity in the Lower (A) and Upper part (B). The median is indicated with a line in the box and the mean is added as a point.*

Figur B9*. Histogram for porøsitet i Nedre og Øvre del. Median værdien er indikeret med en linie i boxen og middelværdien tilføjet som et punkt.*

Permeability statistics

Case 1 – Stevns-1 without marly interval
As mentioned previously the first case for statistics for permeability are based exclusively on the data from the Stevns-1 well and leaving out the low permeability values from the marly interval around 100 meters depth. The permeability distribution for the lower and upper part is shown in two versions, linear and log-scale (Figures B10 and B11). The permeability is often treated as a lognormal distribution which is confirmed in Figure B10(B).

The histograms include the values for the arithmetic means. However, for vertical flow going across the layering, the harmonic mean will be a more relevant estimate of bulk permeability. This calculation gives:
Harmonic mean Upper section (<300meters depth): 2.58
Harmonic mean Lower section (>300meters depth): 0.46

Case 2 – Stevns-1 including marly interval
This case includes the low permeability values from the marly interval around 100 meters depth in Stevns-1 well. The calculated statistics are included in Table B2.

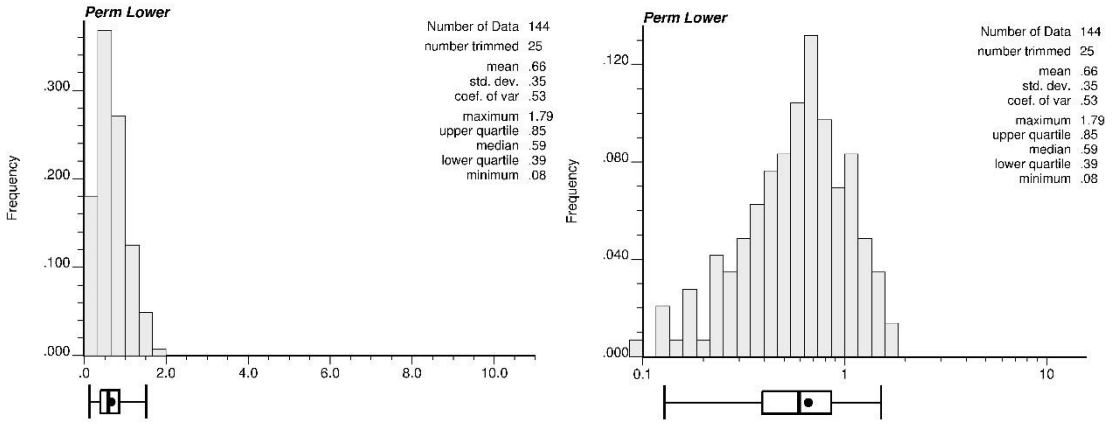

A B

***Figure B10**. Histogram for permeability in the Lower part shown in Linear (A) and Log-scale (B). The median is indicated with a line in the box and the mean is added as a point.*

***Figur B10**. Histogram for permeabilitet i Nedre del vist med linear (A) og logaritmisk (B) skala. Medianværdien er indikeret med en linie i boxen og middelværdien tilføjet som et punkt.*

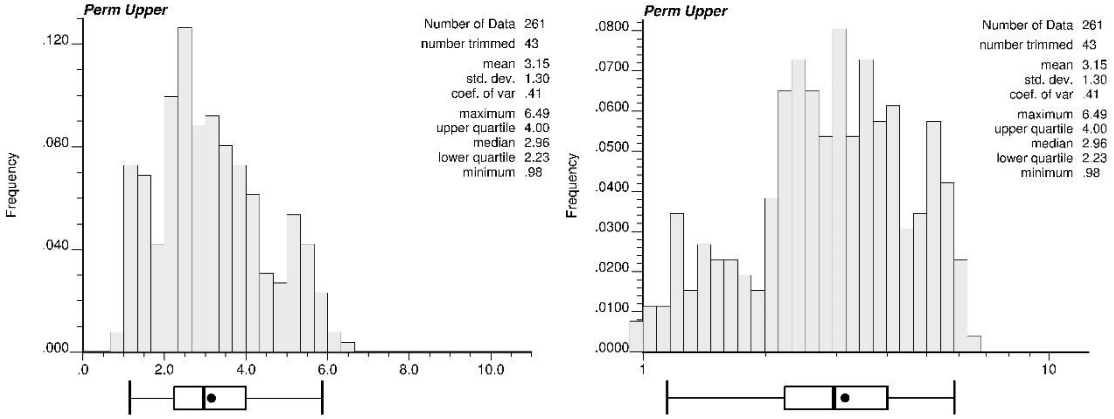

A B

***Figure B11**. Histogram for permeability in the Upper part shown in Linear (A) and Log-scale (B). The median is indicated with a line in the box and the mean is added as a point.*

***Figur B11**. Histogram for permeabilitet i Øvre del vist med linear (A) og logaritmisk (B) skala. Medianværdien er indikeret med en linie i boxen og middelværdien tilføjet som et punkt.*

Case 3 - Permeability statistics for data including Erslev wells and Stevns-1

The following statistics for permeability are based on the merged data from the Stevns-1 well (excluding marl layer around 100 meters depth) and the limited number of plug analyses from the Erslev wells. As mentioned earlier the chalk from the Erslev wells could be deviating from normally compacted chalk at depths around 500–600 meters. It should be noted that the porosities measured on the Erslev samples generally is within the interval given by the Stevns-1 data. The lowered permeabilities could be explained by the presence of a salt diapir

directly underlying the formation and maybe contributing with deeper fluids causing additional diagenesis and cementation. Despite this potential deviation these data are not ignored but included in this supplementary analysis of case 3 and case 4. The permeability distributions are shown in log-scale (Figure B12).

The histograms include the values for the arithmetic means. However, for vertical flow going across the layering, the harmonic mean will be a more relevant estimate of bulk permeability. This calculation gives for the merged data from Stevns-1 and the Erslev wells:
Harmonic mean Upper section (<300meters depth): 2.16
Harmonic mean Lower section (>300m depth): 0.17

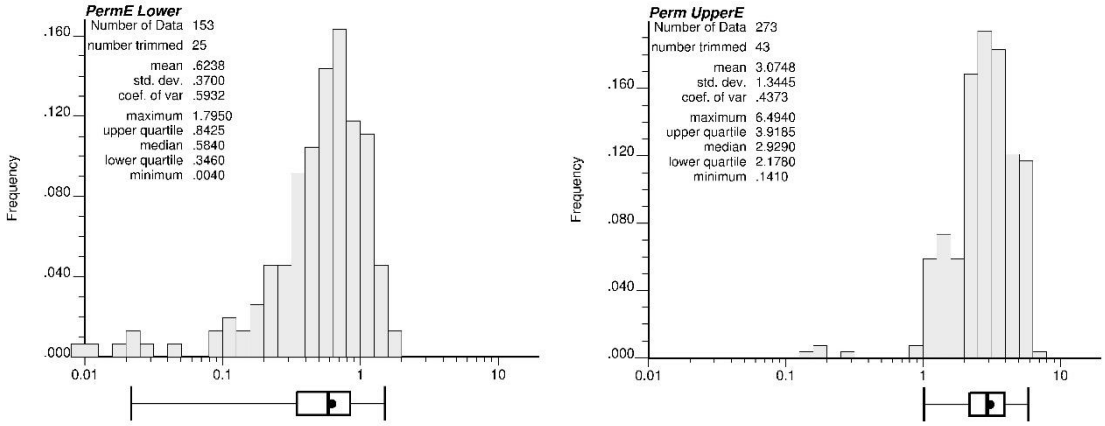

A B

Figure B12*. A: Histogram for permeability (Stevns-1 and Erslev) in the Lower part shown in Log-scale. The median is indicated with a line in the box and the mean is added as a point. B: Histogram/Boxplot for permeability (Stevns-1 and Erslev) in the Upper part shown in Log-scale. The median is indicated with a line in the box and the mean is added as a point.*

Figur B12*. A: Histogram for permeabilitet (Stevns-1 og Erslev) i Nedre del vist med logaritmisk skala. Medianværdien er indikeret med en linie i boxen og middelværdien tilføjet som et punkt. B: Histogram/Boxplot for permeabilitet (Stevns-1 og Erslev) i Øvre del vist med logaritmisk skala. Medianværdien er indikeret med en linie i boxen og middelværdien tilføjet som et punkt.*

Case 4 - Permeability statistics for data including Erslev wells and Stevns-1
The statistics for permeability are based on the merged data from the Stevns-1 well (now including the marl layer around 100 meters depth) and the limited number of plug analyses the Erslev wells. The calculated statistics are included in Table B2.

References

Frykman, P. 2001: Spatial variability in petrophysical properties in Upper Maastrichtian chalk outcrops at Stevns Klint, Denmark. *Marine and Petroleum Geology* 18: 1041–1062.

Gosk, E., Bull, N., Andersen, L.J. 1981: Hydrogeological Main Report, Geological Survey of Denmark, April 1981.

Jakobsen, P.R., Frykman, P., Jakobsen, R. 2021: Studies of geological properties and conditions for deep disposal of radioactive waste, Denmark. Report no. 3. Upper Cretaceous chalk and Paleocene limestone distribution and properties. GEUS Report no. 2021/54. 76 pp.

Mortensen, J., Engstrøm, F., Lind, I., 1998: The relation among porosity, permeability, and specific surface of chalk from the Gorm field, Danish North Sea. SPE 31062, *SPE Reservoir Evaluation & Engineering* 1: 245–251.

Stemmerik, L., Surlyk, F., Klitten, K., Rasmussen, S.L. & Schousbo, N., 2006: Shallow core drilling of the Upper Cretaceous Chalk at Stevns Klint, Denmark. *Geological Survey of Denmark and Greenland Bulletin* 10: 13–16.

Surlyk, F., Rasmussen, S.L., Bousaha, M., Schiøler, P., Schovsbo, N.H., Sheldon, E. Stemmerik, L., Thibault, N., 2013: Upper Campanian–Maastrichtian holostratigraphy of the eastern Danish Basin. *Cretaceous Research* 46: 232–256.

Thibault, N., Anderskouv, K., Bjerager, M., Boldreel, L.O., Jelby, M.E., Stemmerik, L., Surlyk, F., 2015: Upper Campanian–Maastrichtian chronostratigraphy of the Skælskør-1 core, Denmark: correlation at the basinal and global scale and implications for changes in sea-surface temperatures. *Lethaia* 48: 549–560.

Appendix C. Claystone permeabilities

Liquid permeability was measured only in a few cuttings samples from Danish claystone (Pedersen et al., 2021). Thus, average, minimum, and maximum values and standard deviations of liquid permeability for Danish claystone used in the stochastic simulations were estimated using the measured effective porosities and their relation to liquid permeability described in Mbia et al. (2014). Effective porosity values in various claystone formations and the sampling depths were compiled from Olsen and Jørgensen (2008), Mbia et al. (2014), and Springer et al. (2020). Outlier samples, where sandstone was dominating the lithology were removed from the dataset and a set of 152 samples was analyzed. The high content of sand beds in the claystone sections would decrease the transport time and could create preferential flow paths.

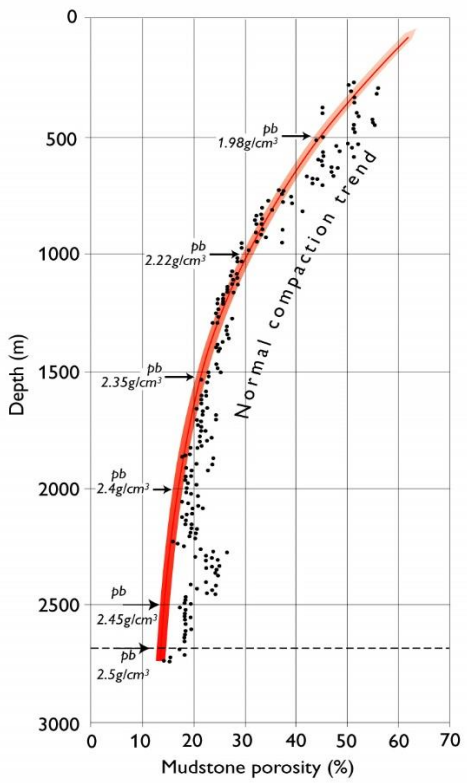

Figure C1*. Compaction trend in mudstones (Magara, 1968).*
Figur C1*. Komprimeringstrenden i lersten (Magara, 1968).*

All available porosity samples are from depths greater than 700 meters and thus the porosity values were migrated to the depth of 500 meters based on the normal compaction trend in mudstones (Magara, 1968, Figure C1). Prior to the porosity correction, each sample depth was increased by 750 meters to account for the compaction related to the glaciations and older deposits, so the porosity values for 500 meters in the Danish claystone correspond to these at 1250 meters. E.g. for the Danish conditions the porosity of 20% measured at 1500 meters. corresponded to porosity of 20% at 2250 meters dept in Figure C1. This value was migrated to 1250 meters. using the red slope in Figure C1.

Median porosity at 500 meters estimated from the corrected dataset equals 29%, which is a typical value for depths greater than 1000 meters. This is due to the glaciations-driven compaction. Minimum and maximum porosities in the dataset were 11 and 44%.

In the next step porosity values were used to read the minimum and maximum claystone permeability from the porosity-permeability relation in shales from the Norwegian-Danish basin (Mbia et al., 2014; Figure C2). Figure C2 shows an impact of the claystone mineralogy on the permeability that varies by a couple of orders of magnitude depending on whether the dominant clay mineral is smectite or kaolinite. Detailed studies of the claystone mineralogy are therefore necessary for the further project stages. The minimum liquid permeability value was 4.5 x 10^{-4} µD, and the maximum was 2710 µD. These values were used to generate a lognormal permeability distribution. A stochastic text file with 1000 values constituting a Gaussian normal distribution was created. These values were then used as exponents to generate the permeability distribution. In an iterative process, the generated exponents were adjusted so that calculated permeability values matched the minimum and maximum liquid permeabilities presented in Figure C2. The histogram with generated permeability values is shown in Figure C3.

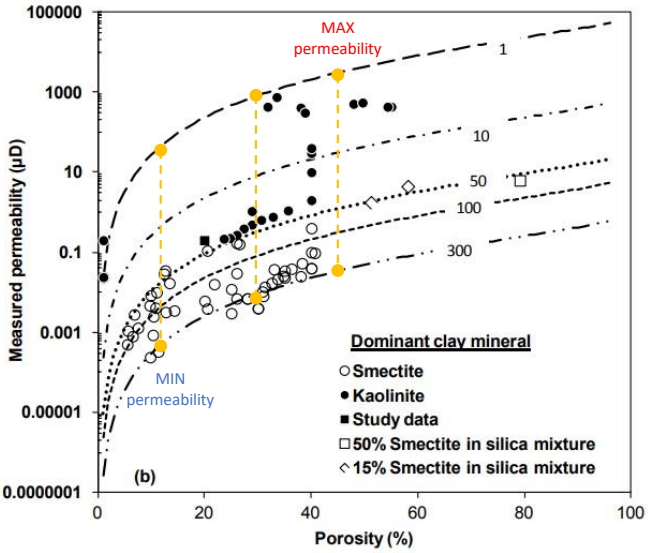

***Figure C2**. Minimum and maximum permeability for Danish claystone from the relation between porosity and permeability in Norwegian-Danish Basin (Mbia et al., 2014).*
***Figur C2**. Minimum og maksimum permeabilitet i danske lersten baseret på porøsitet og permeabilitet forhold i Det Norsk-Danske Bassin (Mbia et al., 2014).*

Average permeability in the generated distribution equals 26 µD, median 1.4 µD, and a harmonic mean of the dataset is 0.06 µD. The generated dataset has a minimum of 4.6 x 10^{-4} µD, a maximum of 2676 µD, and the natural log of the standard deviation is 2.56. For comparison, liquid permeability measured at Fjerritslev Formation was 3 x 10^{-3} to 3200 µD. Permeabilities in µD were transformed into hydraulic conductivities in m/d by multiplying the generated values by 8.64 x 10^{-7}.

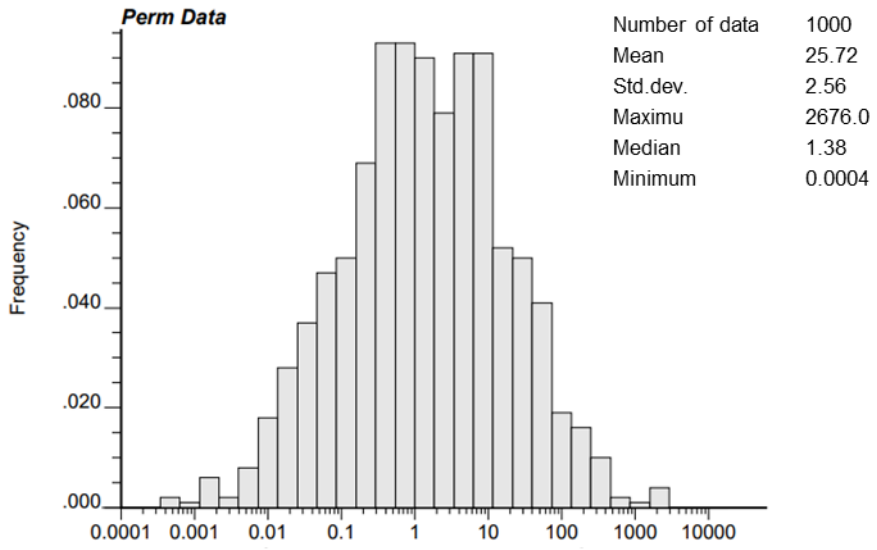

***Figure C3**. Lognormal claystone permeability distribution generated in the iterative process by fitting minimum and maximum permeability to values read from the porosity-permeability relation presented in Mbia et al. (2014).*

***Figur C3**. Histogram for permeabilitet i lersten med logaritmisk skala genereret i den iterative proces ved at tilpasse minimum og maksimum permeabilitet til værdier fra porøsitet-permeabilitet forhold fra Mbia et al. (2014).*

References

Magara, K., 1968: Compaction and migration of fluids in Miocene mudstone, Nagaoka Plain, Japan. *AAPG Bulletin* 52(12): 2466–2501.

Mbia, E.N., Fabricius, I.L., Krogsbøll, A., Frykman, P., Dalhoff, F., 2014: Permeability, compressibility and porosity of Jurassic shale from the Norwegian-Danish Basin. *Pet. Geosci.* 20: 257–281.

Olsen, D., Jørgensen, M., 2008: Conventional core analysis data from 10 Danish onshore wells. Wells Børglum-1, Fjerritslev-2, Frederikshavn-2, Gassum-1, Haldager-1, Horsens-1, Mors-1, Rødby-1, Skagen-2, Vedsted-2. Danmarks og Grønlands Geologiske Undersøgelse Rapport 2008/62. pp.8.

Pedersen, G. K, Lauridsen, B., Sheldon, E., Midtgaard, H. H, 2021: Studies of geological properties and conditions for deep disposal of radioactive waste, Denmark. Report no. 4. Jurassic and Lower Cretaceous claystone distribution, sedimentology, and properties. GEUS Report no. 2021/55. 107 pp.

Springer, N., Dideriksen, K., Holmslykke, H.D., Kjøller, K., Olivarius, M., Schovsbo, N., 2020: Capture, storage and Use of CO2 (CCUS). Danmarks of Grønlands Geologiske Undersøgelse Rapport 2020/30. pp.44.

Appendix D. BTC ensembles in the chalk

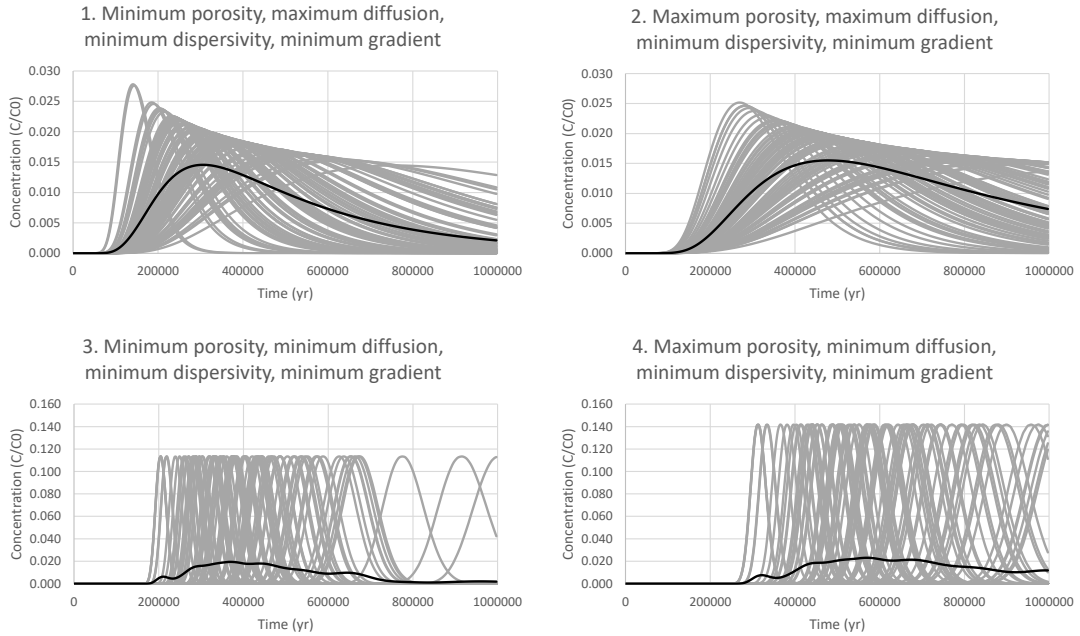

***Figure D1**. BTC ensembles from scenarios 1 to 4 as relative concentration vs. time. The number in the heading of each plot refers to the ensembles listed in Table 4.*
***Figur D1**. Gennembrudskurver for ensemble scenarier 1 til 4 vist som relative koncentrationer vs. tid. Numrene i hver af figuroverskrifterne relaterer til ensemblerne angivet i Tabel 4.*

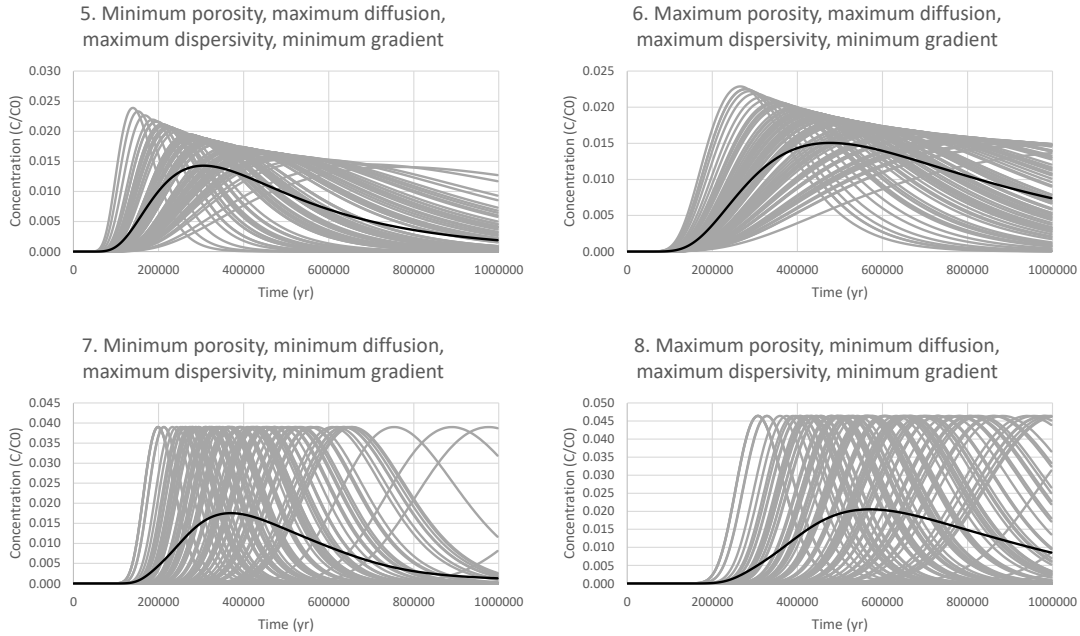

***Figure D2**. BTC ensembles from scenarios 5 to 8 as relative concentration vs. time. The number in the heading of each plot refers to the ensembles listed in Table 4.*
***Figure D2**. Gennembrudskurver for ensemble scenarier 5 til 8 vist som relative koncentrationer vs. tid. Numrene i hver af figuroverskrifterne relaterer til ensemblerne angivet i Tabel 4.*

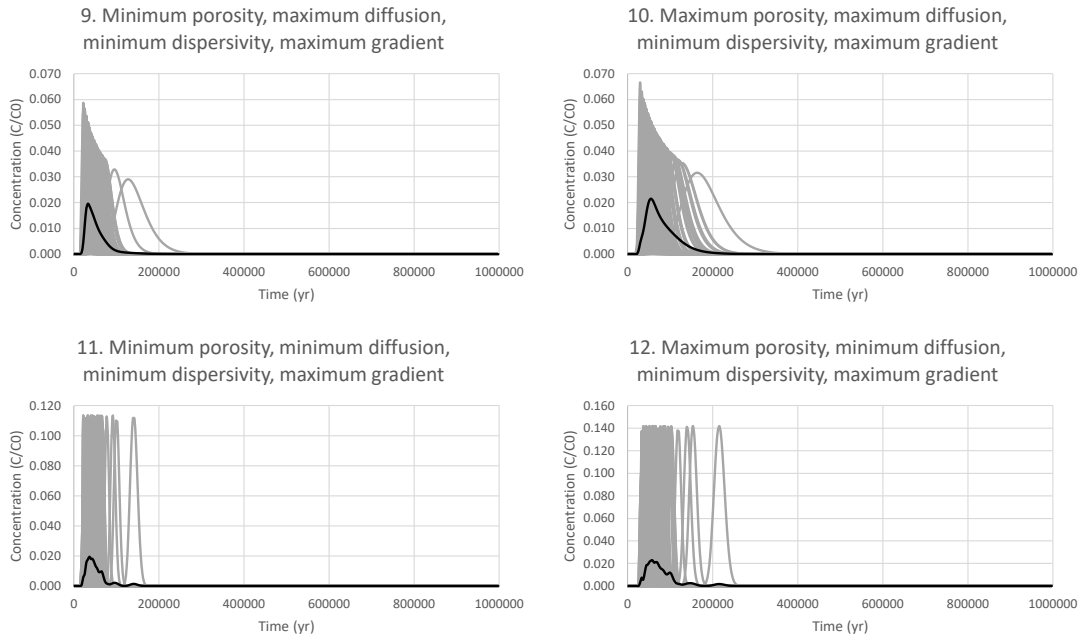

***Figure D3**. BTC ensembles from scenarios 9 to 12 as relative concentration vs. time. The number in the heading of each plot refers to the ensembles listed in Table 4.*
***Figur D3**. Gennembrudskurver for ensemble scenarier 9 til 12 vist som relative koncentrationer vs. tid. Numrene i hver af figuroverskrifterne relaterer til ensemblerne angivet i Tabel 4.*

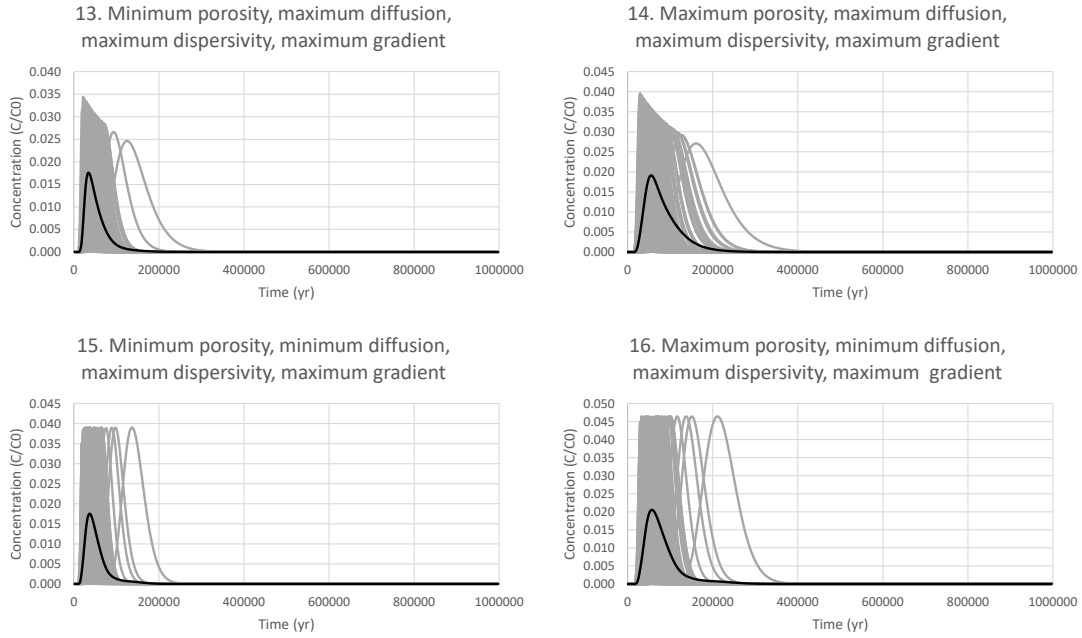

***Figure D4**. BTC ensembles from scenarios 13 to 16 as relative concentration vs. time. The number in the heading of each plot refers to the ensembles listed in Table 4.*
***Figur D4**. Gennembrudskurver for ensemble scenarier 13 til 16 vist som relative koncentrationer vs. tid. Numrene i hver af figuroverskrifterne relaterer til ensemblerne angivet i Tabel 4.*

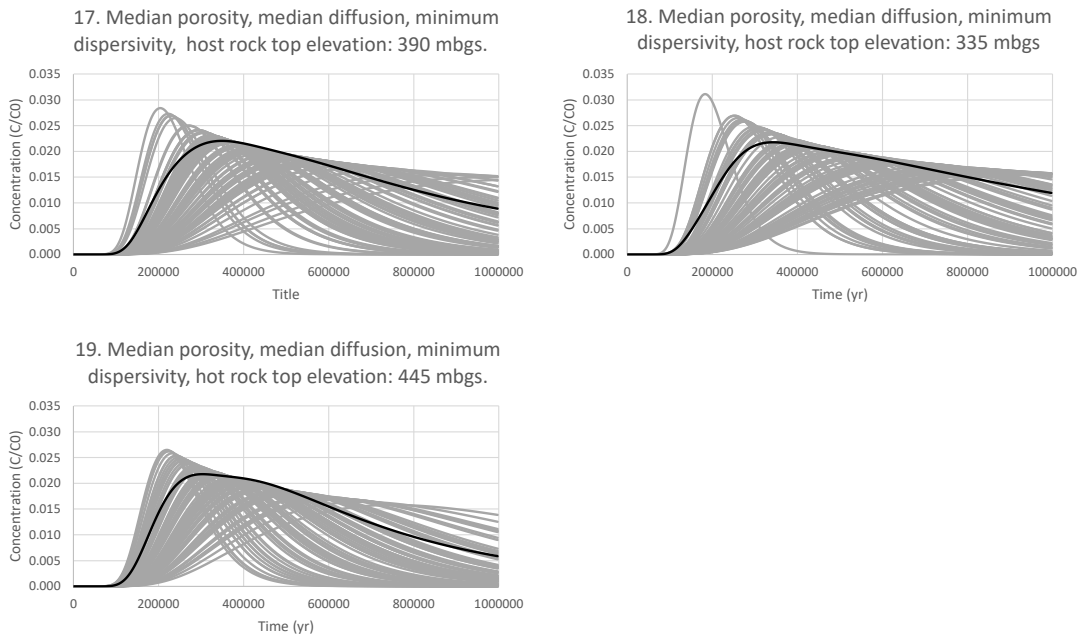

Figure D5*. BTC ensembles from scenarios 17 to 19 as relative concentration vs. time. The number in the heading of each plot refers to the ensembles listed in Table 5.*
Figur D5*. Gennembrudskurver for ensemble scenarier 17 til 19 vist som relative koncentrationer vs. tid. Numrene i hver af figuroverskrifterne relaterer til ensemblerne angivet i Tabel 5.*

Appendix E. BTC ensembles in the claystone

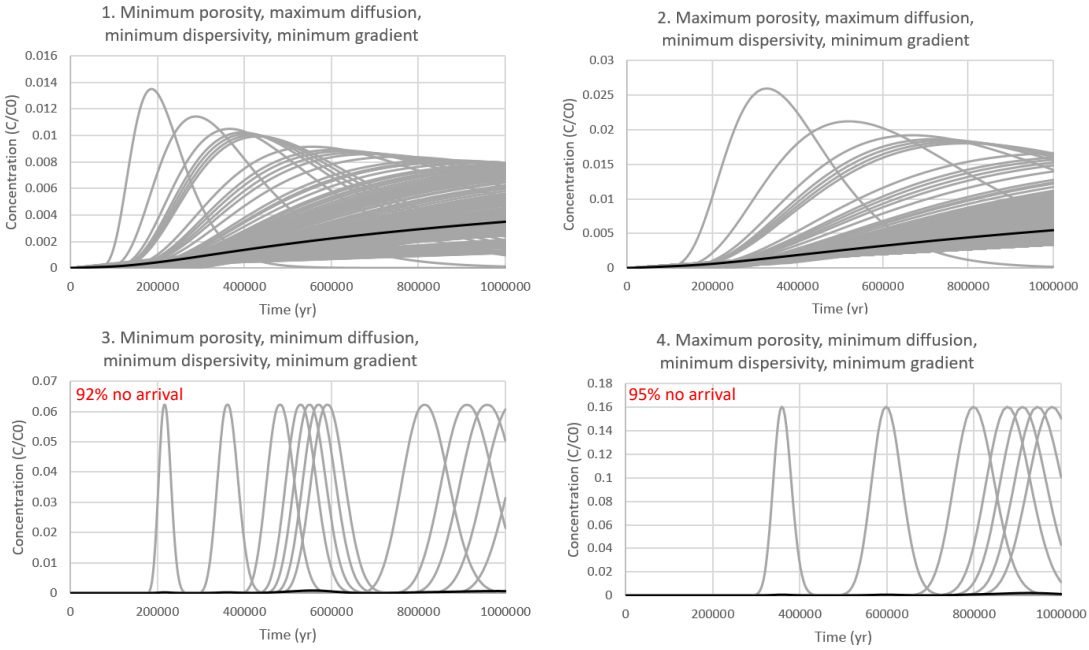

***Figure E1**. BTC ensembles from scenarios 1 to 4 as relative concentration vs. time. The number in the heading of each plot refers to the ensembles listed in Table 4.*
***Figur E1**. Gennembrudskurver for ensemble scenarier 1 til 4 vist som relative koncentrationer vs. tid. Numrene i hver af figuroverskrifterne relaterer til ensemblerne angivet i Tabel 4.*

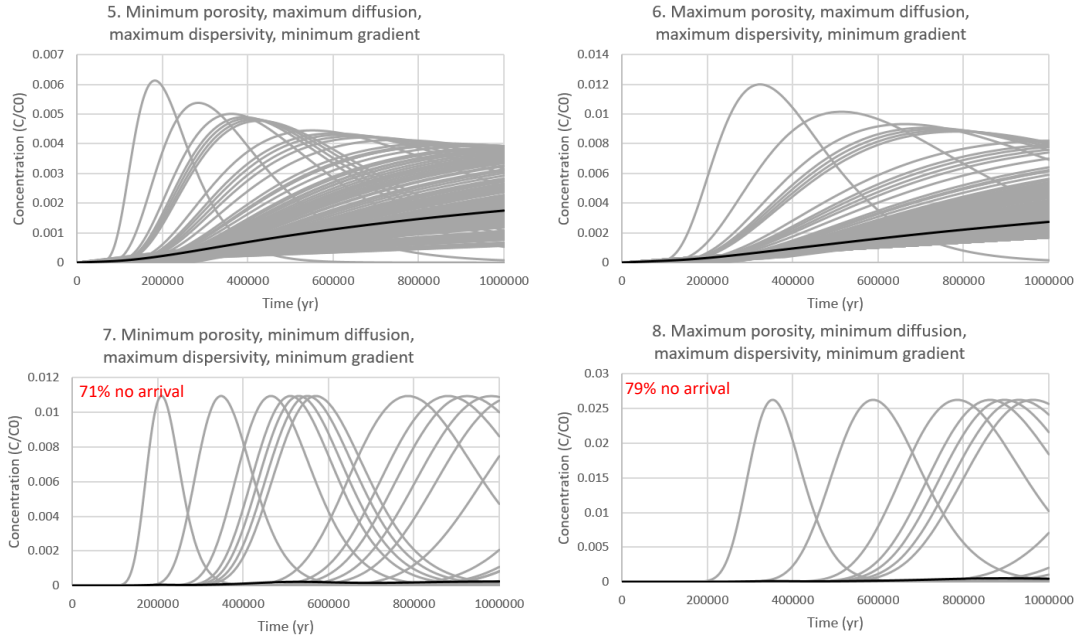

***Figure E2**. BTC ensembles from scenarios 5 to 8 as relative concentration vs. time. The number in the heading of each plot refers to the ensembles listed in Table 4.*
***Figur E2**. Gennembrudskurver for ensemble scenarier 5 til 8 vist som relative koncentrationer vs. tid. Numrene i hver af figuroverskrifterne relaterer til ensemblerne angivet i Tabel 4.*

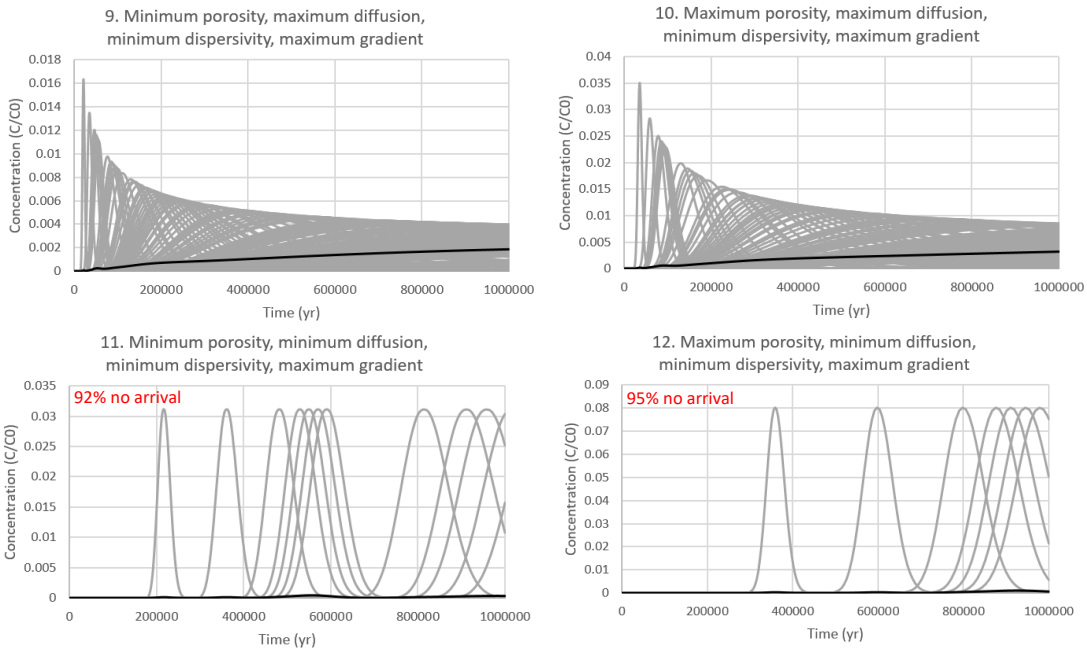

***Figure E3**. BTC ensembles from scenarios 9 to 12 as relative concentration vs. time. The number in the heading of each plot refers to the ensembles listed in Table 4.*
***Figur E3**. Gennembrudskurver for ensemble scenarier 9 til 12 vist som relative koncentrationer vs. tid. Numrene i hver af figuroverskrifterne relaterer til ensemblerne angivet i Tabel 4.*

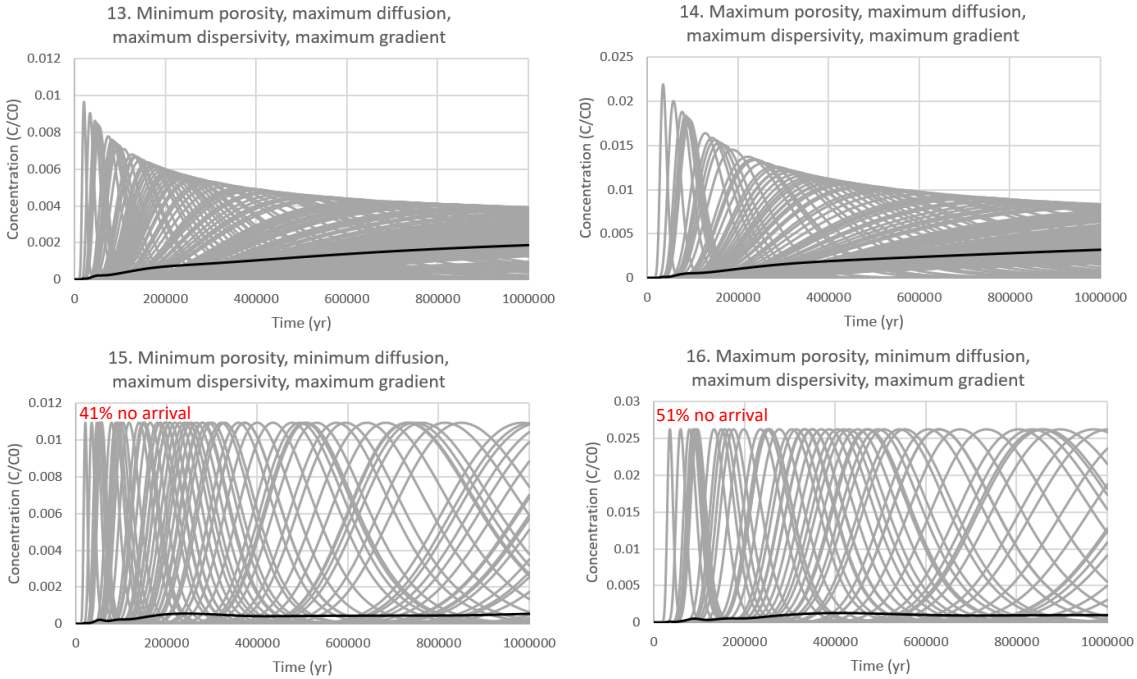

***Figure E4**. BTC ensembles from scenarios 13 to 16 as relative concentration vs. time. The number in the heading of each plot refers to the ensembles listed in Table 4.*
***Figur E4**. Gennembrudskurver for ensemble scenarier 13 til 16 vist som relative koncentrationer vs. tid. Numrene i hver af figuroverskrifterne relaterer til ensemblerne angivet i Tabel 4.*

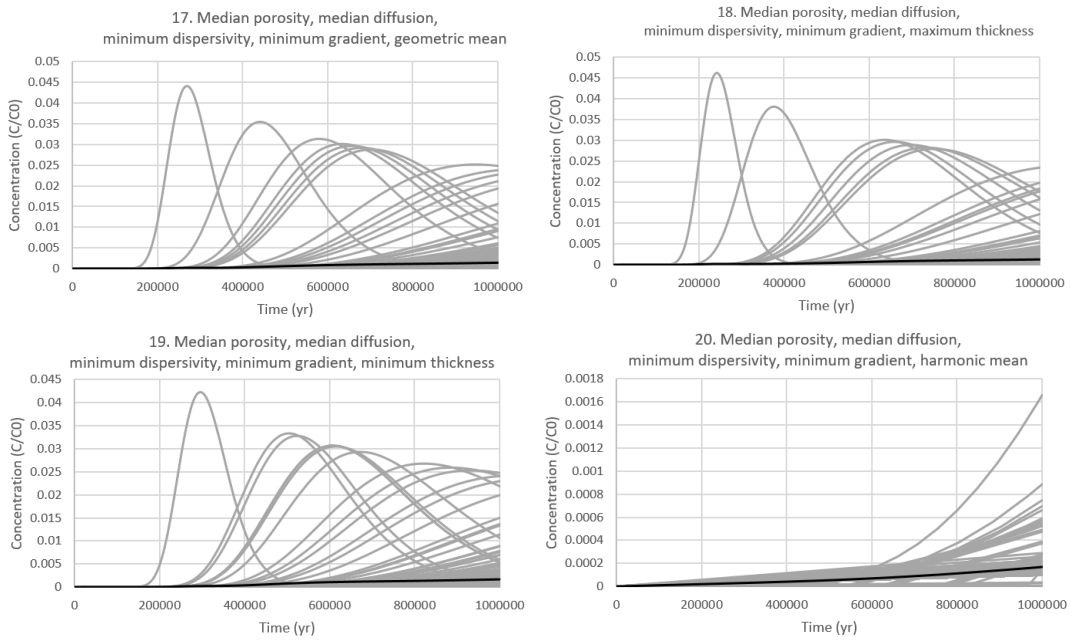

***Figure E5**. BTC ensembles from scenarios 17 to 20 as relative concentration vs. time. The number in the heading of each plot refers to the ensembles listed in Table 5.*
***Figur E5**. Gennembrudskurver for ensemble scenarier 17 til 20 vist som relative koncentration vs. tid. Numrene i hver af figuroverskrifterne relaterer til ensemblerne angivet i Tabel 5.*